

# Unravelling the Mechanisms of GPCR-G Protein Promiscuity

Submitted by  
**Volkan Ozcoban (993442)**

Supervisors  
**Dr. Chris Draper-Joyce**  
and  
**A/Prof. Dan Scott**



Receptor Structure and Drug Discovery  
Laboratory  
The Florey Institute of Neuroscience and  
Mental Health



Department of Biochemistry and Pharmacology  
Faculty of Medicine, Dentistry and Health  
Sciences  
The University of Melbourne

## **Declaration**

This is to certify that:

1. This thesis comprises only my original work toward the BSc (Hons) except where indicated in the text and;
2. Due acknowledgement has been made in all the text to other material used.

Total word count: 10,999

## **Abstract**

The neurotensin receptor 1 (NTSR1) is a G-protein coupled receptor (GPCR) which is promiscuously couple to all four G protein family subtypes ( $G_q$ ,  $G_{i/o}$ ,  $G_s$ , and  $G_{12/13}$ ). Although structural information delineates some molecular mechanisms underlying GPCR-G protein promiscuity, the kinetic and temporal contexts are largely unexploited. Currently, no methodologies contextualise GPCR-G protein signalling in a cell-free format where every proximal factor can be altered. Such a tool would allow observation of underlying biological influences allowing for promiscuity which are difficult to measure with current methodologies, such as GPCR:G protein stoichiometry, lipid composition, and ionic conditions, and also remove potentially confounding factors. Three variants of NTSR1 (human, rat, and an engineered high-expressing rat variant) were used in this study to investigate coupling promiscuity. We hypothesised although these NTSR1 variants are all highly homologous GPCRs capable of binding identical agonists, such as NT1-13 and NT8-13, they possess differences in kinetics with  $G\alpha_{i3}$  and  $G\alpha_q$  heterotrimers. Hence, the aims were to characterise the functionality of two novel tri-cistronic  $G\alpha_{i3}$  and  $G\alpha_q$  bioluminescence resonance energy transfer (BRET) sensors, characterise the coupling of the three NTSR1 variants in whole-cell and pseudo-reductionist BRET assays, and to leverage purification tags on the BRET sensors to begin development of a cell-free assay. We established human and rat NTSR1 are primarily  $G\alpha_q$  coupled whilst showing  $G\alpha_{i3}$ -based secondary coupling and highlighted the capacity of the engineered rat variant to couple with both G proteins. Finally, successful purification of a functionally active  $G\alpha_{i3}$  BRET sensor provides the beginnings for development of a cell-free GPCR-G protein activation BRET assay. These findings highlight how novel tools can be utilised to investigate kinetic patterns of G protein coupling, whilst also paving way for assay development.

## Table of Contents

<b>Unravelling the Mechanisms of GPCR-G Protein Promiscuity .....</b>	1
<b>Declaration .....</b>	2
<b>Abstract .....</b>	3
<b>Table of Contents.....</b>	4
<b>Abbreviations.....</b>	6
<b>Chapter 1: Introduction.....</b>	8
<b>1.1 G protein coupled receptors and their G protein binding partners.....</b>	8
<b>1.2 GPCR promiscuity .....</b>	10
<b>1.2.1 Structural complexities of GPCR-G protein interaction .....</b>	11
<b>1.2.2 ‘Biased agonism’ arising from G protein engagement .....</b>	12
<b>1.2.3 Coordination of G protein coupling by the GPCR lipid environment.....</b>	12
<b>1.3 Major methods for studying G protein coupling .....</b>	13
<b>1.3.1 GTP<math>\gamma</math>S binding assays.....</b>	13
<b>1.3.2 Resonance energy transfer.....</b>	14
<b>1.4 Model GPCRs to interrogate G protein activity: Neurotensin type 1 receptors.....</b>	16
<b>1.4.1 Neurotensin in the human body .....</b>	16
<b>1.4.2 Neurotensin receptors and the neurotensin type 1 receptor.....</b>	16
<b>1.4.3 Human NTSR1.....</b>	16
<b>1.4.4 Rat NTSR1 .....</b>	17
<b>1.4.5 enNTSR1 .....</b>	17
<b>1.5 Study objectives .....</b>	18
<b>Chapter 2: Materials and Methods .....</b>	20
<b>2.1 Mammalian Cell Culture .....</b>	20
<b>2.2 HEK293-F Stable Cell Line Generation .....</b>	20
<b>2.3 Ligands .....</b>	20
<b>2.4 Live Cell BRET Assays .....</b>	21
<b>2.5 Membrane Preparations .....</b>	21
<b>2.6 Membrane Preparation BRET Assays .....</b>	22
<b>2.7 Lentiviral Production and Purification .....</b>	22
<b>2.8 G Protein Expression and Purification.....</b>	22
<b>2.9 Expression and Purification of enNTSR1 .....</b>	23
<b>2.10 Expression and Purification of Rat NTSR1 .....</b>	23
<b>2.11 SDS-PAGE .....</b>	24
<b>2.12 Western Blot Transfer and Detection .....</b>	24

<b>2.13 GTP Turnover Assay .....</b>	24
<b>2.14 Data Analysis .....</b>	25
<b>Chapter 3: Results .....</b>	26
<b>3.1 Determining the signalling functionality of <i>Gai3</i> and <i>Gaq</i> BRET biosensors with prototypical and promiscuous GPCRs .....</b>	26
<b>3.2 Determining the G protein coupling capacity of enNTSR1 .....</b>	33
<b>3.3 Measuring G protein kinetics utilizing membrane preparation-based BRET assays (or pseudo-cell free BRET assays).....</b>	36
<b>3.4 Determining purification potential and catalytic functionality of heterotrimeric G<math>\alpha</math> BRET sensors.....</b>	43
<b>Chapter 4: Discussion.....</b>	50
<b>4.1 Real-time G protein BRET sensors allow kinetic and temporal monitoring of receptor-G protein interaction during the G protein activation cycle.....</b>	50
<b>4.2 enNTSR1 has G protein coupling functionality but is an impaired variant of rat NTSR1 .....</b>	53
<b>4.3 Membrane preparation-based BRET assays further distinguish temporal and pharmacological differences in receptor-G protein interaction .....</b>	54
<b>4.4 Purification of a BRET-based G protein biosensor provides a promising future for reductionist format RET-based assays .....</b>	55
<b>4.5 Future directions and conclusions.....</b>	56
<b>Acknowledgements .....</b>	57
<b>Bibliography.....</b>	59
<b>Appendix .....</b>	i
<b>Appendix Tables .....</b>	i
<b>Appendix Methods.....</b>	ix
<b>Appendix Figures.....</b>	x

## Abbreviations

<b>AR</b>	Adrenergic receptor
<b>AUC</b>	Area under the curve
<b>BRET</b>	Bioluminescence resonance energy transfer
<b>BSA</b>	Bovine serum albumin
<b>cAMP</b>	Cyclic adenosine monophosphate
<b>CHS</b>	Cholesteryl hemisuccinate
<b>CMC</b>	Critical micelle concentration
<b>DAG</b>	Diacylglycerol
<b>DDM</b>	n-Dodecyl- $\beta$ -D-maltoside
<b>DMEM</b>	Dulbecco's modified eagle medium
<b>DPBS</b>	Dulbecco's phosphate-buffered saline
<b>DRD2</b>	D2 dopamine receptor
<b>EC<sub>50</sub></b>	Half-maximal effective concentration
<b>EDTA</b>	Ethylenediaminetetraacetic acid
<b>E<sub>max</sub></b>	Maximum efficacy
<b>enNTSR1</b>	Engineered rat neuropeptid Y receptor 1
<b>ER</b>	Endoplasmic reticulum
<b>FBS</b>	Foetal bovine serum
<b>FRET</b>	Förster resonance energy transfer
<b>FSM</b>	FreeStyle™ 293 Expression Medium
<b>GAP</b>	GTPase-activating protein
<b>GDP</b>	Guanosine diphosphate
<b>GEF</b>	Guanine nucleotide exchange factor
<b>GPCR</b>	G protein coupled receptor
<b>GRK</b>	G protein-coupled receptor kinase
<b>GTP</b>	Guanosine triphosphate
<b>HEK293-F</b>	Human embryonic kidney 293 cells (Freestyle variant)
<b>HEK293-T</b>	Human embryonic kidney 293 cells (Large T antigen expressing variant)
<b>HEPES</b>	4-(2-hydroxyethyl)-1-piperazineethanesulfonic acid
<b>ICL</b>	Intracellular loop
<b>IP<sub>3</sub></b>	Inositol 1,4,5-triphosphate
<b>IPTG</b>	Isopropyl $\beta$ -D-1-thiogalactopyranoside
<b>IRES</b>	Internal ribosome entry site

<b>LMNG</b>	Lauryl maltose neopentyl glycol
<b>MBP</b>	Maltose-binding protein
<b>muGFP</b>	Novel ultra-stable, monomeric green fluorescent protein
<b>nLuc</b>	Nanoluciferase
<b>NMR</b>	Nuclear magnetic resonance
<b>NT1-13</b>	Neurotensin 1-13
<b>NT8-13</b>	Neurotensin 8-13
<b>NTSR1</b>	Neurotensin receptor 1
<b>NTSR2</b>	Neurotensin receptor 2
<b>NTSR3</b>	Neurotensin receptor 3
<b>PAGE</b>	Polyacrylamide gel electrophoresis
<b>PBS</b>	Phosphate-buffered saline
<b>PLC</b>	Phospholipase C
<b>PMSF</b>	Phenylmethylsulphonyl fluoride
<b>POPC</b>	Palmitoyloleoyl phosphatidylcholine
<b>POPG</b>	Palmitoyloleoyl phosphatidylglycerol
<b>PRF</b>	Phenol red-free media
<b>PVDF</b>	Polyvinylidene fluoride
<b>RET</b>	Resonance energy transfer
<b>RLuc</b>	Renilla luciferase
<b>SDS</b>	Sodium dodecyl sulphate
<b>TBS</b>	Tris-buffered saline
<b>TM</b>	Transmembrane domain
<b>WT</b>	Wild type

## Chapter 1: Introduction

### 1.1 G protein coupled receptors and their G protein binding partners

Characterised by their seven  $\alpha$ -helical transmembrane domains, G protein coupled receptors (GPCRs) form the largest class of membrane bound receptor drug targets. GPCRs transduce extracellular signals, ranging from photons to proteins, into diverse downstream signalling pathways, making them one of the most attractive pharmacological targets (Hauser et al., 2018).

GPCRs activate intracellular heterotrimeric G proteins consisting of a  $G\alpha$ ,  $G\beta$ , and  $G\gamma$  subunit in response to external stimuli (Figure 1). Conformational changes relayed to the activated GPCRs intracellular face grants access to an inactive, guanosine diphosphate (GDP)-bound G protein, promoting release of GDP and allowing for high affinity binding of guanosine triphosphate (GTP) within the deserted binding pocket of the  $G\alpha$  subunit (Oldham & Hamm, 2008). Nucleotide exchange results in dissociation of the heterotrimer into  $G\alpha$  and  $G\beta\gamma$  subunits, allowing for interaction with downstream effector molecules initiating G protein-mediated intracellular signalling. Ultimately, signalling ceases when the GTPase activity of the  $G\alpha$  subunit hydrolyses GTP into GDP.

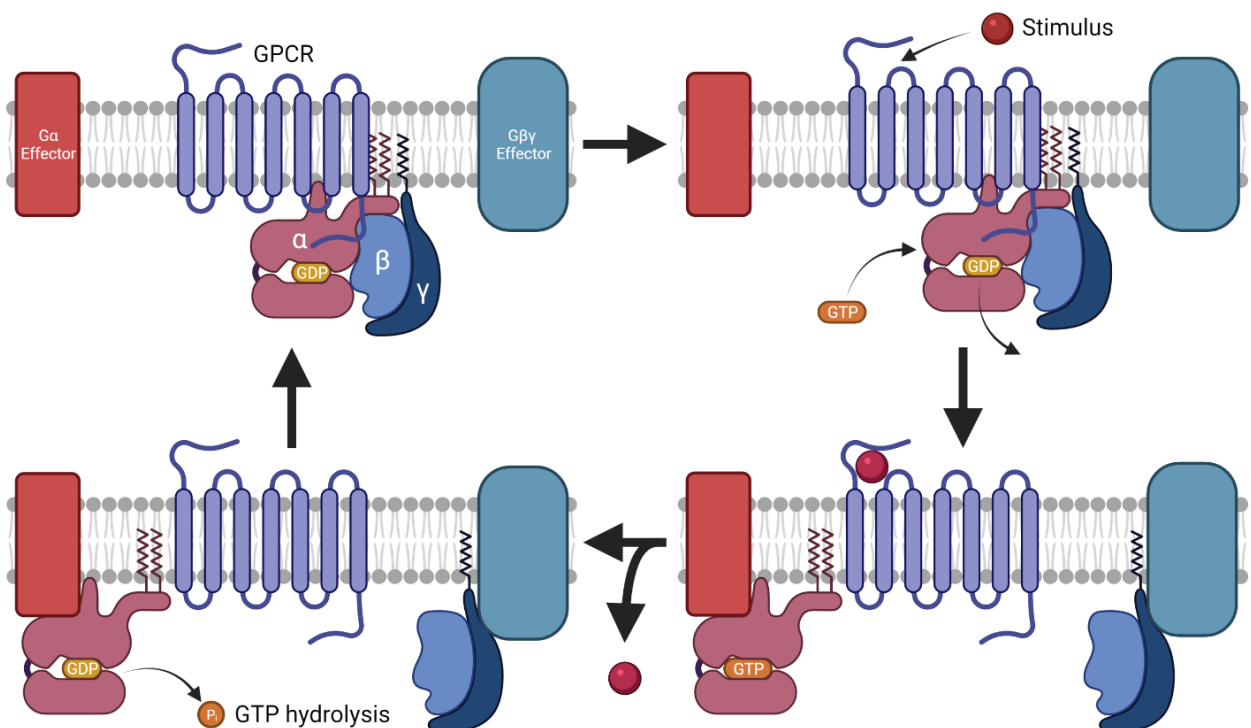


**Figure 1. G protein-based G protein coupled receptor signalling.** The GPCR is inactive whilst the G protein is in a heterotrimeric state (Top left). Stimulus activates the GPCR, allowing the heterotrimeric G protein to bind to the intracellular face of the GPCR, allowing for exchange of GDP for GTP (Top right). Heterotrimer dissociates, resulting in  $G\alpha$  monomers and  $G\beta\gamma$  heterodimers interacting with downstream effector protein (Bottom right). G protein signalling ceases after

hydrolysis GTP by the GTPase activity of the  $G\alpha$  subunit. The G protein heterotrimer reforms and returns the system to the basal state (Bottom left).

Predicated on their sequence and downstream effector response, the 16 human  $G\alpha$  subunits are classified into four major families:  $G\alpha_{q/11}$ ,  $G\alpha_s$ ,  $G\alpha_{i/o}$ , and  $G\alpha_{12/13}$ , with each stimulating distinct signalling cascades (**Figure 2**) (Syrovatkina et al., 2016). Moreover, the five  $G\beta$  and 12  $G\gamma$  isoforms diversify the signalling network, although the complexities introduced by the selectivity for these important G protein subunits is poorly understood (Khan et al., 2013). Importantly, stimulus specificity is critical for selective  $G\alpha$  signal transduction (Neves et al., 2002).

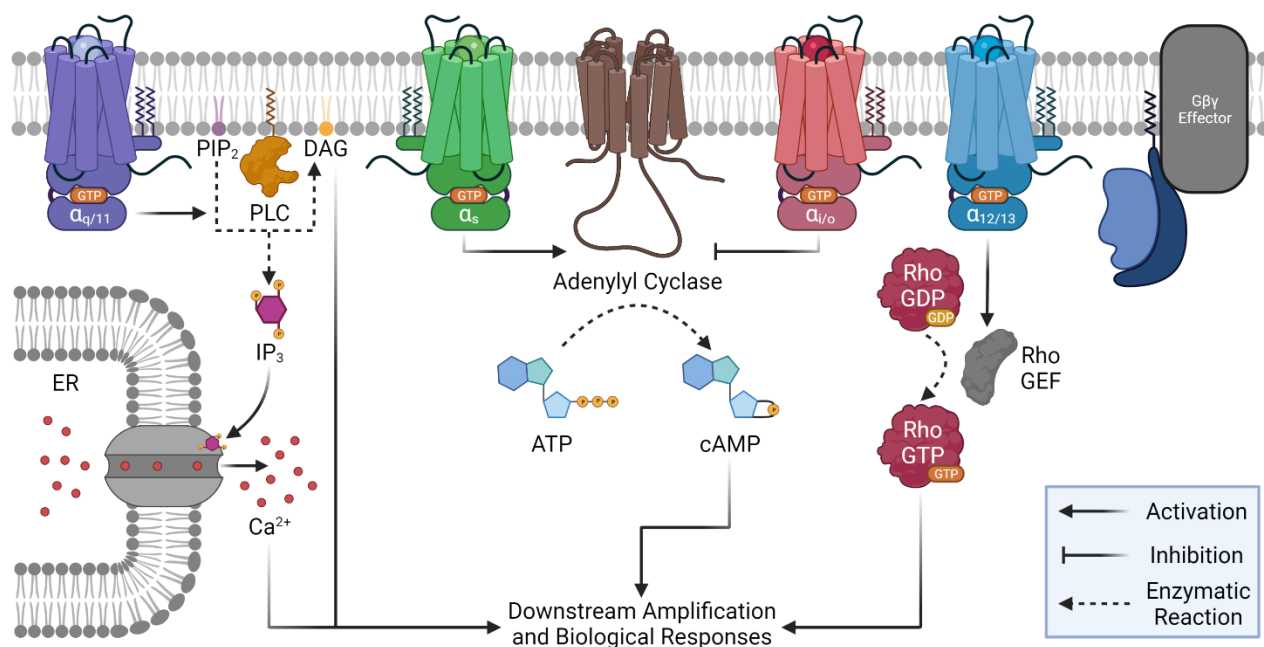


**Figure 2. Schematic of the classical G protein signalling pathways.** Model G protein signalling pathways through the four  $G\alpha$  families ( $G\alpha_{q/11}$ ,  $G\alpha_s$ ,  $G\alpha_{i/o}$ ,  $G\alpha_{12/13}$ ) produce complexity which is system and tissue dependent.  $G\alpha$  proteins can activate or inhibit effector proteins including phospholipase C (PLC), adenylyl cyclase, and Rho guanine nucleotide exchange factors (GEFs) to produce second messengers such as diacylglycerol (DAG), inositol 1,4,5-triphosphate (IP<sub>3</sub>), cyclic adenosine monophosphate (cAMP), and activate protein phosphorylation, respectively. The diverse signalling pathways activated by GPCRS can induce biological responses modulating proliferation, gene regulation, hormone secretion, and much more. Additionally, several  $G\beta$  and  $G\gamma$  subtypes diversify signalling through unique effector molecules e.g., ion transporters, kinases.

In a simplified sense, the GPCR active state is one which is bound to the G protein heterotrimer while the inactive state is not. In reality, GPCRs exist in equilibrium between multiple states. Dynamicity of individual transmembrane domains, loops, and bonds results in subtle shifts between multiple conformations leading to GPCRs being conformationally heterogeneous (Kobilka & Deupi, 2007). This complex behavior (coined conformational equilibrium) highlights different GPCR partners prefer distinct receptor conformations (**Figure 3**). GPCR ligands are capable of shifting the conformational equilibrium of the receptor to varying extents (Kenakin, 2003). Agonists bind the receptor to push the conformational equilibrium towards an active state, inverse agonists stabilise the inactive conformation thereby reducing basal activity, and neutral antagonists block activity of both agonists and inverse agonists without perturbing basal activity (Wacker et al., 2017). However, the modern discovery of ligands capable of selectively engaging distinct downstream pathways has altered our view of optimal therapeutics (Rominger et al., 2014). Uncovering the factors influencing distinct responses may enable development of more efficacious therapeutics for these important drug targets.

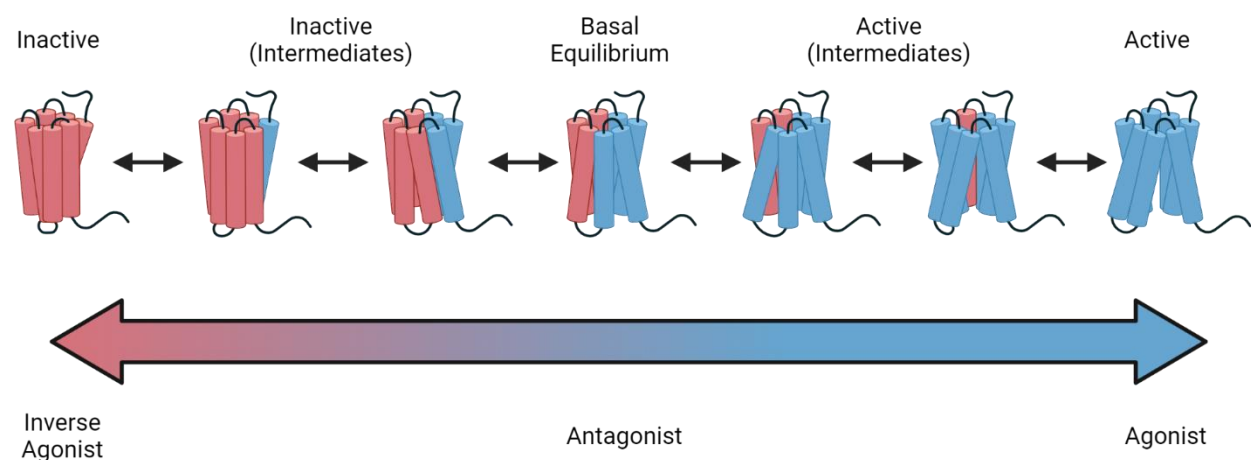


**Figure 3. Conformational heterogeneity in GPCR signaling.** GPCRs exist in a state of constant movement, existing on a spectrum of multiple conformations. GPCRs can transit through multiple intermediate states to reach either extreme: the inactive or active states. The ideal receptor conformations for particular G protein and non-G protein binding partners do not fully overlap but exist along the spectrum, however, the full mechanism remains to be elucidated. The inactive state is stabilized by inverse agonists while the active state is stabilized by agonists. Antagonists block either agonists or inverse agonists from binding receptor, ultimately maintaining the basal equilibrium state.

## 1.2 GPCR promiscuity

Although multiple dissimilar GPCRs can couple to identical G proteins, they ordinarily have sets of disparate functions and pharmacology. For example, the  $\mu$ -opioid (Koehl et al., 2018) and D2

dopamine receptors (DRD2) (Yin et al., 2020) are exclusively  $G\alpha_{i/o}$  coupled, resulting in opioid-induced analgesic effects (James & Williams, 2020) and inhibitory neurotransmission (Seeman et al., 1975), respectively. Crucially, the majority of human GPCRs couple to more than one G protein partner (Inoue et al., 2019). For instance, the neuropeptide Y receptor 1 (NTSR1) couples primarily to  $G\alpha_q$  but can also couple to  $G\alpha_{i/o}$ ,  $G\alpha_s$ , and  $G\alpha_{13}$  (Besserer-Offroy et al., 2017; Tabarean, 2020). Information into the native macroscopic view on GPCR-G protein promiscuity *in vivo* is quite limited. However, of most well-studied GPCRs, the prominent couplers (coined cognate G proteins) are generally known, while secondary couplers are poorly classified and their physiological relevance underappreciated, presenting a cavity in potential GPCR therapeutic discovery.

### 1.2.1 Structural complexities of GPCR-G protein interaction

The lack of general mechanistic insight into G protein selectivity may be attributed to asymmetry in the evolutionary history of GPCRs and G proteins whereby GPCRs have expanded in repertoire and diverged through gene duplication events while G proteins have remained evolutionarily static (Flock et al., 2017). A conserved role for the C-terminal  $\alpha 5$ -helix in various  $G\alpha$  subtypes at the GPCR interface has been highlighted in numerous studies (Draper-Joyce et al., 2018; Flock et al., 2017; Oldham & Hamm, 2008; Rasmussen et al., 2011), whereby, a ‘selectivity barcode’ forms due to subtype-specific residues around the conserved core. These sequence and structural differences around the conserved  $\alpha 5$ -helix allow for delicate rotational and translational movement of the G protein contacts, allowing G protein selectivity for GPCRs. Although the  $G\alpha$  C-terminus is a key determinant for selectivity, an influence of distal spatial regions, such as the  $G\alpha$  subunit core, has been discovered (Kostenis et al., 1997). Structurally distinct regions have been highlighted to play more important roles in governing receptor-G protein selectivity than the  $G\alpha$  C-terminus alone, such as in the D1 dopamine and M3 muscarinic receptors (Okashah et al., 2019). These various studies demonstrate a structural plasticity of GPCRs for recognising distinct G protein families due to no key motifs being conserved across receptors coupling to identical G proteins (Glukhova et al., 2018).

Reciprocal structural and energetic links during GPCR-G protein engagement have been demonstrated by DeVree et al. (2016) whereby G protein coupling allosterically modulates agonist association and dissociation, bringing into question how this influences GPCR-G protein selectivity. The nature of different ligands interacting with a single GPCR allows the receptor to explore distinct conformational landscapes and influence the differential sampling of heterotrimeric G proteins bound to the complex (Furness et al., 2016). This ability of ligands to sample different conformational ensembles has given rise to the concept of ‘biased agonism’.

### **1.2.2 ‘Biased agonism’ arising from G protein engagement**

‘Biased agonism’ is the phenomena by which an agonist may preferentially signal via subsets of transduction pathways over other pathways, and may be determined by ligand residency time, altered receptor kinetics, and stabilisation of discrete receptor conformational states altering transducer coupling (Furness et al., 2016). To date, the breadth of research into ‘biased agonism’ has focused on distal signalling measures and differences in G protein-dependent versus G protein-independent signalling e.g.,  $\beta$ -arrestin-mediated signalling (Onaran et al., 2017). However, the proximal relationship of receptor-G protein selectivity remains poorly understood as a mechanism through which biased signalling may arise. More recently, altered conformational selection in the vasopressin V2 receptor engagement with G proteins across all subfamilies, as well as G protein-independent interaction, could be biased through small structural modifications of its native agonist, suggesting additional bias hot spots in the ligand binding pocket (Heydenreich et al., 2021). Additionally,  $G\alpha$  expression levels can influence agonist efficacy and potency (Onfroy et al., 2017), indicating a critical mechanism through which bias may occur as the receptor is more likely to couple with the abundant subtype. Differential G protein expression is notable in pathological contexts such as cancer (Yajima et al., 2012), whilst also fluctuating in normal tissue e.g., lymphoid development (Grant et al., 1997). In turn, the contemporary design of biased ligands needs to consider *in vitro* approaches to systematically determine causal relationships of receptor-G protein interaction.

### **1.2.3 Coordination of G protein coupling by the GPCR lipid environment**

An additional complexity to GPCR-G protein engagement is the lipid composition within particular cells. Cell membranes contain various lipid subtypes distributed dynamically and in relative proportions which allow for cell type differentiation and compartmentalization (Casares et al., 2019). In addition to the critical role lipid membranes play in anchoring lipidated G protein subunits and driving subunit specific signaling (Álvarez et al., 2015; Vögler et al., 2004), the local membrane charge on the intracellular surface proximal to the receptor is capable of modulating coupling. For instance, *in vitro* perturbations to the  $\beta_2$ -adrenergic receptor ( $\beta_2$ -AR) membrane composition have suppressed  $\beta_2$ -AR- $G\alpha_i$  complex formation while enhancing  $\beta_2$ -AR- $G\alpha_s$  coupling (Strohman et al., 2019), reflecting variations in the fraction of charged and hydrophobic residues lining the heterotrimeric contact surface (Flock et al., 2017). Interestingly, incorporation of  $\text{Ca}^{2+}$  rescues the coupling efficiency of  $\beta_2$ -AR- $G\alpha_{i3}$  complexes without altering  $\beta_2$ -AR- $G\alpha_s$  coupling suggesting electrostatic intermediaries aid in coupling. Furthermore, affinity and nucleotide exchange rates of  $G\alpha_q$ -based heterotrimers to activated NTSR1 have markedly increased in the presence of negatively charged phospholipid head groups without modulating agonist binding (Inagaki et al., 2012).

Ultimately, membrane-lipid alterations are capable of changing GPCR signalling and need to be considered when unravelling agonist action.

Although GPCR-G protein structures emphasise subtle variations in coupling states, the temporal sequence of events during coupling, such as the possibility of a selectivity filter in the intermediate steps of coupling (Du et al., 2019; Kato et al., 2019), is hindered by current methodologies. To understand these subtleties in promiscuity, comprehending the influence of expression levels of GPCRs/G $\alpha$  proteins, membrane composition, and ligand binding are a necessary foundation for understanding the fundamental biology of coupling selectivity (**Figure 4**). Hence, an analytical technique in a cell-free system to control and implicate various parameters in selectivity is needed.

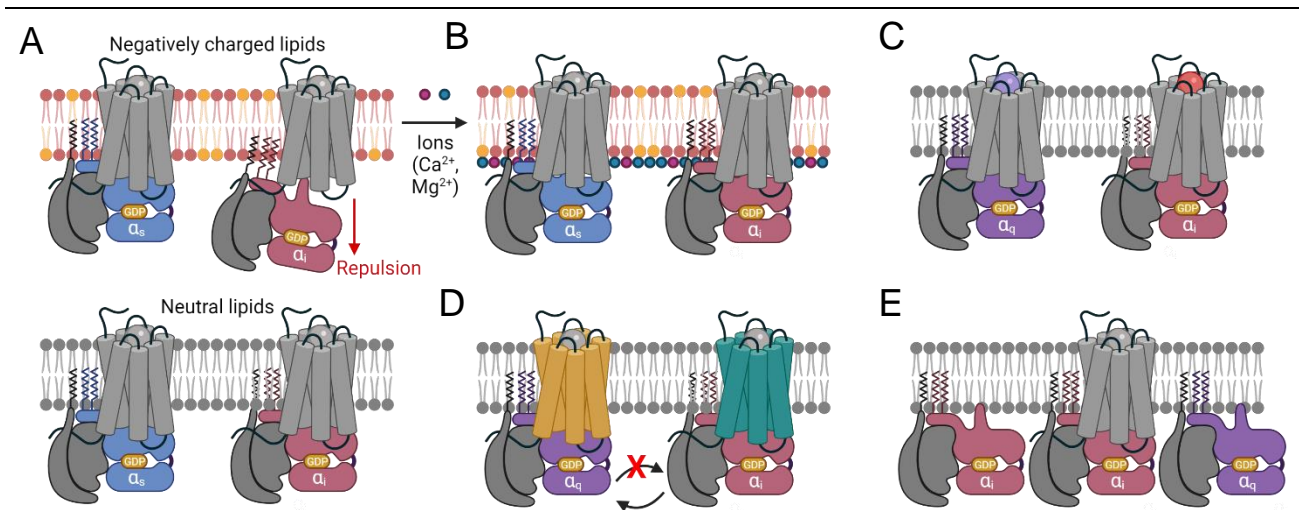


**Figure 4. Summary indicating exemplary factors influencing GPCR-G protein promiscuity.** Factors altering GPCR-G protein coupling interactions include (but are not limited to): (A) specific composition (e.g., phosphatidylcholine, phosphatidylglycerol) and charge (positive/negative/neutral) of lipids in the membrane bilayer, (B) surrounding cellular composition and ionic interactions, (C) selective agonist bound to the GPCR, (D) GPCR subtype, and (E) G $\alpha$  subtype and stoichiometry.

### 1.3 Major methods for studying G protein coupling

#### 1.3.1 GTP $\gamma$ S binding assays

As the initial nucleotide exchange during G protein activation is imperative for GPCR signalling, utilising the non-hydrolysable radiolabelled GTP analogue, [ $^{35}$ S]GTP $\gamma$ S, has allowed for monitoring of the exchange event (Higashijima et al., 1987). GTP $\gamma$ S binding assays allow for utilisation of membrane preparations or permeabilised whole cells containing the GPCR of interest to be incubated with [ $^{35}$ S]GTP $\gamma$ S followed by ligand stimulation to assess GPCR activation (Strange, 2010). However, as [ $^{35}$ S]GTP $\gamma$ S is non-hydrolysable, the forward G protein response induced by the

ligand can be measured while the reformation of heterotrimers cannot be, thereby losing much of the kinetic landscape. Furthermore, a common impediment to GTP $\gamma$ S binding assays is confinement to GPCRs coupling to G $\alpha_{i/o}$  subfamilies due to inefficient detection of [ $^{35}$ S]GTP $\gamma$ S binding to G $\alpha_s$  and G $\alpha_{q/11}$  subfamilies above the high basal signal (Milligan, 2003). Factors compounding such inability are the substantially lower nucleotide exchange rates of G $\alpha_s$  and G $\alpha_q$  species (Berstein et al., 1992; Brandt & Ross, 1986; Jones et al., 2012), and relatively lower levels of expression (Grant et al., 1997; Milligan, 2003).

### 1.3.2 Resonance energy transfer

Resonance energy transfer (RET) uses the process of energy transfer from a fluorescent donor to a fluorescent acceptor to monitor real-time protein-protein interactions (Hamdan et al., 2006), with RET sensors established in two flavours: Förster RET (FRET) and bioluminescence RET (BRET). FRET requires excitation of the donor fluorophore with an external light source while BRET mitigates use of an external excitation laser, instead utilising the light-emitting capability of luciferase-based enzymes thereby reducing noise and photobleaching (Xu et al., 1999). Efficient detection of protein-protein interactions is determined by the donor-acceptor pair being within ~10 nm and spectral overlap between donor emission and acceptor excitation (Stryer, 1978), allowing for unparalleled resolution into the time-based kinetics of GPCR signalling.

G protein BRET sensors are generalisable high-throughput tools to identify ligand pharmacology, with minimal strain placed on live cells (Zhou et al., 2021). Recently, a toolbox for optimal donor fusion sites within the G $\alpha$  subunit for monitoring G protein activity has been developed (Olsen et al., 2020). Nevertheless, inclusion of the three G protein subunits on unique plasmids can lead to experimental variations (**Figure 5A**). To combat this, our laboratory has developed a tri-cistronic plasmid containing all three synthetic G protein subunits as well as a polyhistidine-tag for heterotrimeric purification (**Figure 5B**). Although similar tri-cistronic systems have been developed (Schihada et al., 2021), these assays were conducted in a whole cell format. Purification of these BRET-based G protein sensors would allow for interrogation of GPCR-G protein coupling in a purified format whereby the precise analytical conditions can be intimately controlled, including only having the captured GPCR and G protein of interest present, lipid/detergent environment, GDP/GTP concentration, and GPCR:G protein stoichiometry.

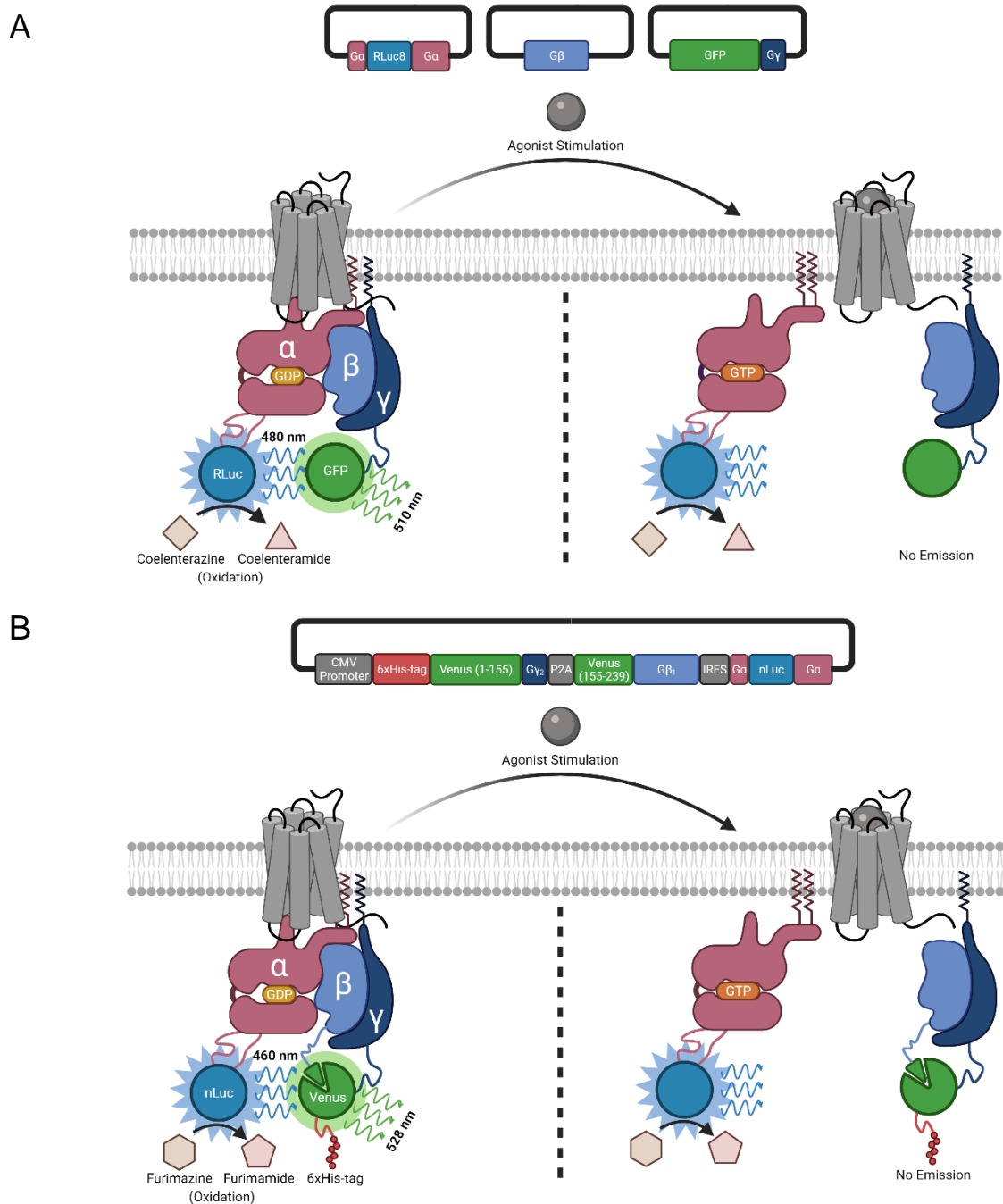


**Figure 5. Schematic of the two generalisable forms of BRET sensors for determining G protein coupling and uncoupling.** (A) Three plasmid transfectable systems are commonly used and optimised for in-cell pharmacological assays of GPCR biology and signal transduction. They generally use luciferase-based enzymes, such as Renilla luciferase (RLuc), as the donor and fluorescent proteins as acceptors. (B) Novel all-in-one tri-cistronic BRET sensor construct with a polyhistidine purification handle. Utilises the brighter nanoluciferase (nLuc) as the bioluminescent donor. In both cases, substrate oxidation results in enzymatic release of light by the donor protein and excitation of the acceptor protein. The ratio of emission from acceptor to donor proteins is used as a relative measure for changes in protein-protein interaction.

## **1.4 Model GPCRs to interrogate G protein activity: Neurotensin type 1 receptors**

### **1.4.1 Neurotensin in the human body**

Neurotensin (NT1-13) is a 13-amino acid (ELYENKPRRPYIL) endogenous regulatory peptide which has both endocrine and neuromodulator activity in the central nervous system and gastrointestinal tract, respectively (Goedert & Emson, 1983; Uhl & Snyder, 1976). Processing of pre-pro-neurotensin results in the production of either NT1-13 or neuromedin N (KIPYL) (Kitabgi, 2006), with outcomes depending on the tissue type. In the brain, pre-pro-neurotensin is processed into both products while in the gut it is primarily processed into NT1-13 (Kitabgi, 2006). Interestingly, it has been shown the six C-terminal residues RRPYIL (NT8-13) are sufficient and necessary for NT1-13 interaction whilst increasing affinity for cognate receptors by 10-fold (Cusack et al., 1995; Granier et al., 1982). Yet, it is not one of the fragments produced *in vivo* (Tyler-McMahon et al., 2000). Hence, NT1-13 and NT8-13 are the primary tools utilized for basic agonist-based research into neurotensin receptor interaction and modulation.

### **1.4.2 Neurotensin receptors and the neurotensin type 1 receptor**

Neurotensin receptors were identified based on their capability to bind NT1-13. This led to classification of the triadic family consisting of NTSR1, NTSR2, and NTSR3 (Chalon et al., 1996; Mazella et al., 1998; Tanaka et al., 1990). The two low affinity receptors for NT1-13 were identified as NTSR2 (sharing 64% homology with NTSR1) and the non-GPCR NTSR3 (Chalon et al., 1996; Mazella et al., 1998). Although NTSR2 signalling pathways are poorly understood, NTSR1 has been the most well-defined of the triad (Wu et al., 2013).

Although NTSR1 has been studied thoroughly since its discovery (Tanaka et al., 1990), subtype selective market-approved compounds for NTSR1 are non-existent. A major facet is high structural homology between NTSR1 and NTSR2, and absence of NTSR2 structures to guide structure-based drug design. An accompanying aspect is the lack of well-defined separation between its supposed primary and secondary G protein coupling partners, as well capability to activate non-G protein-dependent pathways such as  $\beta$ -arrestin mediated internalization (Besserer-Offroy et al., 2017).

### **1.4.3 Human NTSR1**

Human NTSR1 has been suggested to play substantial roles in analgesia (Kleczkowska & Lipkowski, 2013), thermoregulation (Feifel et al., 2010), and blood pressure regulation (Piliponsky et al., 2008). In particular, NTSR1 has been associated in multiple cancers such as the aggressive pancreatic ductal adenocarcinoma which overexpresses both NTSR1 and NT1-13 whilst also increasing expression in line with the stage of disease progression (Takahashi et al., 2021; Wang et al., 2011). However, there are a lack of biased and subtype selective drugs for the treatment of

diseases resulting from alterations in NTSR1 expression or signalling. Additionally, bioavailable biased compounds for NTSR1 could provide a new avenue for the control of severe pain. It may be beneficial to have a novel method for controlling the coupling state of the human NTSR1 as the receptor is incredibly promiscuous, hence why drug candidates are difficult to screen for.

#### 1.4.4 Rat NTSR1

Being the first neurotensin receptor discovered (Tanaka et al., 1990), rat NTSR1 has been the most well-studied. Although not as physiologically relevant as the human NTSR1, studies into rat NTSR1 can be used as comparative tools in studying GPCR species heterogeneity. Moreover, *in vivo* studies of drug candidates and GPCR physiology in mice and rat species have been arduous due to the differential understanding of homologous human and non-human GPCRs, particularly at the GPCR-G protein interaction level. Furthermore, direct evidence of rat NTSR1 and G protein binding in live cells is lacking, with coupling only being demonstrated through modulation of second messenger cascades. Hence, it is critical to understand the direct GPCR-G protein interaction and promiscuity of rat NTSR1 to inform *in vivo* studies.

#### 1.4.5 enNTSR1

enNTSR1 is a high expressing and thermostabilized recombinant GPCR produced via directed evolution of rat NTSR1 (Bumbak, 2016). enNTSR1 has an approximate yield of 0.6 mg/L of culture when expressed in *E. coli*, with high detergent stability lending itself as a prototypical receptor for cell-free analytical methods (Bumbak, 2016; Bumbak et al., 2018) (**Figure 6**). However, to reach high yields and stability, 35 amino acid mutations, a short six C-terminal amino acid truncation, and a long 42 amino acid N-terminal truncation were introduced into rat NTSR1 (Bumbak, 2016; Bumbak et al., 2018). As a research tool, enNTSR1 has only been used for general GPCR-ligand, nanobody binding, and nuclear magnetic resonance (NMR) experiments. However, capacity to interact with signalling partners, such as G proteins and  $\beta$ -arrestin, is largely unknown. Limited evidence through distal IP<sub>1</sub> assays suggests enNTSR1-G $\alpha_q$  interaction (Bumbak et al., 2018). Hence, it is necessary to understand enNTSR1-G protein coupling to pave way for methods development.

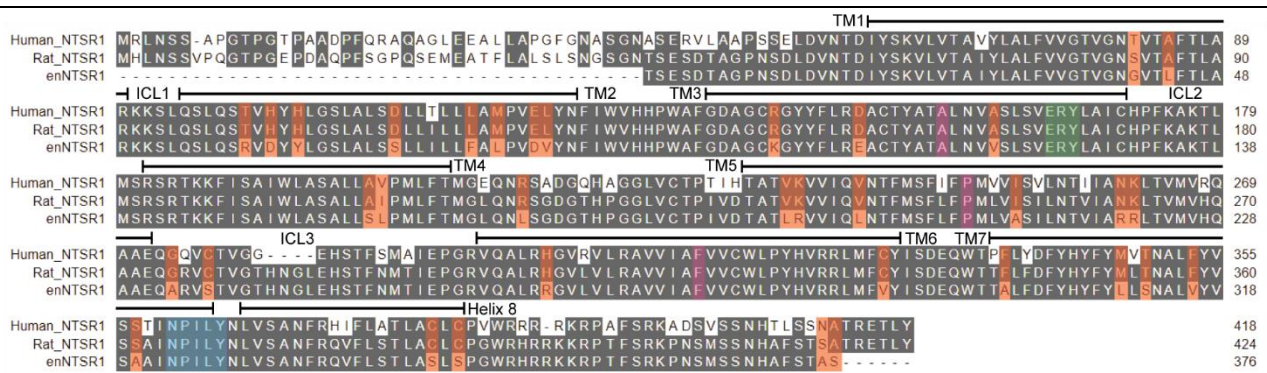


**Figure 6. Sequence alignments of human neurotensin type 1, rat neurotensin type 1, and the engineered rat neurotensin type 1, enNTSR1, receptors.** Identical amino acids are indicated in grey. Amino acid residues mutated to generate enNTSR1 from rat NTSR1 indicated in orange. The three critical ERY/DRY, PAF, and NPxxY microswitches or transmission switches which allow for transmission of the signal generated from the extracellular environment to be transmitted to the intracellular portion of the GPCR are indicated in green, pink, and blue, respectively (Kato et al., 2019). Transmembrane domains (TMs) are indicated by black lines above the sequence alignments. Intracellular loops (ICLs) labelled in the blank space between TMs.

## 1.5 Study objectives

It is unclear what factors of the promiscuity are critical for selectivity. In particular, the kinetic context of the three NTSR1 variants have not been well compared. We hypothesize although human NTSR1, rat NTSR1, and enNTSR1 are all homologous GPCRs capable of binding identical agonists, such as NT1-13 and NT8-13, they possess differences in temporal association with  $G\alpha_{i3}$  and  $G\alpha_q$  heterotrimers. Specifically, investigation into the role of promiscuity and transduction will be conducted on the triad as the wildtype receptors are  $G\alpha_q$ -based primary couplers depicting  $G\alpha_i$ -based secondary coupling while evidence of G protein coupling is deficient for enNTSR1.

The first aim is to characterise the functionality of our laboratories novel  $G\alpha_q$  and  $G\alpha_{i3}$  BRET sensors. Confirming functionality of these BRET sensors would provide a platform for generalizable tools in assessing G protein coupling and bias, allowing for proximal readouts of GPCR-G protein activation with temporal resolution.

The second aim is to characterize the  $G\alpha_{i3}$  and  $G\alpha_q$  G protein coupling interaction with human NTSR1, rat NTSR1, and enNTSR1 using either the potent agonists NT1-13 or NT8-13. Although similar analysis had been conducted for human NTSR1 (Besserer-Offroy et al., 2017), the study lacked any use of the kinetic time-based properties of a BRET sensor. Analyses for rat NTSR1 and enNTSR1 have yet to be conducted, with the latter being unclassified for G protein coupling.

Hence, the third aim would be to begin pipeline development of a cell-free GPCR-G protein assay. A methodology for purifying these sensors and their activity would need to be determined when removed from cells. This would allow progression of potential new tools unable to capture intricacies investigated in the first two aims.

## Chapter 2: Materials and Methods

Refer to **Appendix Table I** for specific reagent/manufacture details, **Appendix Table II** for plasmids, and **Appendix Table III/IV** for G protein BRET sensor subunit nucleotide/amino acid sequences.

### 2.1 Mammalian Cell Culture

HEK293-T cells were grown as adherent cultures. HEK293-F and HEK293-F human NTSR1 IRES mCherry stable cell lines were grown as both adherent and suspension cultures. Adherent cultures (HEK293-T, HEK293-F, and HEK293-F Human NTSR1 WT IRES mCherry stables) were cultured in DMEM supplemented with 10% (v/v) FBS, 1% (v/v) L-glutamine, and 1% (v/v) penicillin/streptomycin (Complete DMEM), kept in an incubator maintaining 5% atmospheric CO<sub>2</sub> at 37°C. Suspension cultures (HEK293-F, HEK293-F Human NTSR1 WT IRES mCherry stables, HEK293-F  $\text{G}\alpha_{i3}$  stables, and HEK293-F HA-ALFA Rat NTSR1 WT IRES mCherry stables) were cultured in FreeStyle<sup>TM</sup> 293 Expression Medium supplemented with 1% (v/v) penicillin/streptomycin (complete FSM), in a shaking incubator (125 rpm) maintaining 8% atmospheric CO<sub>2</sub> at 37°C.

For transfections, a ratio of 1  $\mu\text{g}$ :2  $\mu\text{L}$  DNA:Lipofectamine 2000 was used. Briefly, DNA and Lipofectamine were diluted in Opti-MEM (each in 250  $\mu\text{L}$ /well of a 6 well plate or 120  $\mu\text{L}$ /2  $\mu\text{g}$  of DNA for suspension-based transfections) and incubated at room temperature for 5 minutes. DNA and Lipofectamine 2000 dilutions were mixed and incubated for 20 minutes. Mixtures were then added to cells.

### 2.2 HEK293-F Stable Cell Line Generation

HEK293-T cells were plated at  $3 \times 10^6$  cells/15cm dish in 8 mL complete DMEM. The following day, media was replaced with 8 mL complete FSM and cells transfected with 4.8  $\mu\text{g}$   $\text{G}\alpha_{i3}$  biosensor DNA, 3.12  $\mu\text{g}$  pMDL, 1.2  $\mu\text{g}$  pRSV-Rev, and 1.68  $\mu\text{g}$  pCMV-VSV-G plasmids. Cells were kept at 8% atmospheric CO<sub>2</sub> at 37°C. Two mornings following transfection (~9 am), lentivirus-containing media was harvested (and fresh FSM added), filtered through a 0.45  $\mu\text{m}$  Millex-HV syringe filter unit (Merck Millipore Ltd), supplemented with 4  $\mu\text{g}/\text{mL}$  polybrene, and mixed with  $2 \times 10^6$  HEK293-F cells. This was repeated the following morning (24 hours later). In the afternoon (~5 pm), HEK293-F cells were centrifuged ( $400 \times g$ , 5 minutes), resuspended in FSM, and grown until high density ( $\geq 30 \times 10^6$  cells) for fluorescence-activated cell sorting.

### 2.3 Ligands

NT8-13 synthetically produced by GL Biochem (Shanghai, China). Endogenous NT1-13 kindly provided by Kazem Asadollahi (Bio21 Institute).

## 2.4 Live Cell BRET Assays

Adherent cells were plated in a six-well plate at 500,000 cells/well in complete DMEM. Cells were transfected 24 hours later. For human NTSR1 experiments, HEK293-F human NTSR1 IRES mCherry stables were plated from adherent cultures and transfected with 250 ng/well of G $\alpha_{i3}$  or G $\alpha_q$  BRET biosensor DNA. For rat NTSR1/enNTSR1 experiments, HEK293-F cells were plated from adherent cultures and transfected with 750 ng of pCSC enNTSR1 (M208) Strep. IRES mCherry, pcDNA3.1/Zeo(+) Rat NTSR1 WT, or pcDNA3.1/Zeo(+), alongside 250 ng of BRET biosensor DNA. For  $\beta$ -arrestin assays, 250 ng of nanoluciferase-fused receptor and 600 ng of venus-fused  $\beta$ -arrestin were transfected into HEK293 cells (**Appendix Table II**). 24 hours later, cells were washed using DPBS and resuspended in phenol red-free DMEM supplemented with 10% (v/v) FBS, 1% (v/v) L-glutamine, 1% (v/v) penicillin/streptomycin, and 25 mM HEPES (complete PRF-DMEM). Cells were plated in white opaque 96-well microplates (PerkinElmer) at 40,000 cells/well/80  $\mu$ L. 24 hours later, PRF-DMEM was aspirated and replaced with 90  $\mu$ L of assay solution (ratio of 1  $\mu$ L Nano-Glo® Luciferase Assay Substrate (Promega):450  $\mu$ L PRF-DMEM for a 1.11X assay solution). Plates were equilibrated at 37°C for 10-15 minutes in a PHERAstar® FSX microplate reader (BMG LABTECH) (LUM 535 450 optics module). After restarting the reader for ~3 minutes, the reader was paused, plate ejected, and 10  $\mu$ L of 10X peptide dilutions or vehicle manually dispensed before reads allowed to continue to completion.

## 2.5 Membrane Preparations

Cells were transfected with receptor and G protein BRET sensors proportional to the cell number used in the Live Cell BRET Assay protocol. Cells were harvested 72 hours after transfection, collected by high-speed centrifugation (2,300  $\times g$ , 10 minutes, 4°C), snap frozen, and stored at -80°C. Cells were resuspended in lysis buffer (20mM HEPES pH 7.5, 100 mM NaCl, 10  $\mu$ M GDP, MgCl<sub>2</sub>, and EDTA pH 7.5) and homogenised on ice using an Ultra Turrax IKA T18 basic (24,000 rpm, 10-20 seconds). Homogenates were centrifuged (530  $\times g$ , 10 minutes, 4°C). Supernatant was decanted into a fresh tube and centrifuged again (43,800  $\times g$ , 1 hour, 4°C). Supernatants were disposed of, with membrane pellets resuspended in resuspension buffer (20 mM HEPES, 100 mM NaCl). The pellet was disrupted using 18-to-30-gauge needles (Terumo Medical Products), aliquoted, snap frozen, and stored at -80°C. Concentrations were determined using the Pierce™ BCA Protein Assay Kit (Thermo Fisher Scientific).

## **2.6 Membrane Preparation BRET Assays**

The following is for per well mixtures in optimised receptor-GPCR membrane preparation assays. In a single 96-well OptiPlate™ (PerkinElmer), 10  $\mu$ g of membrane preparations (made up in 20  $\mu$ L of resuspension buffer supplemented with 1.25  $\mu$ M GDP and 10 mM MgCl<sub>2</sub>), 1  $\mu$ L of 101 mM dithiothreitol (DTT), and 60  $\mu$ L of assay solution (ratio of 1  $\mu$ L Nano-Glo® Luciferase Assay Substrate:300  $\mu$ L resuspension buffer for a 1.67X assay solution) were mixed together. Plate incubation and reading was identical to the Live Cell BRET Assay protocol. The only difference being 10  $\mu$ L of 100  $\mu$ M GTP and 10  $\mu$ L of 10X peptide dilutions (both diluted in resuspension buffer) were added sequentially to the plate after ejecting.

For 384-well OptiPlate™ (PerkinElmer) assays during optimisation, an identical set up (at half the total volume) was utilised, however, without DTT, at a temperature of 37C, and in 50  $\mu$ L total.

## **2.7 Lentiviral Production and Purification**

HEK293-T cells were plated at  $10 \times 10^6$  cells/15cm dish in 17 mL complete DMEM. The following day, media was replaced with 17 mL fresh complete DMEM and cells transfected with 12  $\mu$ g G $\alpha_{i3}$  biosensor DNA, 7.8  $\mu$ g pMDL, 3  $\mu$ g pRSV-Rev, and 4.2  $\mu$ g pCMV-VSV-G plasmids. The viral-containing media was collected 48-60 hours post-transfection. The media was centrifuged ( $300 \times g$ , 5 minutes) and cell pellet discarded. The viral-containing media was filtered through 0.45  $\mu$ m Millex-HV syringe filter units (Merck Millipore Ltd). Viral media was ultracentrifuged under a vacuum ( $52,600 \times g$ , 2.5 hours, 4°C). Media was discarded and tubes allowed to dry. 40  $\mu$ L of ice-cold DPBS was dispensed into the bottom of each tube and incubated (16 hours, 4°C). The viral-pellet was dissolved by pipetting, aliquoted, and stored at -80°C.

## **2.8 G Protein Expression and Purification**

HEK293-F cells were suspended in a shake flask (Corning) at  $1 \times 10^6$  cells/mL FSM. 1  $\mu$ L of lentivirus/ $10^6$  cells were mixed into cultures supplemented with 4 mg/mL polybrene. 24 hours after transduction, cells were centrifuged ( $400 \times g$ , 5 minutes) and resuspended in fresh media. For the final purification, cultures were harvested 72 hours post infection. Cells were collected by high-speed centrifugation ( $2,300 \times g$ , 10 minutes, 4°C), snap frozen, and stored at -80°C.

Cells were lysed in hypotonic lysis buffer (10 mM Tris pH 7.5, 150  $\mu$ M MgCl<sub>2</sub>, 1 mM  $\beta$ -mercaptoethanol, 10  $\mu$ M GDP, 1  $\mu$ L Benzonase, and protease inhibitors (2 mM PMSF and 1 cComplete™ EDTA-free Protease Inhibitor Cocktail) for 1 hour at 4°C with gentle shaking. The lysate was supplemented with an equivalent volume of 2X solubilisation buffer (40 mM HEPES pH 7.5,

200 mM NaCl, 2% (w/v) sodium cholate, 0.1% (v/v) n-dodecyl- $\beta$ -d-malatoside (DDM), 10 mM MgCl<sub>2</sub>, 1 mM  $\beta$ -mercaptoethanol, 20  $\mu$ M GDP, protease inhibitors). Cell debris was homogenised with a glass douncer, sonicated, and solubilised (2 hours, 4°C). Insoluble debris was removed by centrifugation (32,300  $\times g$ , 30 minutes, 4°C). 500  $\mu$ L of Talon® Metal Affinity Resin (1 mL of slurry) per 20 mL seeding culture was equilibrated with 3×5 resin volumes of 1X solubilisation buffer. After centrifugation, the supernatant was mixed with equilibrated resin (1 hour, 4°C) with gentle rotation. After binding, the mixture was placed into a glass gravity flow column (Bio-Rad) and allowed to drain. The resin was washed with 3×5 resin volumes of 1X solubilisation buffer. Bound proteins were eluted in a total of 2 mL elution buffer (1X solubilisation buffer supplemented with 250 mM imidazole) with 15-minute incubations at room temperature. Elution fractions were pooled, concentrated (Amicon® Ultra-15-100 kDa cutoff Centrifugal Filter Unit), snap frozen, and stored at -80°C (identical for all purifications).

## 2.9 Expression and Purification of enNTSR1

enNTSR1 was expressed in C43(DE3) competent *E. coli* cells utilizing as previously described (Bumbak et al., 2018). Briefly, cells were transformed with enNTSR1 plasmid (**Appendix II**), cultured, and induced with 0.25 mM Isopropyl  $\beta$ -D-1-thiogalactopyranoside (IPTG) overnight at 16°C. Cells were sonicated in solubilisation buffer (100 mM HEPES, pH 8, 400 mM NaCl, 20% (v/v) glycerol, 100 mg Lysozyme, 2  $\mu$ L benzonase, protease inhibitors), solubilized by adding 1% (v/v) DDM, 0.1% Cholestryl Hemisuccinate Tris Salt (CHS), and 0.8% (w/v) 3-((3-cholamidopropyl) dimethylammonio)-1-propanesulfonate (CHAPS), and mixed with Talon® Metal Affinity Resin equilibrated using wash buffer 1 (30 mM HEPES, pH 7.5, 500 mM NaCl, 10 mM MgCl<sub>2</sub>, 10 mM imidazole, 30% (v/v) glycerol, 0.1% (v/v) DDM, 0.01% (v/v) CHS). The resin was washed with wash buffer 1 and wash buffer 1 supplemented with 8 mM ATP. Resin-bound protein was gradient exchanged into LMNG exchange buffer (30 mM HEPES, pH 7.5, 250 mM NaCl, 10 mM imidazole, 0.1% (v/v) Lauryl Maltose Neopentyl Glycol (LMNG), 0.01% (v/v) CHS). Resin-bound protein was eluted using LMNG 10X CMC buffer (30 mM HEPES, pH 7.5, 250 mM NaCl, 10 mM imidazole, 0.01% (v/v) LMNG, 0.001% CHS (v/v)) supplemented with 300 mM imidazole.

## 2.10 Expression and Purification of Rat NTSR1

HEK293-F HA-ALFA Rat NTSR1 WT IRES mCherry stable cells were grown to a density of  $4 \times 10^6$  cells/mL, harvested, snap frozen, and stored at -80°C. The pellet was lysed with hypotonic lysis buffer (10 mM Tris, pH 7.5, 1 mM EDTA, 1 mM MgCl<sub>2</sub>, 2  $\mu$ L benzonase, protease inhibitors) for 1 hour. Cell debris was pelleted by centrifugation (32,300  $\times g$ , 10 minutes, 4°C), resuspended in solubilisation buffer (30 mM HEPES, pH 7.5, 1% (v/v) LMNG, 0.1% (v/v) CHS, 750 mM NaCl,

30% (v/v) glycerol, 1 mM MgCl<sub>2</sub>, 2 µL benzonase, protease inhibitors), and solubilised (2 hours, 4°C). Insoluble cell debris was removed by centrifugation (32,300 × *g*, 30 minutes, 4°C) and supernatant mixed with wash buffer 1 (30 mM HEPES, pH 7.5, 0.01% (v/v) LMNG, 0.001% (v/v) CHS, 750 mM NaCl, and 10% (v/v) glycerol) equilibrated ALFA Selector Peptide Elutable resin (4% cross-linked agarose) for 1.5 hours at 4°C. The resin was collected in a glass column, washed with wash buffer 1 and wash buffer 2 (20 mM HEPES, pH 7.5, 0.01% (v/v) LMNG, 0.001% (v/v) LMNG, and 150 mM NaCl). Bound proteins were eluted using wash buffer 2 supplemented with 0.4 mg/mL ALFA elution peptide.

## 2.11 SDS-PAGE

BenchMark™ Fluorescent Protein Standard (~11-155 kDa) and Precision Plus Protein™ All Blue Prestained Protein Standard (~10-250 kDa) used as molecular weight ladders for SDS-PAGE and Western Blot analyses, respectively. Protein samples were mixed with 5X SDS loading dye (0.02% (w/v) bromophenol blue, 30% (v/v) glycerol, 10% (w/v) SDS, and 250 mM Tris-Cl) for receptor analysis or dye supplemented with 5% (v/v) β-mercaptoethanol and denatured at 95°C for 2 minutes for G protein analysis (ratio of 4:1 Protein:Dye). Using a Mini-PROTEAN® System (Bio-Rad), 10 µL of samples were loaded onto a 4-15% Mini-PROTEAN® TGX Stain-Free™ Protein Gel in 1X SDS Buffer (25 mM Trizma® base, 192 mM glycine, 1% (w/v) SDS). Electrophoresis was conducted at 200 V for 30 minutes at room temperature. Gels imaged using a BioRad ChemiDoc XRS+ System.

## 2.12 Western Blot Transfer and Detection

After SDS-PAGE, proteins were transferred onto a Immun-Blot® PVDF membrane using the Mini Trans-Blot® Cell system (BioRad) as per the manufacturer's guidelines. Transfers were conducted in 1X wet transfer buffer (25 mM Trizma® base, 192 mM glycine, 20% (v/v) methanol) (100 V, 1 hour, 4°C). Following transfer, membranes were rinsed in 1X TBS (20 mM Trizma® base, 150 mM NaCl) containing 0.1% (w/v) TWEEN® 20 (1X TBS-T). Membranes were blocked in blocking solution (5% (w/v) bovine serum albumin (BSA), 0.02% (v/v) NaN<sub>3</sub> in 1X TBS-T) for 1 hour at room temperature with gentle shaking. Primary and secondary antibodies were applied at the appropriate dilutions, temperatures, and times desired (**Appendix Table V** for details) with gentle shaking. Membranes were washed 3 times over 15 minutes with 1X TBS-T after each antibody application. Membranes were imaged using the Li-Cor Odyssey Infrared Imaging System 9120.

## 2.13 GTP Turnover Assay

Gα<sub>i3</sub> biosensor turnover assays were conducted using the GTPase™-Glo Assay Kit (Promega) with modifications. Purified Gα<sub>i3</sub> biosensor and control samples were diluted stepwise in GTPase/GAP

buffer. The GTP turnover reaction was begun in a 96-well OptiPlate™ by mixing 5  $\mu$ L of protein mixtures with 5  $\mu$ L 2X GTP solution (10  $\mu$ M GTP, 1 mM DTT in GTPase/GAP buffer) and incubated at room temperature for 60 minutes. 10  $\mu$ L of reconstituted GTPase-Glo™ reagent component (1X GTPase-Glo Reagent and ADP in GTPase-Glo™ Buffer) was added to the GTPase reaction and incubated for 30 minutes at room temperature. 20  $\mu$ L of detection reagent was added and incubated for 10 minutes at room temperature. Luminescence was measured in a PHERAstar® FSX microplate reader (LUM plus optic module).

## 2.14 Data Analysis

Data were analysed using GraphPad Prism 9. Data are presented as mean  $\pm$  standard error of the mean (SEM) of  $n$  independent experiments (unless otherwise stated). BRET ratios were defined as acceptor emission/donor emission (ratio of Venus-emission-to-nanoluciferase-emission). Net BRET ratios were calculated as the difference in ratio of ligand-treated and vehicle-treated conditions. Dose-response curves fit to a nonlinear regression with three parameters.  $\log_{10}(EC_{50})$  over time curves fit to a simple linear regression. One-way ANOVA (Tukey's multiple comparison) used for statistical analyses at a significance level of  $p = 0.01$ .

## Chapter 3: Results

### 3.1 Determining the signalling functionality of $G\alpha_{i3}$ and $G\alpha_q$ BRET biosensors with prototypical and promiscuous GPCRs

First, the functionality of our novel  $G\alpha_{i3}$  and  $G\alpha_q$  BRET biosensors was determined by monitoring the induction of nucleotide exchange and G protein dissociation after stimulation of NTSR1 with NT8-13 and NT-13 (**Figure 7A, Appendix Figure A1**). In all four combinations of G protein and agonist (**Figures 7B-E**), agonist-induced decrease in the BRET ratio to a minimum occurred after ~15 minutes. This likely corresponds to equilibrium shifts of G proteins from inactive to active G protein states, where GDP is exchanged for GTP and heterotrimer dissociates. At the minima, there was a gradual increase in BRET ratio over time towards baseline implying potential modulation of the G protein at the cell membrane and receptor recycling. The former occurs due to the assay being a population-based assay which accounts for both inactivate and activate G proteins with endogenous G proteins also being present. Interestingly, although minimal differences are observed between agonists within G protein groups (comparing **Figure 7B to 7C** and **7D to 7E**), between G protein groups highlights more rapid kinetic upturns for  $G\alpha_q$  activation compared to  $G\alpha_{i3}$  activation by the human NTSR1 (comparing **Figure 7B to 7D** and **7C to 7E**). These data highlight the G protein biosensors are functional when expressed in a tri-cistronic manner.

An area under the curve (AUC) approach to determine the dose-response characteristics of NT8-13 and NT1-13 with  $G\alpha_{i3}$ - and  $G\alpha_q$ -based G proteins (**Figure 7F**). An unexpected rightward shift in both peptide dose-response curves were observed with  $G\alpha_q$  compared to  $G\alpha_{i3}$ , contradicting previous findings both agonists are more potent in activating  $G\alpha_q$  signalling (Besserer-Offroy et al., 2017). This suggests the analytical framework of taking AUC of the net BRET ratio may not be ideal for comparing dose-response characteristics. Rather, the strength of the assay and datasets is the ability to observe temporal effects of receptor activation. These temporal alterations may highlight the importance of receptor-ligand kinetics. Additionally, the maximal effect of peptides ( $E_{max}$ ) at the human NTSR1 receptor between  $G\alpha_{i3}$ - and  $G\alpha_q$ -based G proteins is starkly different. This is due to the magnitudes in BRET ratios being dependent on the insertion positions of the nanoluciferase/split-Venus proteins in disordered loops, and differences in protein structure and function between subtypes, rather than efficacy differences. Hence, taking single time-points or an average over time to express dose-response misrepresents general efficacy and half-maximal effective concentration (EC<sub>50</sub>) measurements. This may highlight AUC dose-response analyses take averages of efficacy and potency which is not suitable in GPCR-G protein kinetic analyses (**Figure 7F**).

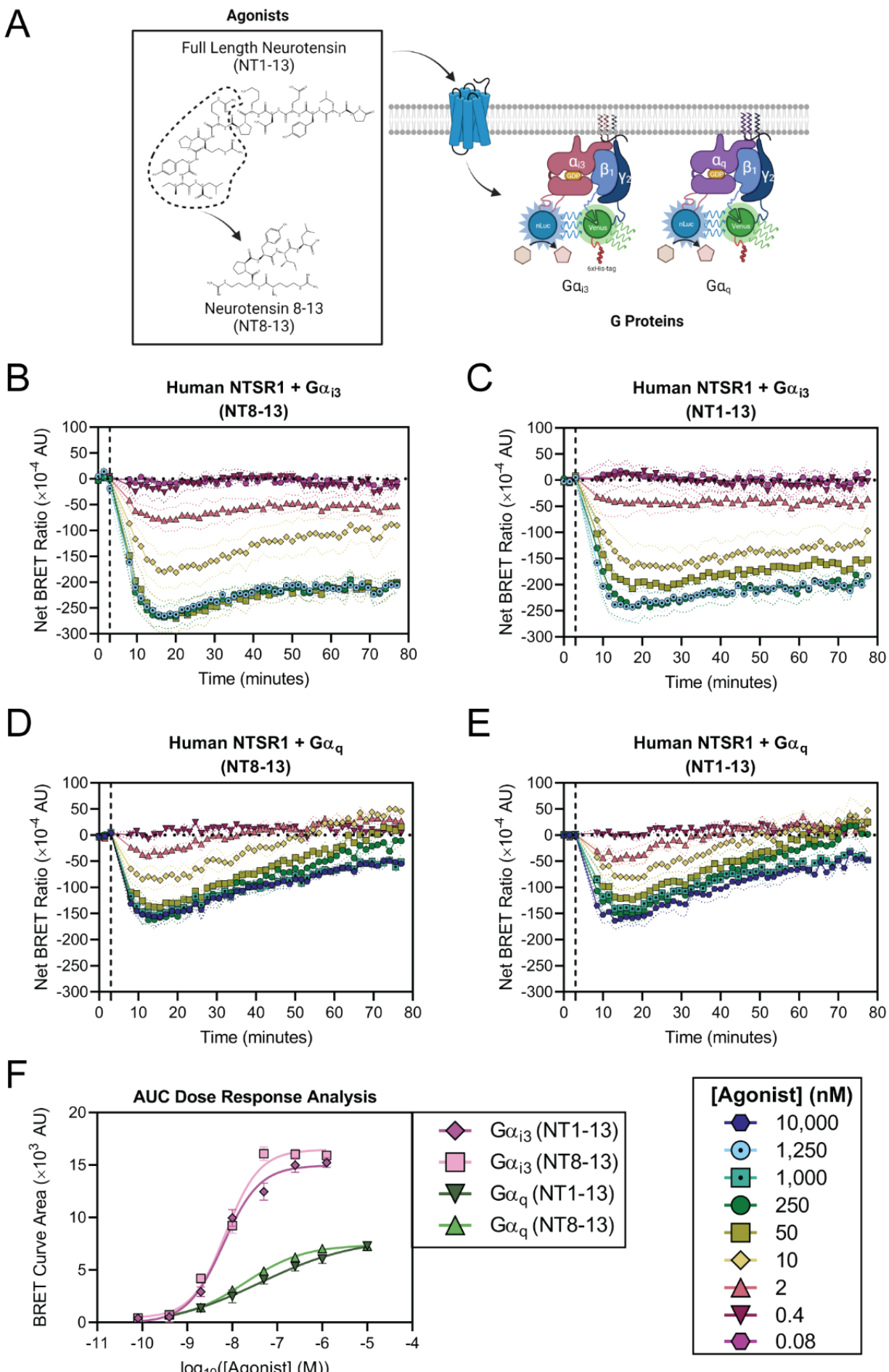


**Figure 7. Human NTSR1 presents distinct signalling and dose-response characteristics when coupling to  $G\alpha_{i3}$  and  $G\alpha_q$  G proteins.** (A) Summary of the agonists (NT8-13 and NT1-13) utilised in measuring the signalling functionality of the two novel  $G\alpha_{i3}$  and  $G\alpha_q$  BRET-based biosensors. This combination was utilised in subsequent BRET experiments. Change in BRET ratio over time in HEK293-F cells expressing human NTSR1 for the activation of (B)  $G\alpha_{i3}$  in the presence of NT8-13, (C)  $G\alpha_{i3}$  in the presence of NT1-13, (D)  $G\alpha_q$  in the presence of NT8-13, and (E)  $G\alpha_q$  in the presence of NT1-13. The data were baseline corrected against the average of three luminescent signal reads (90 second between each; 3 minutes total) prior to the addition of agonist (vertical black dotted lines). Values are expressed as mean  $\pm$  SEM (dotted lines). (F) Corresponding dose-response curves determined by area under the curve calculations of the net BRET ratio. Values are expressed as mean  $\pm$  SD. All values represent three independent experiments conducted in duplicate where duplicates were averaged before calculating SEM and/or SD.

---

Instead, by monitoring the change in BRET ratio over time, real-time agonist dose-response curves for both NT8-13 and NT1-13 were obtained. Dose-response curves for each agonist depicted unique temporal patterns (**Figure 8A-D**). Both agonists elicit similar profiles in the presence of  $G\alpha_{i3}$  which are difficult to separate as these are agonists which only differ in binding affinity (**Figure 8A/B**). Collectively, a gradual decrease in both  $E_{max}$  and potency were observed over time. This would be expected from natural desensitization of the human NTSR1 ( $\beta$ -arrestin driven internalization (Inagaki et al., 2012)), rather than signaling finishing. Moreover, as the assay is population-based, this degree of plasticity is expected for G proteins transitioning from equilibrium back to baseline. Both agonist dose-response curves in the presence of  $G\alpha_q$  decreased rapidly in  $E_{max}$  and potency over 75-minutes compared to their  $G\alpha_{i3}$  counterparts (**Figure 8C/D**).

The time-based analysis allowed a linear regression analysis of the  $\log_{10}(EC_{50})$  values for data points after the minima of the BRET response curves (**Figure 7B-E**). Plotting  $\log_{10}(EC_{50})$  values over time depicted values remain almost identical for both peptides within identical G protein groups (**Figure 8E**). Indeed, changes in  $\log_{10}(EC_{50})$  values accelerate upwards for the agonists after initiation of the  $G\alpha_q$  compared to the  $G\alpha_{i3}$  signalling cascade for the human NTSR1. At the 15-minute minima, pEC<sub>50</sub> values (defined as the negative of the  $\log_{10}(EC_{50})$ ) for all four combinations began at approximately identical values (left-most datapoints in **Figure 8E**). This indicates human NTSR1 is equally promiscuous with  $G\alpha_q$  and  $G\alpha_{i3}$ . However, we speculated one could analyze the overall initial pEC<sub>50</sub> values of a particular ligand by inspecting the initial value of the regression line (**Figure 8E**). Both agonists had equally similar potencies within G protein groups as would be

expected for agonists differing only in affinity ( $p = 0.4159$  for  $G\alpha_{i3}$ ,  $p = 0.6690$  for  $G\alpha_q$ ). Indeed, the potency for the agonists to induce  $G\alpha_q$  signal transduction was greater than  $G\alpha_{i3}$  ( $p < 0.01$ ; both agonists) (**Table I**). As it was beyond the project, further mathematical validation as to whether linear regression analysis is optimal for deriving overall pEC<sub>50</sub> values was not conducted. Nevertheless, these findings suggest NT8-13 and NT1-13 have a greater bias towards  $G\alpha_q$  coupling with the human NTSR1 compared to  $G\alpha_{i3}$ , in line with previous conclusions the receptor is primarily  $G\alpha_q$  coupled (Besserer-Offroy et al., 2017; Kato et al., 2019). Additionally, the pEC<sub>50</sub> values derived and differences observed are in line with the only other study comparing G protein promiscuity at the human NTSR1 using proximal readouts (Besserer-Offroy et al., 2017).

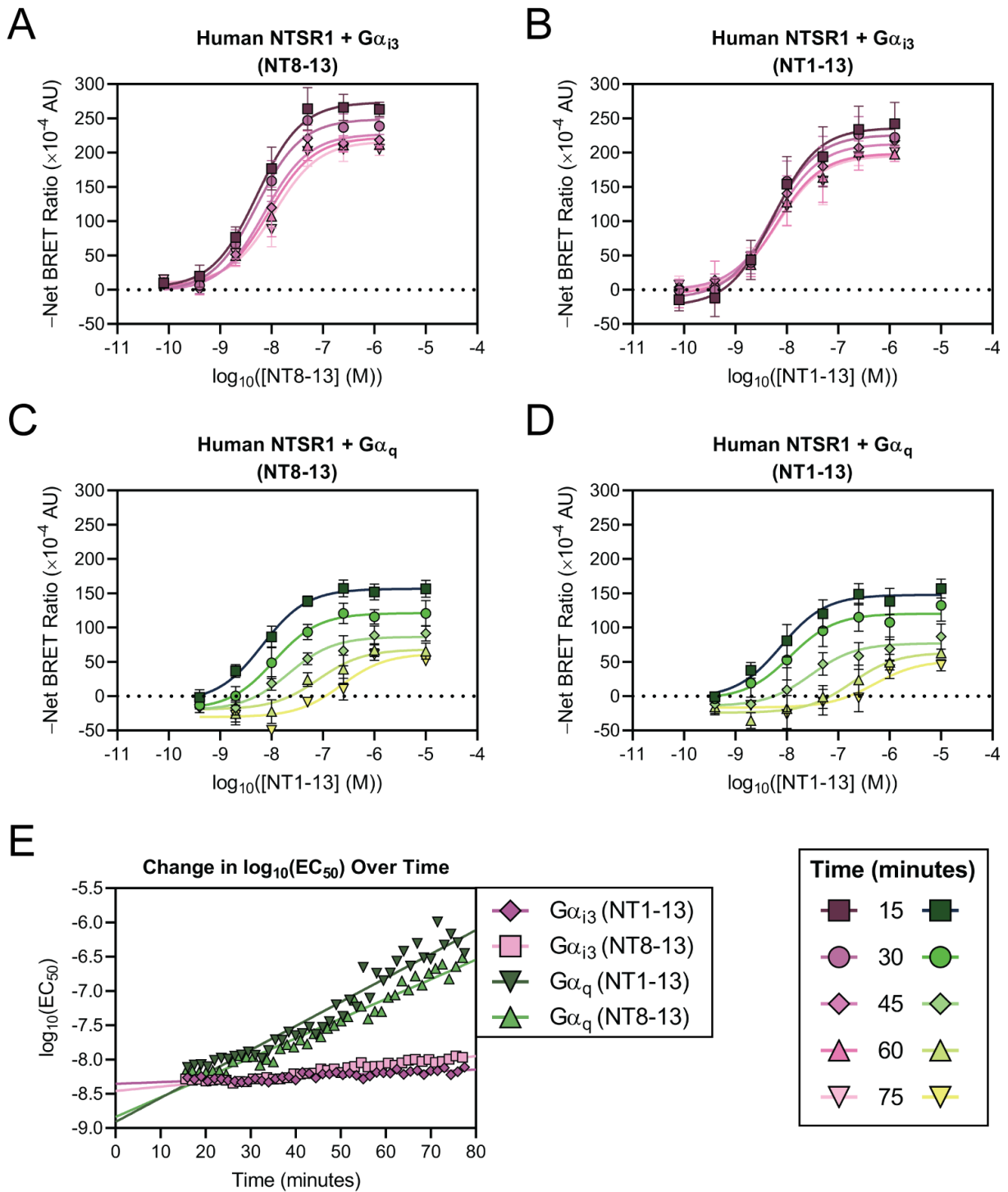


**Figure 8. Human NTSR1 agonists display distinct kinetic signalling profiles in potency and efficacy over time.** Agonist dose-response curves against human NTSR1 at distinct time points for the activation of (A)  $G\alpha_{i3}$  in the presence of NT8-13, (B)  $G\alpha_{i3}$  in the presence of NT1-13, (C)  $G\alpha_q$  in the presence of NT8-13, and (D)  $G\alpha_q$  in the presence of NT1-13. All values are expressed as mean  $\pm$  SEM for three independent experiments conducted in duplicate where duplicates were averaged before calculating SEM. (E) Corresponding change in  $\log_{10}(EC_{50})$  values over time with simple linear regression fits.

Having characterized the functionality of the  $G\alpha_{i3}$  and  $G\alpha_q$  BRET sensors, cells expressing the wildtype rat NTSR1 alongside the BRET sensors were exposed to the same agonists to determine the time-based kinetics of G protein coupling as these have not, to our knowledge, been previously undertaken. All BRET response curves (**Figures 9A/C/E/G**) and associated dose-response curves for NT8-13 and NT1-13 (**Figures 9B/D/F/H**) present striking disparity to their homologous human NTSR1 sibling. The dissociation of G protein after agonist stimulation was rapid for the rat NTSR1, reaching equilibrium within seconds. Such rapid G protein coupling kinetics may imply a pre-coupled rat NTSR1-G protein complex compared to human NTSR1. Additionally, the drop in BRET ratio associated with stimulation does not prolong further after equilibrium is attained, with sharp upturns observed at ~4 minutes in all four cases (**Figures 9A/C/E/G**). These upturns were far more rapid for the  $G\alpha_{i3}$ -based coupling compared to  $G\alpha_q$ -based coupling responses (**Figures 9A/C** compared to **Figures 9E/G**). However, the minimum BRET ratio may not have been reached during activation of the  $G\alpha_{i3}$  response as it occurred too rapidly after manual ligand addition. This was a limitation of the plate reader's injection system lacking capacity. Furthermore, for both  $G\alpha_{i3}$ -based BRET response curves, signaling returned to baseline at or slightly below the baseline within 50 minutes (**Figures 9A/C**). Contradictorily,  $G\alpha_q$ -based response curves surpass the baseline average (**Figures 9E/G**). Additional upturn above the initial baseline measurement may suggest the system returns to a reduced G protein coupled state after ligand activation.

On observing the associated dose-response curves for each agonist-G protein pair (**Figures 9B/D/F/H**), a downward shift in NT8-13 and NT1-13 efficacy was observed in the first 10 minutes of  $G\alpha_{i3}$  activation with no shifts in potency (**Figures 9B/D**). Contrastingly,  $G\alpha_q$  dose-response curves indicated slower downward shifts in efficacy to baseline after ~50 minutes with subtle rightward shifts in potency (**Figures 9F/H**). These changes in potency were reflected in  $\log_{10}(EC_{50})$  values over time as  $G\alpha_{i3}$  activation potencies stagnate over time while decreasing for  $G\alpha_q$  transduction (**Figures 9I**). Linear regression analysis was conducted to capture baseline pEC<sub>50</sub> values for each agonist at the rat NTSR1 (**Table I**). No correlation between potency and time were illustrated for both agonists in mediating  $G\alpha_{i3}$  coupling. In contrast,  $G\alpha_q$  coupling highlighted positive correlations between potency and time (decrease in potency over time). The higher pEC<sub>50</sub> of NT8-13 and NT1-13 during  $G\alpha_q$  transduction illustrates  $G\alpha_q$  is favoured over  $G\alpha_{i3}$  by the rat NTSR1 receptor with these two agonists. Moreover, greater separation in potency between agonists was observed with higher pEC<sub>50</sub> value for NT8-13 compared to NT1-13 in stimulating  $G\alpha_{i3}$  coupling ( $p < 0.0001$ ), while the potency for activating  $G\alpha_q$  responses were indifferent ( $p = 0.6955$ ) (**Figure 9I, Table I**). This may suggest the conformational heterogeneity of the rat NTSR1 is substantially different to human NTSR1, owing to potentially different pre-coupled states.

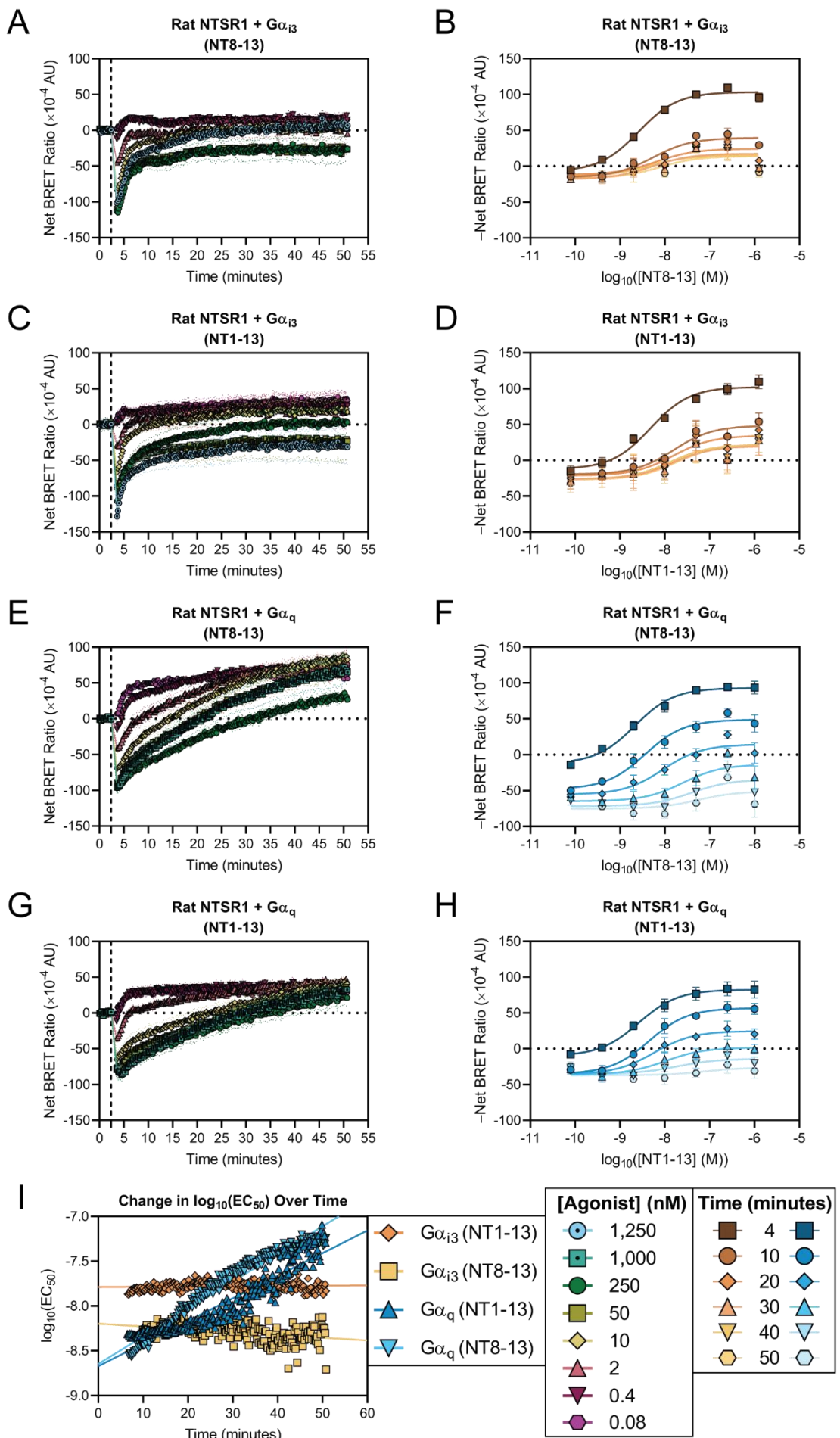


**Figure 9. Rat NTSR1 displays faster alterations in potency and efficacy over time with both  $\text{G}\alpha_{i3}$  and  $\text{G}\alpha_q$  G proteins.** Change in BRET ratio over time in HEK293-F cells expressing rat NTSR1 with the corresponding dose-response curves at distinct time points for the activation of (A, B)  $\text{G}\alpha_{i3}$  in the presence of NT8-13, (C, D)  $\text{G}\alpha_{i3}$  in the presence of NT1-13, (E, F)  $\text{G}\alpha_q$  in the presence of NT8-13, and (G, H)  $\text{G}\alpha_q$  in the presence of NT1-13. The data were baseline corrected against the average of 13 luminescent signal reads (12 second between each; 2 minutes 24 seconds total) prior to the addition of agonist (vertical black dotted lines). All values are expressed as mean  $\pm$  SEM for three independent experiments conducted in duplicate where duplicates were averaged before calculating SEM. (I) Corresponding change in  $\log_{10}(EC_{50})$  values over time with simple linear regression fits.

### 3.2 Determining the G protein coupling capacity of enNTSR1

Moving forward, the goal of measuring G protein kinetics in a purified system was to remove confounding factors, such as endogenous G proteins and altered receptor-G protein stoichiometry. However, this is difficult to conduct with wild-type GPCRs as these are generally low-expressing and unstable when purified. The exemplary control GPCR, enNTSR1, is generally utilized by our laboratory owing to its favorably high expression and stability in bacteria. Yet, its capacity to couple to any G protein family is unknown. Hence, our two BRET sensors were used to determine whether enNTSR1 retained G protein coupling capacity.

After reaching a minimum at ~15 minutes,  $\text{G}\alpha_{i3}$  transduction plateaus when activated with 250 nM or greater NT8-13 while a downward trend in activation is observed at agonist concentrations below this value (**Figure 10A**). The difference in activation at concentrations of NT8-13 below 250 nM may indicate a level of constitutive activity present in enNTSR1. Taking dose-response analyses, it appeared for NT8-13 in the presence of  $\text{G}\alpha_{i3}$  had minimal upward shifts in efficacy and no dramatic change in potency with time (**Figure 10B**). Interestingly, the leftward tail of the dose-response curves shift upwards in concert with time, which is in line with the postulated constitutive activity of the receptor.

For enNTSR1 coupling with  $\text{G}\alpha_q$  (**Figure 10C**), we observed similar changes as  $\text{G}\alpha_{i3}$ , albeit differences at various NT8-13 concentration were difficult to separate due to a subdued magnitude in BRET. However, the similarity in plateaus observed between  $\text{G}\alpha_{i3}$  and  $\text{G}\alpha_q$  suggests alterations in G protein coupling which are far-reaching and not bound to a single family. The corresponding NT8-13 dose-response curves with  $\text{G}\alpha_q$  are also difficult to separate (**Figure 10D**), but general trends suggest similar perturbations in efficacy and potency which were observed for  $\text{G}\alpha_{i3}$ . A time-based analysis of  $\log_{10}(EC_{50})$  values highlight little difference in NT8-13 potency in initiating  $\text{G}\alpha_{i3}$  and

$G\alpha_q$  signal transduction ( $p = 0.0385$ ) (**Figure 10E**). In both cases,  $\log_{10}(EC_{50})$  is positively correlated with time from an almost identical basal pEC<sub>50</sub> (**Table I**). In addition, although previous studies identified binding affinities are not different from rat NTSR1, the lower basal pEC<sub>50</sub> values of enNTSR1 compared to rat NTSR1 suggest either structural changes within the transmembrane domain or intracellular domains alter the magnitude of G protein activation.

Given the cell surface expression of enNTSR1 is greater than the wildtype rat NTSR1 receptor (Bumbak, 2016) and human NTSR1 (**Appendix Figure A2**), reduced G protein signaling (BRET ratio) in enNTSR1 is not due to reduced expression (**Figures 10A/C**). This is likely a cumulative reduction in  $G\alpha_{i3}$  and  $G\alpha_q$  coupling with enNTSR1 due to the array of mutations required to increase expression and thermostability. Additionally, the downward trend in signal after NT8-13 stimulation is slower for both  $G\alpha_{i3}$  and  $G\alpha_q$  at enNTSR1 compared to rat NTSR1 (**Figures 10A/C** compared to **Figures 9A/E**). There are likely conformational aberrations in the transmembrane domain or intracellular G protein contact points of the enNTSR1 structure.

Parallel experiments conducted identified enNTSR1 lacks coupling capacity with  $\beta$ -arrestin compared to rat NTSR1 (**Figure 10F** compared to **Figure 10G**).  $\beta$ -arrestin coupling deficit provides context to the plateaus observed for the net BRET ratio curves, as the signal upturn observed for human and rat NTSR1 were hypothesized to be receptor recycling processes (**Figures 7/9**). The phenotype suggests these G protein BRET sensors have the range to divide both G protein-mediated and membrane-dependent kinetic effects across the temporal landscape of transduction.

Further understanding and optimization of the enNTSR1-G protein interaction is required before such a system can be taken to a cell-free environment. Nonetheless, the clear activation of G proteins by enNTSR1 suggests a promising foundation for using enNTSR1 as a prototypical receptor in purified format G protein-based coupling experiments.

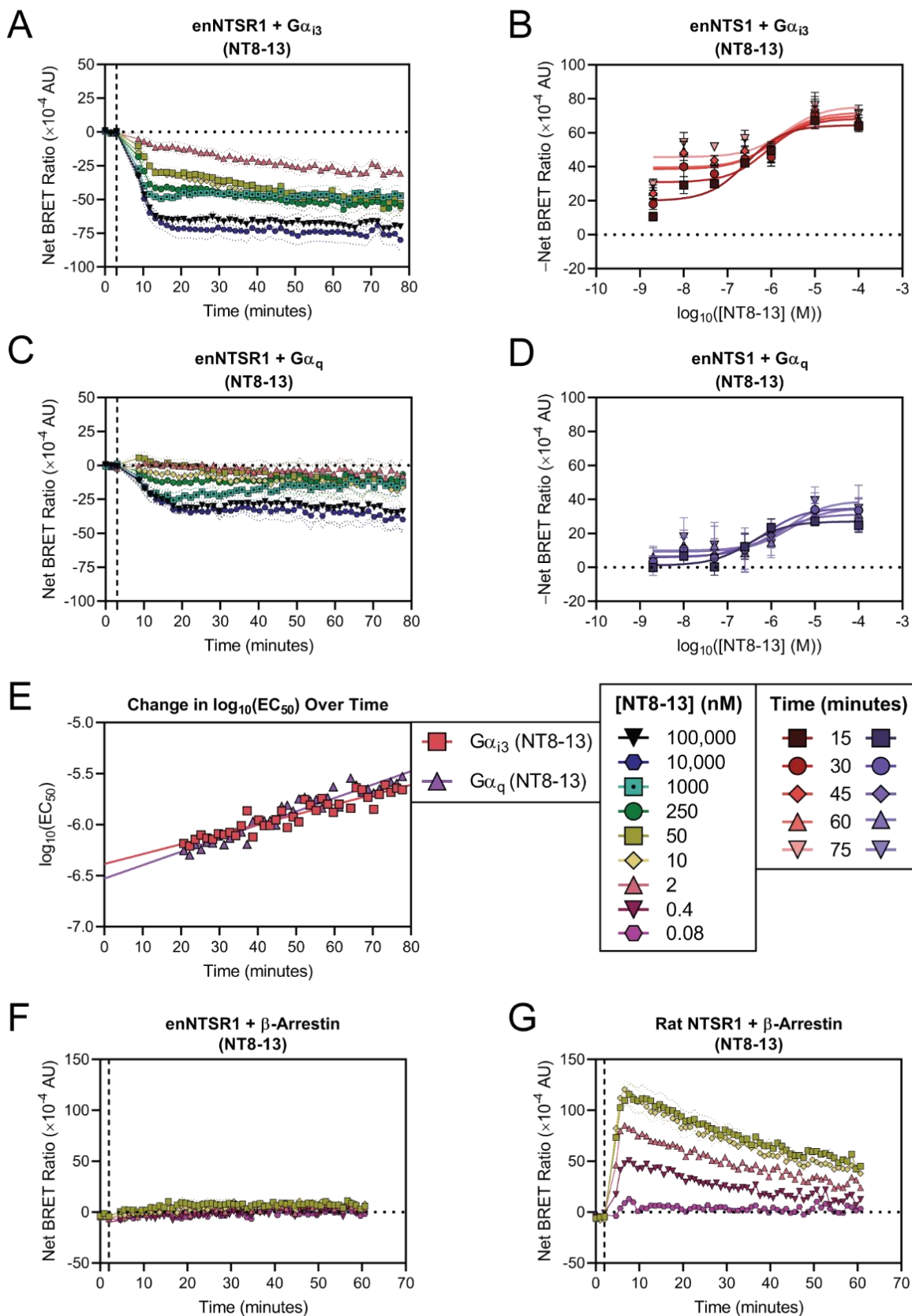


**Figure 10.** A highly expressing, thermostabilised rat NTSR1 mutant, enNTSR1, couples weakly to G $\alpha_{i3}$  and G $\alpha_q$  G proteins. Change in BRET ratio over time in HEK293-F cells expressing enNTSR1 with the corresponding dose-response curves at distinct time points for the activation of

**(A, B)**  $G\alpha_{i3}$  in the presence of NT8-13, and **(C, D)**  $G\alpha_q$  in the presence of NT8-13. The data were baseline corrected against the average of three luminescent signal reads (90 seconds between each; 3 minutes total) prior to the addition of agonist (vertical black dotted lines). Values are expressed as mean  $\pm$  SEM for four independent experiments conducted in duplicate where duplicates were averaged before calculating SEM. **(E)** Corresponding changes in  $\log_{10}(EC_{50})$  values over time with simple linear regression fits.  $\beta$ -arrestin coupling activated by NT8-13 for **(F)** enNTSR1, and **(G)** rat NTSR1. Data for **(F)** and **(G)** kindly provided by Andrew Zhang (Scott Laboratory, Florey). Values are expressed as mean  $\pm$  SEM for three independent experiments conducted in duplicate where duplicates were averaged before calculating SEM.

---

**Table I. Summary of  $pEC_{50} \pm$  SEM values for NT8-13 and NT1-13 in live cell-based BRET assays.**

Agonist	G Protein Subtype	Human NTSR1	Rat NTSR1	enNTSR1
NT8-13	$G\alpha_{i3}$	$8.459 \pm 0.014$	$8.198 \pm 0.017$	$6.385 \pm 0.03$
	$G\alpha_q$	$8.838 \pm 0.048$	$8.648 \pm 0.014$	$6.528 \pm 0.03$
NT1-13	$G\alpha_{i3}$	$8.356 \pm 0.015$	$7.789 \pm 0.008$	—
	$G\alpha_q$	$8.911 \pm 0.073$	$8.672 \pm 0.020$	—

---

### 3.3 Measuring G protein kinetics utilizing membrane preparation-based BRET assays (or pseudo-cell free BRET assays)

In asking whether it was possible to extend BRET assays to a reductionist format, a pseudo-reductionist method utilizing cell-based membrane preparations was employed to study GPCR-G protein kinetics and further analyze G protein-based BRET sensors. In this method, cells expressing either the human or rat NTSR1 and the  $G\alpha_{i3}$  or  $G\alpha_q$  BRET sensor were homogenized into membrane sheets. These GPCR-G protein membrane preparations act as surrogates for a cell-free BRET-based assay as they contain the overexpressed GPCR and G protein of interest, but also house all other cellular membrane components in the absence of detergent. The internal cellular machinery, which may impose restrictions on GPCR-G protein interaction during or after activation, is completely removed. For example, the formation of clathrin-coated pits through  $\beta$ -arrestin mediated internalization should be absent. Additionally, assays benefited from loss of non-specific GPCR-G protein interactions potentially elicited by NT8-13/NT1-13 (**Appendix Figure A3**).

Initially, assay conditions had to be optimized for membrane amounts, ionic concentrations, temperature, and presence of reducing agents. This was undertaken on the human NTSR1-G $\alpha_{i3}$  combination as this receptor depicted a generally greater magnitude in the BRET response compared to rat NTSR1 and the G $\alpha_{i3}$  heterotrimer is functionally more stable than the G $\alpha_q$  subtype. First, the amount of membranes and ionic factors were optimized (**Figure 11A-C**). 10  $\mu$ g membrane homogenates per well was chosen due to a slightly greater magnitude compared to 5  $\mu$ g, necessary for retrieving dose-response curves. Interestingly, GDP concentration had little-to-no effect on signal, however, a correlation between increasing Mg $^{2+}$  concentration and signal blunting was observed. Therefore, lower concentrations of GDP and MgCl<sub>2</sub>, alongside saturating concentrations of 10  $\mu$ M GTP, were selected. Finally, presence of the reducing agent, DTT, has been indicated to potentiate G protein transduction markedly, even in the absence of GDP (Florio & Sternweis, 1989; Hermans et al., 1997). Presence of 1 mM DTT did increase signal magnitude (**Figure 11D**). Additionally, increasing temperature led to reduction in BRET signal (**Figure 11D**). Therefore, 25°C was ideal. Final membrane preparation assay conditions were: 10  $\mu$ g of membrane preparations per assay well, 0.25  $\mu$ M GDP, 10  $\mu$ M GTP, 2 mM MgCl<sub>2</sub>, and 1 mM DTT conducted at 25°C.

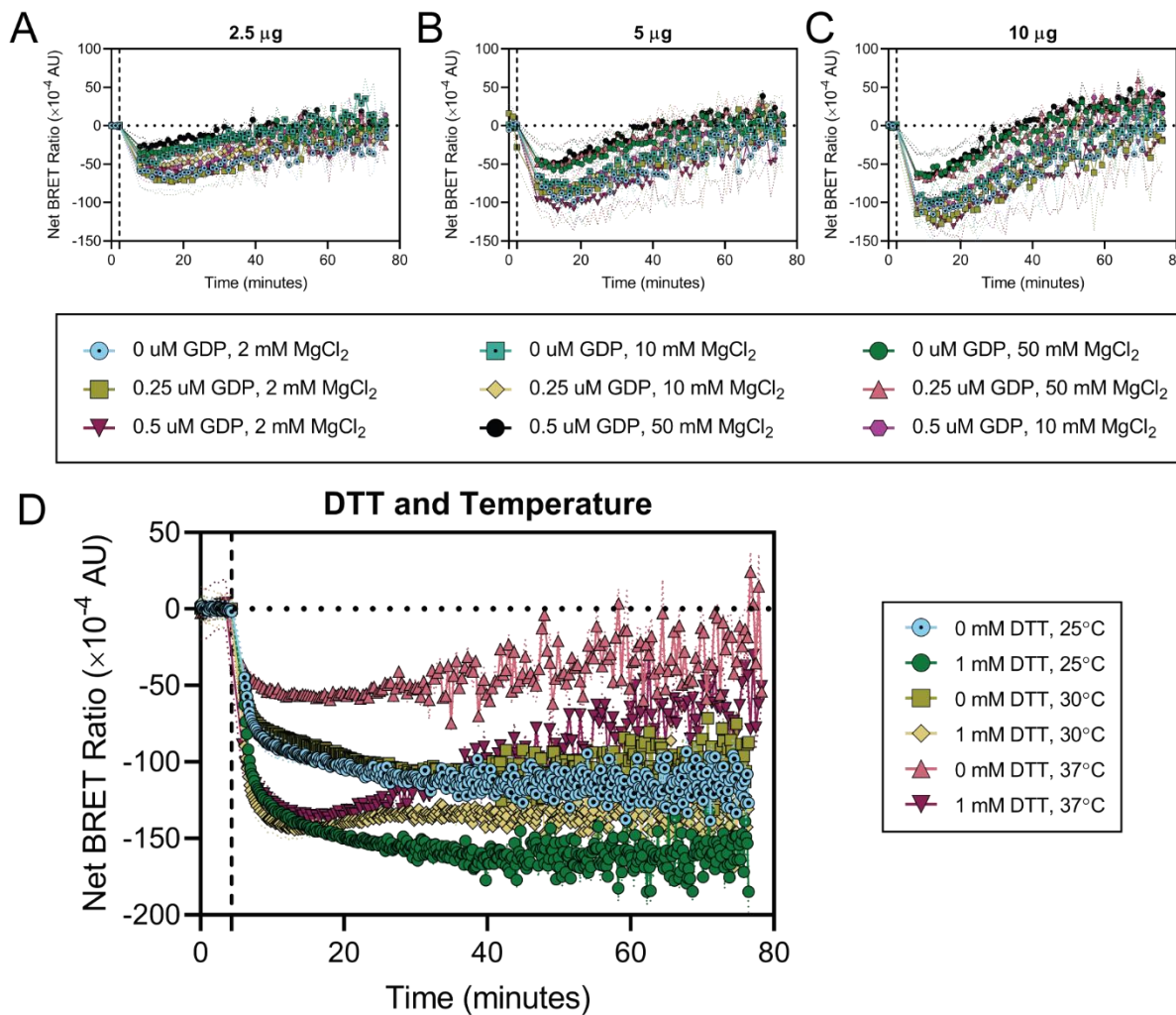


**Figure 11. Optimisation of human NTSR1-G $\alpha$ <sub>i3</sub> membrane preparation-based BRET assays.**

(A) 2.5  $\mu$ g, (B) 5  $\mu$ g, and (C) 10  $\mu$ g of total homogenised membrane preparations were utilised to determine the optimal amount of membrane and ideal ionic conditions to utilise in subsequent BRET assays. Membrane amounts and ionic conditions were optimised in 384-well OptiPlates<sup>TM</sup>. The data were baseline corrected against the average of three luminescent signal reads (67 second between each; 2 minutes 14 seconds total) prior to the addition of 10  $\mu$ M NT8-13 (vertical black dotted lines). (D) Presence of DTT and temperature perturbations were optimised in 96-well OptiPlates<sup>TM</sup> utilising 10  $\mu$ g of membrane preparations, 0.25  $\mu$ M GDP, and 2 mM MgCl<sub>2</sub>. The data were baseline corrected against the average of 27 luminescent signal reads (10 second between each; 4 minutes 20 seconds total) prior to the addition of 10  $\mu$ M NT8-13 (vertical black dotted lines). All values are expressed as mean  $\pm$  SEM (dotted lines) for two independent experiments conducted in triplicate where triplicates were averaged before calculating SEM. Optimisation was only undertaken for  $n = 2$  independent experiments as only general trends were being optimized rather than pharmacological values being acquired.

---

Undoubtedly, the BRET signal curves (**Figures 12A/C/E/G**) and their corresponding dose-response curves (**Figures 12B/D/F/H**) depicted phenotypic, potency, and efficacy modifications compared to whole-cell BRET assay counterparts (**Figures 7-9**). In human NTSR1 expressing G $\alpha$ <sub>i3</sub> membranes, the signal-to-noise fidelity of the ratiometric signal was compromised after ~40 minutes (**Figures 12A/C**). Likely, the decrease in signal-to-noise presents itself as the total amount of G protein BRET sensors within the membrane cannot be controlled. Membrane preparation-based assays are unable to account for receptor:G protein stoichiometries, accounting for a severe limitation in the assay. Ultimately, this led to more rapid nanoluciferase substrate turnover. Hence, in subsequent analyses, the datasets were truncated at 40-minutes.

Notably, with both human and rat NTSR1 receptors, the phenotype of the temporal signalling profile was altered compared to whole-cell counterparts (**Figure 7/9**), with signal response curve magnitudes blunted. G protein equilibrium was reached, although this was sustained. This is identical to the  $\beta$ -arrestin lacking phenotype observed for enNTSR1 (**Figures 10A/C/E**). The loss of internal cellular machinery from the production of cellular homogenates supports the notion the signal upturn observed in live cell BRET assays after the signal minima were re-establishment of the basal GPCR-G protein state due to membrane proximal processes, such as receptor internalization. However, the signal curves for rat NTSR1 did not display previously characteristic G protein activation kinetics (**Figure 9**). This potentially suggests membrane alterations due to homogenization may lead to

changes in receptor conformational heterogeneity, or loss of intracellular machinery which may be necessary in activation kinetics for rat NTSR1- $G\alpha_{i3}$  transduction.

Additionally, as expected, the dose-response curves for human and rat NTSR1 were sustained with minimal alterations in efficacy and potency past the 10-minute equilibrium region (**Figures 12B/D/F/H**). However, comparing dose-response curves for NT8-13 with NT1-13 highlights for both receptor-G protein pairs, there is greater separation in potency between both agonists (**Figures 12B/F** compared to **Figures 12D/H**). Hence, NT-13 appears to be less potent than NT8-13.

Profiles for the time-dependent change in  $\log_{10}(EC_{50})$  were analysed between 10-to-40 minutes (**Figure 12I**). Slight downward trends in  $\log_{10}(EC_{50})$  and time for both agonists were observed. In contrast to live cell BRET-based assays, the pEC<sub>50</sub> values were greater for NT8-13 compared to NT-13 with both human and rat NTSR1 (**Table II**), highlighting, in a pseudo-reductionist format, NT8-13 has greater potency than NT1-13 to initiate a  $G\alpha_{i3}$ -based response ( $p < 0.0001$ ). Reduced NT1-13 potency may be a consequence of the experimental conditions derived for the assay, although it is difficult to draw specific conclusions.

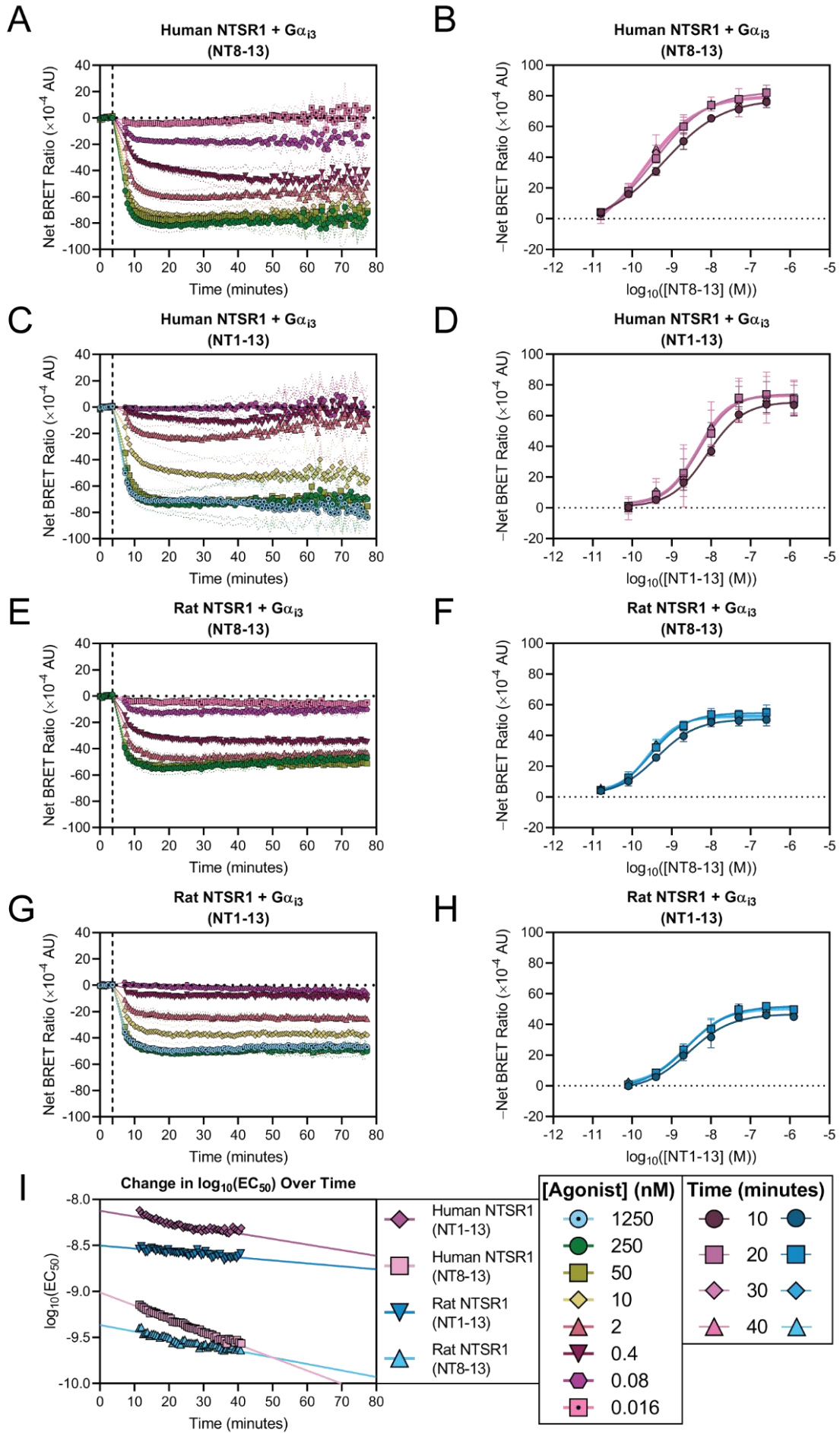


**Figure 12. BRET assays conducted using membrane preparations allow for further disentanglement of specific  $G\alpha_{i3}$ -based coupling interactions in human and rat NTSR1 subtypes.** Change in BRET ratio over time in membrane preparations containing overexpressed human NTSR1 with the corresponding dose-response curves at distinct time points for the activation of (A, B)  $G\alpha_{i3}$  in the presence of NT8-13, and (C, D)  $G\alpha_{i3}$  in the presence of NT1-13. Change in BRET ratio over time in membrane preparations containing overexpressed rat NTSR1 with the corresponding dose-response curves at distinct time points for the activation of (E, F)  $G\alpha_{i3}$  in the presence of NT8-13, and (G, H)  $G\alpha_{i3}$  in the presence of NT1-13. The data were baseline corrected against the average of seven luminescent signal reads (36 second between each; 3 minutes 36 seconds total) prior to the addition of agonist (vertical black dotted lines). Values are expressed as mean  $\pm$  SEM for three independent experiments conducted in triplicate where quadruplicates were averaged before calculating SEM. (I) Corresponding change in  $\log_{10}(EC_{50})$  values over time with simple linear regression fits.

---

Comparatively, membrane preparation-based BRET assays for both rat and human NTSR1 with our  $G\alpha_q$  biosensor was futile (**Figure 13**). Under  $G\alpha_{i3}$  membrane preparation conditions, no BRET response or dose-response separation was observed. Both nanoluciferase and Venus luminescence were approximately equal to the  $G\alpha_{i3}$ -based assays. Furthermore, the  $G\alpha_i$  family of G proteins is likely more receptive to different ionic conditions compared to  $G\alpha_q$ . This highlights optimization for each G protein must be scrutinized and is required for each receptor-G protein combination in any cell-free assay. Additionally, GPCR- $G\alpha_q$  coupling interactions are notoriously difficult to work with outside of a cellular environment, with all GPCR- $G\alpha_q$  structures published being those utilizing hybrid chimeric  $G\alpha_q$  and  $G\alpha_s$  proteins called mini- $G\alpha_q$  proteins (Nehmé et al., 2017). Due to time constraints, optimization of membrane preparation assay conditions for the  $G\alpha_q$ -based BRET biosensor was not conducted. These optimization conditions may need to consider ionic concentration ratios and potential inclusion of chaperones, such as RIC8A (Nishimura et al., 2006), or other unknown stabilizing factors.

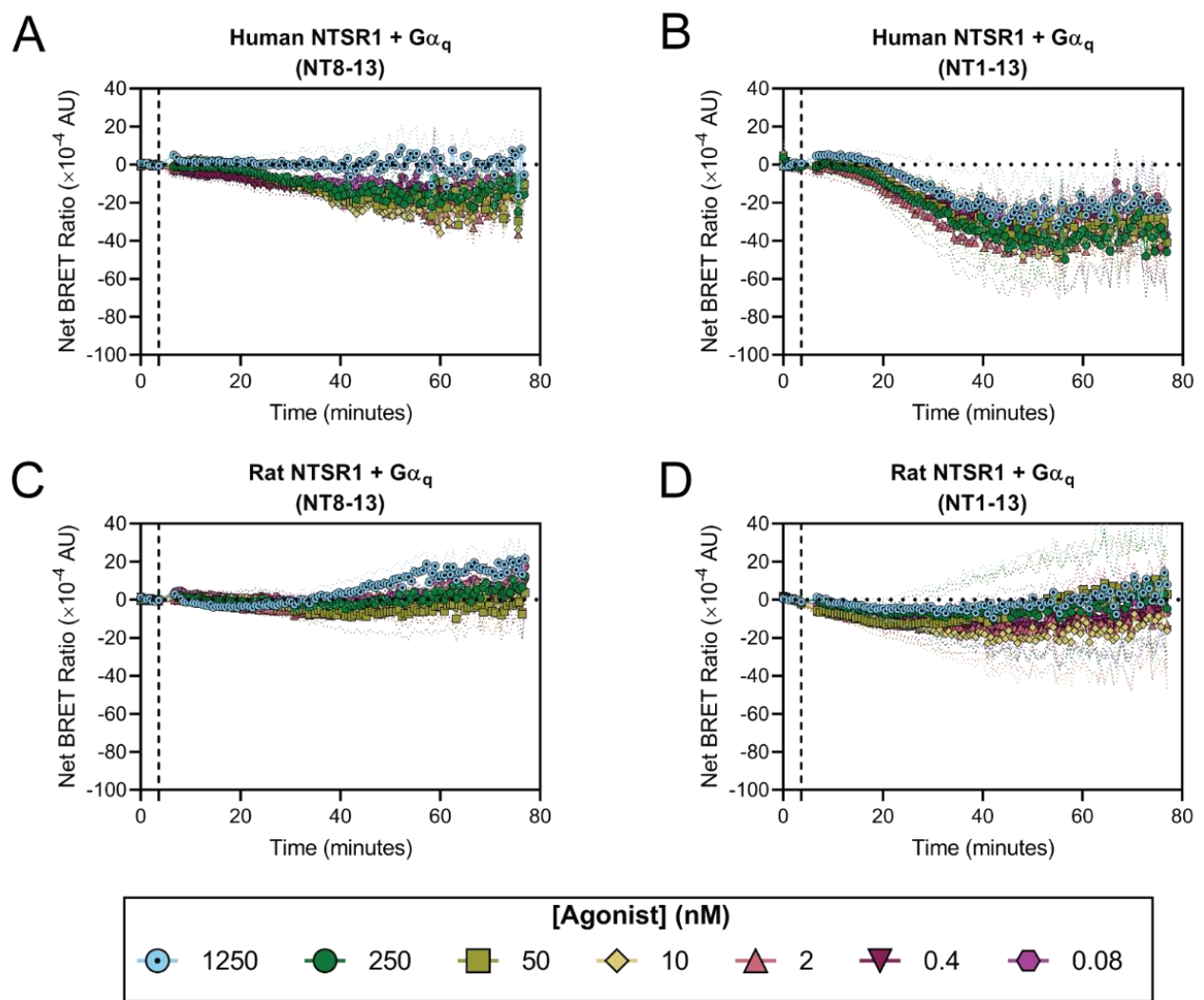


**Figure 13. NTSR1 subtype coupling with  $G\alpha_q$  is potentially challenged by locally different coupling conditions such as GDP and  $MgCl_2$  concentrations.** Change in BRET ratio over time in membrane preparations containing overexpressed human NTSR1 for the activation of (A)  $G\alpha_q$  in the presence of NT8-13, and (B)  $G\alpha_q$  in the presence of NT1-13. Change in BRET ratio over time in membrane preparations containing overexpressed rat NTSR1 for the activation of (C)  $G\alpha_q$  in the presence of NT8-13, and (D)  $G\alpha_q$  in the presence of NT1-13. The data were baseline corrected against the average of seven luminescent signal reads (36 second between each; 3 minutes 36 seconds total) prior to the addition of agonist (vertical black dotted lines). Values are expressed as mean  $\pm$  SEM (dotted lines) for three independent experiments conducted in triplicate where triplicates were averaged before calculating SEM.

**Table II. Summary of pEC<sub>50</sub> ± SEM values for NT8-13 and NT1-13 in membrane preparation-based BRET assays.**

Agonist	G Protein Subtype	Human NTSR1	Rat NTSR1	enNTSR1
NT8-13	G $\alpha_{i3}$	9.011 ± 0.007	9.365 ± 0.010	—
	G $\alpha_q$	—	—	—
NT1-13	G $\alpha_{i3}$	8.125 ± 0.013	8.502 ± 0.009	—
	G $\alpha_q$	—	—	—

### 3.4 Determining purification potential and catalytic functionality of heterotrimeric G $\alpha$ BRET sensors

Having shown the wide-ranging capability of these G $\alpha_{i3}$ - and G $\alpha_q$ -based BRET biosensors as kinetic exploratory tools in discerning the G protein-based signaling features between the three homologous NTSR1. The capability to purify our G protein biosensors needed to be determined. The G $\alpha_{i3}$  BRET biosensor was selected to be an example for building up such a methodology due to its ease of working with compared to G $\alpha_q$ .

First, we needed to assess the ideal overexpression method of the G $\alpha_{i3}$  BRET biosensor in mammalian HEK293-F cells. Although both lentiviral transduction and stable expression are forms of overexpression, transduction is transient while stable production is long-lasting. The G $\alpha_{i3}$ -nanoluciferase subunit is largely nonexistent in stable cells while overexpressed after short-term transduction (**Figure 14A**) Contrastingly, G $\beta$  subunit expression (and by inference G $\gamma$ ) was unrestricted in cells stably expressing the biosensor heterotrimer and cells transiently expressing the biosensor after 72 hours (**Figure 14B**). This suggests G $\beta$  overexpression has minimal-to-no effects on cell health. These two findings indicate the G $\alpha_{i3}$  subunit exhibits a cytotoxic pressure when overexpressed in mammalian cells over the long-term and is selectively suppressed over time compared to the G $\beta$  subunit (**Figure 14C**). Therefore, production of heterotrimeric G proteins in mammalian HEK293-F cells was advanced using the lentiviral transduction method of expression.

Subsequently, the timepoint post-transduction yielding the highest total amount of G protein subunits was determined. The expression of both the G $\alpha_{i3}$  and G $\beta$  subunits plateaued at 72-to-96 hours post-transduction (**Figure 14D/E, Appendix Figure A4**). Hence, the 72-hour timepoint was employed to ensure overexpression of the G $\alpha_{i3}$  BRET biosensor had the least burden on cell health which could detrimentally change yield with each expression batch.

Finally, the optimization process was coalesced to purify the  $G\alpha_{i3}$  BRET sensor in bulk (**Figure 14F-H**). Although the purification process was not completely rid of impurities after elution (**Appendix Figure A5**), it managed to successfully capture a large degree of the  $G\alpha_{i3}$  BRET sensor in its heterotrimeric state. Several non-specific bands were observed in immunoblots (**Figures 14G/H**), however, the identity of the proteins of interest were controlled for throughout prior optimization steps. The majority of nanoluciferase-tagged  $G\alpha_{i3}$  subunits were successfully rescued during purification (**Figure 14G, comparing lane 4 to 5**). The remaining nanoluciferase-tagged  $G\alpha_{i3}$  subunits likely never bound to the chromatography resin due to association with endogenous  $G\gamma$  subunits. Moreover, minimal endogenous wildtype  $G\beta$  subunits contaminated the heterotrimeric state of the  $G\alpha_{i3}$  BRET sensor (**Figure 14H, Lane 7**). Ultimately, although impure, polyhistidine purification of the  $G\alpha_{i3}$  BRET sensor was successful.

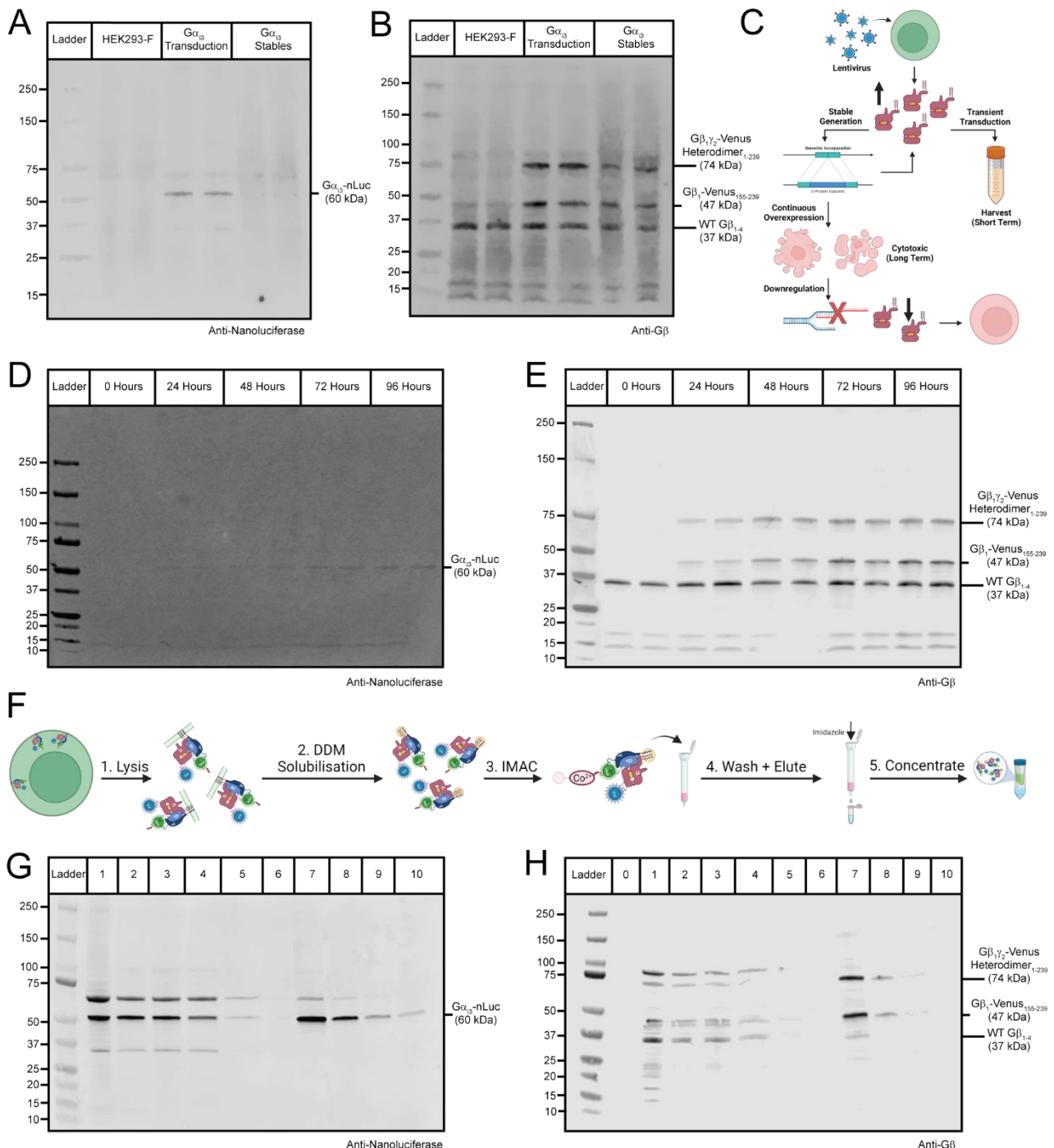


**Figure 14. Optimisation and purification of a 6x-Histidine tagged G $\alpha_i_3$  BRET sensor expressed in HEK293-F mammalian cells.** (A, B) Immunoblot comparison of total G $\alpha_i_3$  BRET biosensor production efficiency when HEK293-F cells were either transduced with lentivirus packaged with biosensor RNA or stably expressing the biosensor. (C) Summary schematic of the differences in lentiviral transduction of the G $\alpha_i_3$  BRET-based biosensor leading to either the generation of stable cell lines or immediate harvesting of cells at the peak expression time. (D, E) Immunoblot time course of production of HEK293-F cells transduced with lentivirus packaged with the G $\alpha_i_3$  biosensor RNA. A, B, D, and E were conducted in duplicate from starter cultures of 2 million cells in 2 mL of culture

media lysed in 250  $\mu$ L of lysis buffer. **(F)** Schematic representation of the purification process of the  $G\alpha_{i3}$  BRET sensor. **(G, H)** Purification of the 6X-Histidine tagged  $G\alpha_{i3}$  BRET sensor from an 80 mL starter culture. A, D, and G are immunoblotted with a nanoluciferase antibody while B, E, and H are immunoblotted with a  $G\beta$  antibody. Lanes correspond to (total volumes samples were taken from in brackets): 0, SDS-PAGE ladder lane; 1, Cell lysate (25 mL); 2, Post-solubilisation (50 mL); 3, Post-centrifugation solubilisation supernatant (50 mL); 4, Unbound protein flow through (50 mL); 5, Wash 1 (15 mL); 6, Wash 2 (15 mL); 7, Elution 1 (2 mL); 8, Elution 2 (2 mL); 9, Elution 3 (2 mL); 10, Elution 4 (2 mL). Ladder markers are in kDa. All blots are representative of at least three independent experiments.

---

Having successfully purified the  $G\alpha_{i3}$  BRET biosensor heterotrimer, we wanted to assess whether the heterotrimer was still functionally capable of turning over GTP. Assessing GTP hydrolysis as a measure of the  $G\alpha_{i3}$  subunits activity outside of a cell, a  $G\alpha_{i3}$ -dependent decrease in GTP was observed (**Figure 15A**). This aided as a proxy for heterotrimer capacity to dissociate allowing it to be used in its purified state. The purified  $G\alpha_{i3}$  BRET sensor had a corresponding  $\log_{10}(EC_{50})$  of  $3.076 \pm 0.194$  (an approximate EC<sub>50</sub> value of 1,191 ng). This follows the overall trend and EC<sub>50</sub> values which have been observed for purified wildtype  $G\alpha_i$  (Mondal et al., 2015), although the specific subtype was not mentioned which may not account for differences in GTP hydrolysis rates between G protein subtypes (Fields & Casey, 1997). Moreover, the increased GTP turnover of the  $G\alpha_{i3}$  BRET sensor was not due to background GTPase purification. Overall, increasing GTP hydrolysis correlated with increasing GTPase concentration. Furthermore, nanoluciferase luminesced in the presence of substrate (**Figure 15B**) and Venus was functional through concentration determination using fluorescence detection. Ultimately, purification of a G protein BRET-based biosensor did not hinder its capacity to function, necessary for a purified-state cell-free GPCR-G protein BRET assay.

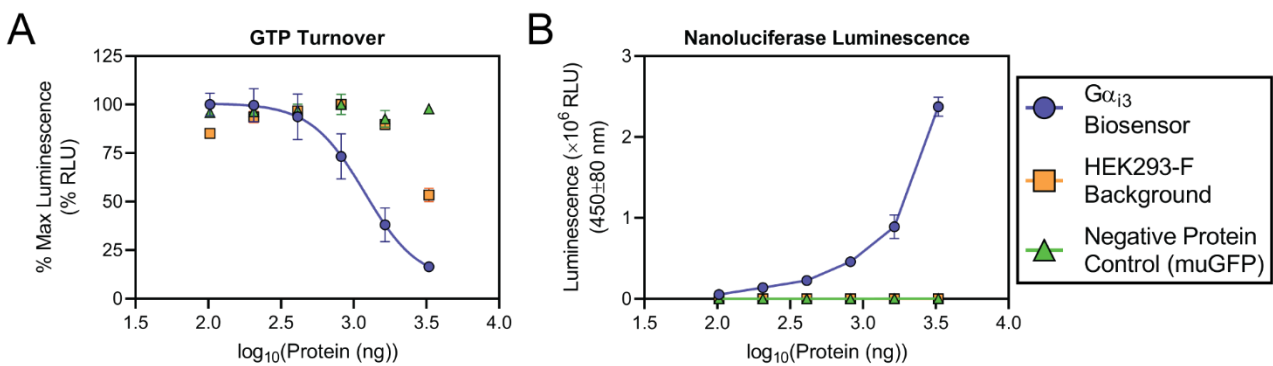


**Figure 15. Purified  $\text{G}\alpha_{i3}$  BRET-based biosensors are both catalytically and functionally active in a cell-free environment.** (A) GTP turnover to assess the catalytic activity of the  $\text{G}\alpha$  GTPase domain. Conducted in the presence of  $\text{G}\alpha_{i3}$ -based BRET sensor, background HEK293-F proteins, and a negative control protein (muGFP) (kindly provided by Lisa Williams, Scott Laboratory, Florey). (B) Enzymatic activity of the nanoluciferase fused to the  $\text{G}\alpha$  subunit through nanoluciferase luminescence of the three samples in the presence of 1X Nano-Glo® Luciferase Assay Substrate (Furimazine). Values are expressed as mean  $\pm$  SEM for three independent experiments conducted in quadruplicate where quadruplicates were averaged before calculating SEM.

To develop a pharmacological reductionist format assay, purification of a receptor was necessary. Both enNTSR1 and rat NTSR1 were purified from bacterial and mammalian cultures (**Figure 16**), respectively, as these were prototypical GPCRs available for purification. muGFP-tagged enNTSR1 was present at lower than the expected molecular weight of  $\sim 117 \text{ kDa}$  (**Figure 16B**), however, this has been observed before (Bumbak et al., 2018). The identity of muGFP-enNTSR1 was confirmed by in-gel fluorescence which identified the presence of the high molecular weight fusion complex (**Figure 16C**). Contrastingly, rat NTSR1 purified out of mammalian cells (**Figure 16D**) was not present in adequate yields in the elution fractions to be observed in-gel (**Figure 16E**). An ALFA-tag immunoblot confirmed presence of rat NTSR1 in what is likely heterogeneous glycosylated isoforms (**Figure 16F**), however, glycosidases were unavailable to confirm this. Elution fractions were substantially purer in the rat NTSR1 samples compared to the enNTSR1 samples due to the presence of the ALFA epitope (**Figure 16E** compared to **Figure 16B**). Approximate total protein yield was 8.5 mg from enNTSR1 purification compared to 5  $\mu\text{g}$  from purification of wild-type rat NTSR1. The markedly reduced yield and high cost in purifying rat NTSR1 indicated selective mutations must be introduced to increase expression with little alteration to ligand binding and G protein kinetics to continue methods development.

Finally, attempts were made to measure GTP turnover by the  $G\alpha_{i3}$  BRET sensor in the presence of enNTSR1 (**Appendix Figure A6**). Methods were adapted from a previous study accounting for GTP turnover in the presence of human NTSR1 with altered lipid charge (Strohman et al., 2019). No significant difference in mean GTP turnover was observed in the presence of enNTSR1 reconstituted in either palmitoyloleoyl phosphatidylcholine (POPC, neutral charge) or palmitoyloleoyl phosphatidylglycerol (POPG, negative charge) compared to sensor alone. Further work is necessary to reconstitute the enNTSR1-G protein signalling complex.

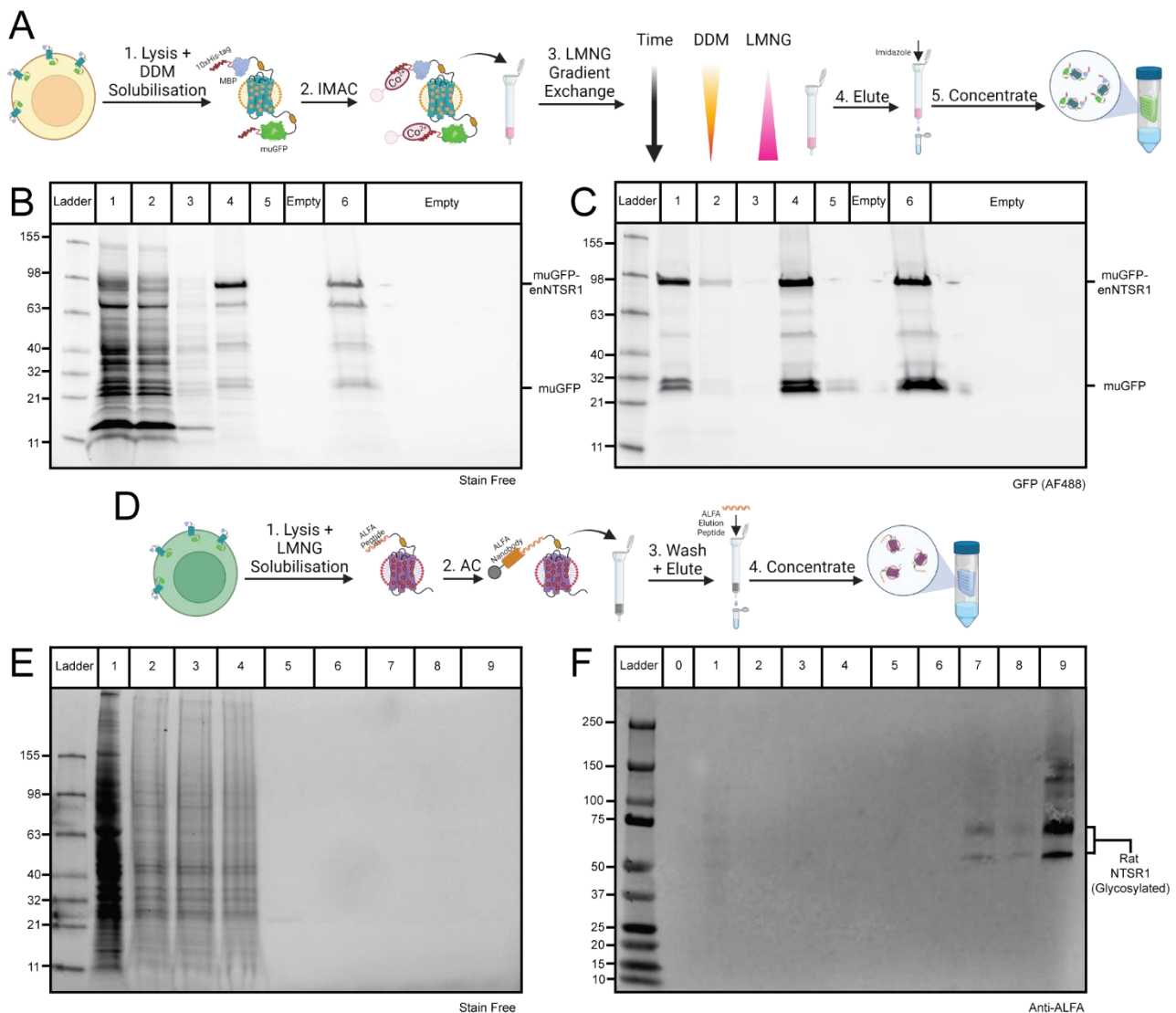


**Figure 16. Purification of enNTSR1 and parental receptor, rat NTSR1. (A)** Summary schematic representation of the enNTSR1 purification workflow. **(B, C)** Samples from purification of enNTSR1 from a 3 L C43 (DE3) bacterial cell culture. Images kindly provided by Eddy Yang (Scott Laboratory, Florey). enNTSR1 stain-free gel images lanes correspond to (total volumes samples were taken from in brackets): 1, Post-solubilisation (70 mL); 2, Unbound protein flow through (70 mL); 3, Washes (200 mL); 4, Elutions (20 mL); 5, Concentrator flow through (19.5 mL); 6, Concentrated elution's

(500  $\mu$ L). **(D)** Summary schematic representation of the wild-type rat NTSR1 purification workflow. **(E, F)** Samples from purification of rat NTSR1 from a 700 mL HEK293-F mammalian cell culture. Rat NTSR1 purification stain-free gel and immunoblot image lanes correspond to (total volumes samples were taken from in brackets): 0, SDS gel ladder lane; 1, Cell lysate (100 mL); 2, Post-solubilisation of membrane pellet (200 mL); 3, Post-centrifugation solubilisation supernatant (200 mL); 4, Unbound protein flow through (200 mL); 5, Wash 1 (50 mL); 6, Wash 2 (50 mL); 7, Elution 1 (500  $\mu$ L); 8, Elution 3 (500  $\mu$ L); 9, Concentrated Elution's 1-4 (200  $\mu$ L). All ladder markers are in kDa.

---

## Chapter 4: Discussion

GPCR research has been confounded by the mysteries surrounding G protein activation. Structural insights have given snapshots of GPCR-G protein interaction while cell-based assays can confound interpretation due to the presence of endogenous molecules. The present study sought to characterize two novel G protein biosensors to unravel granular details of GPCR activation and G protein transduction in a proximal setting. The specialty of these sensors is they can be purified to be used in a reductionist system. The well-defined prototypical receptor system, NTSR1, was selected as tools to study these biosensors as these GPCRs show pleiotropic characteristics with  $G\alpha_{i3}$  and  $G\alpha_q$ . The array of tools available for NTSR1 receptors allowed for broad characterization of the delicate difference in promiscuity at a temporal level for three homologous NTSR1 receptors. Moreover, selectively targeting GPCRs has been a herculean effort. Identifying drugs for market-approval has been challenging, owing to the biochemically difficult nature of studying GPCRs. Stabilised GPCRs, such as enNTSR1, can overcome inherent bottlenecks of studying GPCRs in purified states. Despite the disease-relevance of NTSR1, no biased drugs are available on the market. We sought to begin developing a foundation for a reductionist format GPCR-G protein assay for compound screening. By utilizing both live cell and membrane preparation-based BRET assays, we have generated data that provides a stepping-stone for future use of these tools in a purified format.

### 4.1 Real-time G protein BRET sensors allow kinetic and temporal monitoring of receptor-G protein interaction during the G protein activation cycle.

Agonist-induced kinetic and temporal changes were investigated by monitoring GPCR-G protein signalling events through more proximal readouts at the receptor interface. Using more proximal readouts of GPCR activation allows for direct interrogation of the kinetic behavior of receptors, such as NTSR1, over time, rather than distal outputs prone to crosstalk and artefacts.

Prior studies have investigated the specific efficacy and potency of NT8-13 and NT1-13 for activating human NTSR1 and initiating G protein coupling utilizing BRET-based G protein biosensors (Besserer-Offroy et al., 2017). However, this study, and many other similar GPCR-G protein coupling studies using BRET-based biosensors, have been conducted by transfecting individual G protein subunits. This can substantially affect replicability between experiments and alter efficacy/potency readouts for ligands. Importantly, the study utilized a single time-point (10 minutes after ligand addition) for determining dose-response outputs, belittling the power of a kinetic time-based readout provided by BRET-based biosensors. This arbitrary assignment of a single time-point to investigate dose-response does not consider the population-based nature of the BRET assay. The timeframe of the BRET assay needs to be taken into consideration, as variation will be invoked

by distinct GPCR and G protein combinations. Traditional endpoint assays do not consider the temporal kinetics involved in the biological process of signal transduction which ultimately leads to misjudgment in ligand efficacy and potency values.

Indeed, when investigating the change in pEC<sub>50</sub> over time in live cells for NT8-13 and NT1-13 activation of human NTSR1, rat NTSR1, and enNTSR1 (**Figures 8E/9I/10E**), data points before G protein equilibration were excluded as perturbations in G protein coupling still occurred. This owes to the fact G protein-based BRET assays are a population-based assay, containing subsets of both heterotrimeric and completely dissociated G proteins. Agonism directs the receptor conformations towards the active state, thereby resulting in a greater population of dissociated subunits compared to the baseline. At some timepoint the active and inactive populations of G protein reach an equilibrium. That is, during activation of G proteins the BRET response is quite volatile to small perturbations as the set of receptors bound to agonist have yet to allow the G protein population to reach the hypothetical equilibrium. However, the factors resulting in the upturn of the BRET ratio response back towards the baseline state are harder to define.

For instance, when observing alterations in G $\alpha_q$  coupling kinetics with human NTSR1, a notably rapid shift in efficacy and potency was observed (**Figure 8C/D**). This may be from a combination of desensitization of the receptor, G $\alpha_q$  instability, and switch in G protein signalling. The latter is of more intrigue as NT1-13-induced human NTSR1-G $\alpha_q$  signaling stimulates the inositol phosphate signaling cascade and therefore intracellular calcium release. This can lead to calcium-dependent increase in cAMP levels (Carraway & Mitra, 1998). Mechanistically, as G $\alpha_i$  activation negatively regulates cAMP, the active receptor may divert towards G $\alpha_i$  signalling. Pertussis toxin, a selective inhibitor of G $\alpha_{i/o}$  (Locht et al., 2011), could be employed to confirm the potential role of G protein signalling over time. Furthermore, endogenous G protein knockout cells could be harnessed to determine whether the shift in efficacy and potency for G $\alpha_q$  is retained.

Rapid activation of rat compared to human NTSR1 reveals variations in response to NT8-13 and NT1-13 between NTSR1 homologues at a temporal level. The difference in rapid activation of the G $\alpha_{i3}$  and G $\alpha_q$  G protein signalling pathways by the rat compared to human NTSR1 in whole-cells may suggest evidence for a functional pre-coupled complex of the rat NTSR1 with heterotrimeric G proteins. In this paradigm, the inactive GDP-bound G protein heterotrimer may interact with the receptor resulting in a stabilized pre-coupled complex (Mafi Amirhossein et al., 2022). It remains in a resting complex which can be rapidly activated in the presence of a ligand. Whether pre-coupled complexing between receptor and G protein occurs or whether diffusive mechanisms direct coupling after agonist exposure is still debated. For example, biochemical

evidence suggest the  $\alpha$ 2-adrenoreceptor pre-couples with heterotrimeric  $G\alpha_{i/o}$  (Galés et al., 2006; Nobles Muriel et al., 2005), however, others contest it does not occur through RET-based and fluorescence recovery after photobleaching assays (Hein et al., 2005; Qin et al., 2008). Hence, an exact mechanism of pre-coupled activation has only been proposed *in silico* and not observed mechanistically *in vitro* (Mafi Amirhossein et al., 2022). To test this hypothesis, alternative BRET-based methods could be utilized by fusing a nanoluciferase to the receptor and Venus protein to the G proteins of interest (Ayoub et al., 2007). It would be expected a level of basal Venus luminescence would be observed in the rat NTSR1 compared to the human NTSR1 if pre-coupling occurs. Additionally, the swing in conformational heterogeneity of pre-coupled rat NTSR1 may be populated towards an active state at basal equilibrium. The agonist may be more rapidly stabilized by the presence of pre-bound G protein due to positive cooperativity between these two components (DeVree et al., 2016). However, as the receptor was not found in its endogenous environment, whether other factors, such as unknown membrane-associated proteins, within human cells are responsible for this difference is unknown.

A downfall in utilizing G protein BRET sensors to comparatively measure differences in efficacy is the lack of controls to compare between G protein subtypes. Unfortunately, we were unable to determine appropriate controls. To our knowledge, there is no intrinsic control for comparing efficacies of unbiased compounds in activating different G protein subtypes. The broad consensus has been to utilize the maximal response induced by reference agonists for normalization (Kenakin et al., 2012; Klein Herenbrink et al., 2016; Olsen et al., 2020). This would imply every one of these control agonists is shifting the conformational equilibrium to equally favor all its potential G protein partners. However, this misrepresents receptor conformational selection by ligands. Studies are unable to normalize across different subtypes, for example, responses between  $G\alpha_{i3}$  and  $G\alpha_q$  subtypes presented in this study. Although not a confounding source of variability in determining potency values, more nuanced comparisons between  $G\alpha_{i3}$  and  $G\alpha_q$  bias and differential coupling of subtypes are unable to be adequately addressed. A potential method for controlling differences in G protein subtypes could be to utilize membrane preparation-based assays. Hypothetically, a saturating concentration of the non-hydrolysable analogue of GTP, GTP $\gamma$ S, could be fed into the system to activate G protein signalling in an agonist-independent manner. The maximal change in luminescence could be utilized as a normalization control. Ultimately, consideration of advantages and disadvantages in sensor variants during design of experiments will be necessary to prevent confounding findings.

#### **4.2 enNTSR1 has G protein coupling functionality but is an impaired variant of rat NTSR1**

Analyses of enNTSR1 highlighted G protein biosensors could emphasize the influence of membrane-associated perturbations, such as the loss of  $\beta$ -arrestin interaction (**Figure 10F/G**). Interestingly, potency values were almost identical for NT8-13 when activating  $G\alpha_q$  and  $G\alpha_{i3}$  G protein pathways (**Figure 10E, Table I**). As potency values were almost identical and as the binding affinity of NT8-13 is not significantly different to rat NTSR1 (Bumbak et al., 2018), the active receptor conformation may be altered to favour all G protein interactions similarly. As similar analyses for  $G\alpha_s$  and  $G\alpha_{12/13}$  were not conducted, it is difficult to determine whether this quirk in enNTSR1 signaling generalizes to all G protein families. Studies have demonstrated rat NTSR1 signals through  $G\alpha_s$  subtypes (Skrzydelski et al., 2003; Yamada et al., 1993), while no line of evidence for  $G\alpha_{12/13}$  signalling exists in rat NTSR1, although inference of signaling in human NTSR1 suggests the latter is highly likely for rat NTSR1 (Besserer-Offroy et al., 2017). It is speculated enNTSR1 signals through  $G\alpha_s$  and  $G\alpha_{12/13}$ .

As enNTSR1 contains multiple amino acid mutations, and N- and C-terminal truncation, it is difficult to identify which variations result in the differential binding of G proteins and the loss of  $\beta$ -arrestin mediated internalization (**Figures 10A/C/F/G**). For the latter, it is possible the six amino acid truncations in the C-terminal tail play a notable role in the loss of  $\beta$ -arrestin interaction (**Figure 6**). It has been hypothesized GPCR phosphorylation by GPCR receptor kinases (GRKs) is important for  $\beta$ -arrestin coupling resulting in the foundation of the “barcode” hypothesis (Gurevich & Gurevich, 2019; Huang et al., 2020; Matthees et al., 2021). The loss of Thr419 could be one factor leading to the loss in  $\beta$ -arrestin coupling, although additional mutagenesis-based experiments of the wild-type rat NTSR1 would need to be conducted to support this. It would also be interesting to see whether back-mutation of enNTSR1 at these potentially critical residues can rescue  $\beta$ -arrestin coupling or increase signaling capacity through  $G\alpha_{i3}$  and  $G\alpha_q$ . The conformational heterogeneity of enNTSR1 is likely affected by the mutations, as noted by the differential levels of G protein coupling compared to rat NTSR1. Hence, alterations in structural conformation are likely key driving factor in both the change in G protein and non-G protein ( $\beta$ -arrestin) coupling. Further studies aimed at understanding the nature of enNTSR1-G protein and  $\beta$ -arrestin promiscuity, as well as the basis for overexpression, would prove fruitful in not only how alterations in receptor amino acids manifest and relate these properties, but in also developing a better basis for the interconnectedness of G protein and non-G protein coupling.

#### **4.3 Membrane preparation-based BRET assays further distinguish temporal and pharmacological differences in receptor-G protein interaction**

Membrane preparations containing our G protein BRET sensors were harnessed as a pseudo-reductionist format assay. Interestingly,  $G\alpha_{i3}$  receptor responses with human and rat NTSR1 (**Figure 12**) mimicked an almost identical phenotype to enNTSR1 (**Figure 10A/C/E/G**). While it does not discount other factors responsible for phenotypic changes for the human and rat NTSR1, the similarity highlights the observed upturns in BRET signal following equilibration are likely due to membrane-dependent receptor internalization. Likely, the lack of internal cellular components, such as  $\beta$ -arrestin, bring about the plateau in kinetic signalling. This form of inference has not been previously shown for these forms of BRET sensors, highlighting the breadth of data available from this analytical methodology.

$G\alpha_q$  coupling was unable to be observed with human and rat NTSR1 receptors in a membrane preparation-based BRET assay (**Figure 13**). This finding highlighted a potential role of local ionic pools at or near the inner cell membrane where GPCR-G protein coupling is occurring. Indeed, positive ionic factors, like sodium ions, are known to act as endogenous allosteric modulators of GPCRs by shifting the equilibrium towards an inactive state (Zou et al., 2022).  $Mg^{2+}$  ions have been indicated to enhance agonist and GTP binding resulting in a differential increase in stimulation at low concentrations (< 10 mM) whilst above this threshold they present a strong inhibitory effect (Szekeres & Traynor, 1997). This biphasic effect underscores the importance of ions in heterotrimer coupling. However, there are a lack of studies into other ionic factors effecting G protein activation, including GTP:GDP stoichiometry. Inability to observe  $G\alpha_q$  coupling also suggests the interaction required to form a  $G\alpha_q$  coupling response may be orchestrated by a factor not directly present in the cell membrane as these factors have been stripped from the assay.  $G\alpha_q$  isotypes have stringent requirements for the chaperone, Ric8A, to be trafficked to the cell membrane and correctly folded (Gabay Meital et al., 2011). Moreover, Ric8A is a critical element for guanine nucleotide coordination by the  $G\alpha$  subunit of the heterotrimer and is a quality control mechanism for GTP binding (Seven et al., 2020). Therefore, lack of cytosolic Ric8A in membrane preparation assays may be responsible for the disparity in distinguishable  $G\alpha_q$ -based G protein response when rat and human NTSR1 are stimulated with NT8-13 and NT1-13. Hence, further validation of the effects of nucleotide and proteinaceous parameters are required for developing  $G\alpha_q$ -based cell-free assay systems.

#### **4.4 Purification of a BRET-based G protein biosensor provides a promising future for reductionist format RET-based assays**

$G\alpha_{i3}$ -based heterotrimeric BRET biosensors were successfully purified (**Figure 14**) and functionality of the purified heterotrimeric complex confirmed by a general  $G\alpha_{i3}$  protein dependent trend associated with a reduction in GTP over time (**Figure 15**). However, there are several major issues within our novel tri-cistronic BRET-based biosensor which need to be addressed and circumvented prior to developing a reductionist format BRET-assay.

A caveat in the purification process was introduction of impurities due to the use of mammalian cells for expression of a polyhistidine-tagged fusion protein. Although a FLAG<sup>®</sup> epitope tag could have been utilized, this is prohibitively expensive. Alternatively, the nanobody-based epitope tag, the ALFA-tag, which has been shown to outperform the FLAG<sup>®</sup>-tag (Götzke et al., 2019), would be utilized in place of a 6xHis-tag or FLAG<sup>®</sup>-tag for the purification of G proteins from mammalian cell cultures (**Figure 16D-F** highlights ALFA-tag specificity in mammalian-based purification). Furthermore, additional purification steps could be used. For instance, anion-exchange chromatography could separate proteins based on the net surface charge. Subsequently, fluorescence-detection size-exclusion chromatography would have been employed based on the fluorescence of the Venus protein attachment to further sequester the heterotrimer. However, without high G protein yields, loss between each purification step would reduce total yield substantially, hence why additional purification steps were not undertaken. G protein expression was particularly hampered by the cost and time associated with the production of lentiviral particles. Theoretically, an ideal system for G protein overexpression in mammalian cells would be to use an inducible gene expression system, such as the tetracycline-controlled inducible operator system (Kallunki et al., 2019). By integrating the G protein genes under the control of an inducible promoter, cytotoxicity introduced by  $G\alpha$  subunit overexpression and selection against the overexpressing  $G\alpha$  phenotype could be overcome.

Finally, a cell-free assay system requires tool receptors. Highly expressing GPCR variants like enNTSR1 are desirable compared to low expressing wild-type variants. A notably disease-relevant signalling-capable tool receptor would be that utilized to resolve the human NTSR1 in complex with  $G\alpha_{i1}$  containing a single point mutation to increase expression (Kato et al., 2019). A fine balance is required to keep expression high whilst minimizing loss of G protein coupling.

#### **4.5 Future directions and conclusions**

This study set out to lay foundations for a cell-free reductionist format BRET assay to combat the lack of methodologies for assessing GPCR-G protein promiscuity and ligand bias. Development of two novel  $G\alpha_{i3}$  and  $G\alpha_q$ -based BRET biosensors with purification handles were used to assess the different coupling interactions of three prototypical NTSR1 receptors. The sensors provide a kinetic context to agonist-induced G protein responses in wildtype human and rat NTSR1 but also mutant enNTSR1. Both human and rat NTSR1 were found to couple primarily to  $G\alpha_q$  G proteins whilst showing secondary  $G\alpha_{i3}$  coupling. Comparatively, enNTSR1 was found to transduce G protein signals, albeit to a lesser extent, whilst lacking capacity to couple  $\beta$ -arrestin. The finding of enNTSR1-G protein coupling paves way for producing a cell-free reductionist format G protein assay. However, further work is required to reconstitute the two purified components. Being able to isolate GPCRs and G protein-based RET sensors from cells would not only provide a platform for assessing ligand bias and receptor promiscuity for developing biased and safer therapeutics but also as a tool for other areas of GPCR biology. For example, tool development would aid in assessing ideal conditions in GPCR-G protein structural biology and in NMR with unnatural amino acid incorporation which cannot be conducted in whole-cells.

## Acknowledgements

The year would not have been as bearable and exciting without the kind, intelligent, and understanding people around me. It was a monumental year which was overwhelming and stressful but also one filled with excitement and fun that I will look back at fondly.

Of course, the experience could not have been made possible without two of the best supervisors and scientific role models, Chris Draper-Joyce and Dan Scott. Both of you exude the energy and passion for scientific endeavours which every scientist should hope to have. Thank you for dedicating the time and passion towards my project. Chris, you have been excellent primary supervisor and teacher. Thank you for all the advice and guidance you've given me, especially answering the ridiculous amounts of questions I had every day, however small, stupid, or arbitrary they may have been. Dan, thank you so much for originally taking me on as a student through the Undergraduate Research Opportunities Program. I don't know if I would have been where I am if you hadn't given me that opportunity. Your trust and thought to leave Chris and I to our own devices throughout the year was very appreciated. I am a better scientist having met both of you.

An enormous thanks goes out to everyone in the lab and all the friends I've made along the way. Tiffany for the conversations in the lab and random banter about science; Eddy for the long and thoughtful talks about everything, especially all the pop culture related stuff; Lisa for answering literally every question about science and for letting me annoy you at our desk (and of course, I can't forget to mention Jon who taught me so much before starting Honours); Andy for your extremely obscure questions about life and your amazingly kind attitude with everyone; Brad for always keeping the energy in the lab high and having a cheerful attitude for everything (and the coveted conference pens you gave me); Riley for the top tips and help you gave me throughout the year; Kazem and Saharnaz for being the iconic duo I could talk to about GPCRs with; Jei Min and Evaline for always asking me about random stuff; Sharon and Tania for always keeping the lab going (I don't know what the lab would be like without you two around).

A particular hurrah goes to my fellow Honours partner in the Bathgate Laboratory, Quinn! It's been fantastic to have someone else going through the same madness of failing experiments and being able to support each other throughout the year (the random conversations in tissue culture over the weekends helped). We've finally made it!

Finally, I'd like to thank my family and friends for supporting me but also being understanding of why I was out of touch in some instances and perpetually working. In particular, a big thank you to my father for always having meals ready after a long day in the laboratory, it definitely kept me going throughout the year.

Again, words cannot describe the sincerity of my thoughts in how you have all made this year amazing, and I can't thank you all enough!

And, of course, thanks to all the contributions from others in the lab:

- enNTSR1 and rat NTSR1  $\beta$ -arrestin BRET assays by Andy Zhang (**Figure 10F/G**).
- Purified muGFP samples produced by Lisa Williams (**Figure 15**)
- enNTSR1 purification gel images by Eddy Yang (**Figure 16B/C**)

## Bibliography

- Álvarez, R., López, D. J., Casas, J., Lladó, V., Higuera, M., Nagy, T., Barceló, M., Busquets, X., & Escribá, P. V. (2015). G protein–membrane interactions I: G $\alpha$ i1 myristoyl and palmitoyl modifications in protein–lipid interactions and its implications in membrane microdomain localization. *Biochimica et Biophysica Acta (BBA) - Molecular and Cell Biology of Lipids*, 1851(11), 1511–1520. <https://doi.org/10.1016/j.bbalip.2015.08.001>
- Ayoub, M. A., Maurel, D., Binet, V., Fink, M., Prézeau, L., Ansanay, H., & Pin, J.-P. (2007). Real-Time Analysis of Agonist-Induced Activation of Protease-Activated Receptor 1/G $\alpha$ i1 Protein Complex Measured by Bioluminescence Resonance Energy Transfer in Living Cells. *Molecular Pharmacology*, 71(5), 1329–1340. <https://doi.org/10.1124/mol.106.030304>
- Berstein, G., Blank, J. L., Smrcka, A. V., Higashijima, T., Sternweis, P. C., Exton, J. H., & Ross, E. M. (1992). Reconstitution of agonist-stimulated phosphatidylinositol 4,5-bisphosphate hydrolysis using purified m1 muscarinic receptor, G $\alpha$ q/11, and phospholipase C-beta 1. *Journal of Biological Chemistry*, 267(12), 8081–8088. [https://doi.org/10.1016/S0021-9258\(18\)42410-6](https://doi.org/10.1016/S0021-9258(18)42410-6)
- Besserer-Offroy, É., Brouillette, R. L., Lavenus, S., Froehlich, U., Brumwell, A., Murza, A., Longpré, J.-M., Marsault, É., Grandbois, M., Sarret, P., & Leduc, R. (2017). The signaling signature of the neurotensin type 1 receptor with endogenous ligands. *European Journal of Pharmacology*, 805, 1–13. <https://doi.org/10.1016/j.ejphar.2017.03.046>
- Brandt, D. R., & Ross, E. M. (1986). Catecholamine-stimulated GTPase cycle. Multiple sites of regulation by beta-adrenergic receptor and Mg $^{2+}$  studied in reconstituted receptor-Gs vesicles. *Journal of Biological Chemistry*, 261(4), 1656–1664. [https://doi.org/10.1016/S0021-9258\(17\)35991-4](https://doi.org/10.1016/S0021-9258(17)35991-4)
- Bumbak, F. (2016). *Characterising the Conformational Diversity of the Neurotensin Receptor 1* [PhD]. The University of Melbourne.
- Bumbak, F., Keen, A. C., Gunn, N. J., Gooley, P. R., Bathgate, R. A. D., & Scott, D. J. (2018). Optimization and  $^{13}\text{CH}_3$  methionine labeling of a signaling competent neurotensin receptor 1 variant for NMR studies. *Biochimica et Biophysica Acta (BBA) - Biomembranes*, 1860(6), 1372–1383. <https://doi.org/10.1016/j.bbamem.2018.03.020>
- Carraway, R. E., & Mitra, S. P. (1998). Neurotensin enhances agonist-induced cAMP accumulation in PC3 cells via Ca $^{2+}$ -dependent adenylyl cyclase(s). *Molecular and Cellular Endocrinology*, 144(1), 47–57. [https://doi.org/10.1016/S0303-7207\(98\)00154-3](https://doi.org/10.1016/S0303-7207(98)00154-3)
- Casares, D., Escribá, P. V., & Rosselló, C. A. (2019). Membrane Lipid Composition: Effect on Membrane and Organelle Structure, Function and Compartmentalization and Therapeutic

- Avenues. *International Journal of Molecular Sciences*, 20(9).
- <https://doi.org/10.3390/ijms20092167>
- Chalon, P., Vita, N., Kaghad, M., Guillemot, M., Bonnin, J., Delpech, B., Le Fur, G., Ferrara, P., & Caput, D. (1996). Molecular cloning of a levocabastine-sensitive neurotensin binding site. *FEBS Letters*, 386(2–3), 91–94. [https://doi.org/10.1016/0014-5793\(96\)00397-3](https://doi.org/10.1016/0014-5793(96)00397-3)
- Cusack, B., McCormick, D. J., Pang, Y.-P., Souder, T., Garcia, R., Fauq, A., & Richelson, E. (1995). Pharmacological and Biochemical Profiles of Unique Neurotensin 8-13 Analogs Exhibiting Species Selectivity, Stereoselectivity, and Superagonism \*. *Journal of Biological Chemistry*, 270(31), 18359–18366. <https://doi.org/10.1074/jbc.270.31.18359>
- DeVree, B. T., Mahoney, J. P., Vélez-Ruiz, G. A., Rasmussen, S. G. F., Kuszak, A. J., Edwald, E., Fung, J.-J., Manglik, A., Masureel, M., Du, Y., Matt, R. A., Pardon, E., Steyaert, J., Kobilka, B. K., & Sunahara, R. K. (2016). Allosteric coupling from G protein to the agonist-binding pocket in GPCRs. *Nature*, 535(7610), 182–186. <https://doi.org/10.1038/nature18324>
- Draper-Joyce, C. J., Khoshouei, M., Thal, D. M., Liang, Y.-L., Nguyen, A. T. N., Furness, S. G. B., Venugopal, H., Baltos, J.-A., Plitzko, J. M., Danev, R., Baumeister, W., May, L. T., Wootten, D., Sexton, P. M., Glukhova, A., & Christopoulos, A. (2018). Structure of the adenosine-bound human adenosine A1 receptor–Gi complex. *Nature*, 558(7711), 559–563. <https://doi.org/10.1038/s41586-018-0236-6>
- Du, Y., Duc, N. M., Rasmussen, S. G. F., Hilger, D., Kubiak, X., Wang, L., Bohon, J., Kim, H. R., Wegrecki, M., Asuru, A., Jeong, K. M., Lee, J., Chance, M. R., Lodowski, D. T., Kobilka, B. K., & Chung, K. Y. (2019). Assembly of a GPCR-G Protein Complex. *Cell*, 177(5), 1232–1242.e11. <https://doi.org/10.1016/j.cell.2019.04.022>
- Feifel, D., Goldenberg, J., Melendez, G., & Shilling, P. D. (2010). The acute and subchronic effects of a brain-penetrating, neurotensin-1 receptor agonist on feeding, body weight and temperature. *Neuropeptides*, 58(1), 195–198. <https://doi.org/10.1016/j.neuropharm.2009.07.001>
- Fields, T. A., & Casey, P. J. (1997). Signalling functions and biochemical properties of pertussis toxin-resistant G-proteins. *Biochemical Journal*, 321(3), 561–571. <https://doi.org/10.1042/bj3210561>
- Flock, T., Hauser, A. S., Lund, N., Gloriam, D. E., Balaji, S., & Babu, M. M. (2017). Selectivity determinants of GPCR–G-protein binding. *Nature*, 545(7654), 317–322. <https://doi.org/10.1038/nature22070>
- Florio, V. A., & Sternweis, P. C. (1989). Mechanisms of muscarinic receptor action on Go in reconstituted phospholipid vesicles\*. *Journal of Biological Chemistry*, 264(7), 3909–3915. [https://doi.org/10.1016/S0021-9258\(19\)84939-6](https://doi.org/10.1016/S0021-9258(19)84939-6)

- Furness, S. G. B., Liang, Y.-L., Nowell, C. J., Halls, M. L., Wookey, P. J., Dal Maso, E., Inoue, A., Christopoulos, A., Wootten, D., & Sexton, P. M. (2016). Ligand-Dependent Modulation of G Protein Conformation Alters Drug Efficacy. *Cell*, 167(3), 739-749.e11. <https://doi.org/10.1016/j.cell.2016.09.021>
- Gabay Meital, Pinter Mary E., Wright Forrest A., Chan PuiYee, Murphy Andrew J., Valenzuela David M., Yancopoulos George D., & Tall Gregory G. (2011). Ric-8 Proteins Are Molecular Chaperones That Direct Nascent G Protein  $\alpha$  Subunit Membrane Association. *Science Signaling*, 4(200), ra79–ra79. <https://doi.org/10.1126/scisignal.2002223>
- Galés, C., Van Durm, J. J. J., Schaak, S., Pontier, S., Percherancier, Y., Audet, M., Paris, H., & Bouvier, M. (2006). Probing the activation-promoted structural rearrangements in preassembled receptor–G protein complexes. *Nature Structural & Molecular Biology*, 13(9), 778–786. <https://doi.org/10.1038/nsmb1134>
- Glukhova, A., Draper-Joyce, C. J., Sunahara, R. K., Christopoulos, A., Wootten, D., & Sexton, P. M. (2018). Rules of Engagement: GPCRs and G Proteins. *ACS Pharmacology & Translational Science*, 1(2), 73–83. <https://doi.org/10.1021/acsptsci.8b00026>
- Goedert, M., & Emson, P. C. (1983). The regional distribution of neurotensin-like immunoreactivity in central and peripheral tissues of the cat. *Brain Research*, 272(2), 291–297. [https://doi.org/10.1016/0006-8993\(83\)90576-0](https://doi.org/10.1016/0006-8993(83)90576-0)
- Götzke, H., Kilisch, M., Martínez-Carranza, M., Sograte-Idrissi, S., Rajavel, A., Schlichthaerle, T., Engels, N., Jungmann, R., Stenmark, P., Opazo, F., & Frey, S. (2019). The ALFA-tag is a highly versatile tool for nanobody-based bioscience applications. *Nature Communications*, 10(1), 4403. <https://doi.org/10.1038/s41467-019-12301-7>
- Granier, C., Van Rietschoten, J., Kitabi, P., Poustis, C., & Freychet, P. (1982). Synthesis and Characterization of Neurotensin Analogues for Structure/Activity Relationship Studies. *European Journal of Biochemistry*, 124(1), 117–125. <https://doi.org/10.1111/j.1432-1033.1982.tb05913.x>
- Grant, K. R., Harnett, W., Milligan, G., & Harnett, M. M. (1997). Differential G-protein expression during B- and T-cell development. *Immunology*, 90(4), 564–571. <https://doi.org/10.1046/j.1365-2567.1997.00196.x>
- Gurevich, V. V., & Gurevich, E. V. (2019). GPCR Signaling Regulation: The Role of GRKs and Arrestins. *Frontiers in Pharmacology*, 10. <https://doi.org/10.3389/fphar.2019.00125>
- Hamdan, F. F., Percherancier, Y., Breton, B., & Bouvier, M. (2006). Monitoring Protein-Protein Interactions in Living Cells by Bioluminescence Resonance Energy Transfer (BRET). *Current Protocols in Neuroscience*, 34(1), 5.23.1-5.23.20. <https://doi.org/10.1002/0471142301.ns0523s34>

- Hauser, A. S., Chavali, S., Masuho, I., Jahn, L. J., Martemyanov, K. A., Gloriam, D. E., & Babu, M. M. (2018). Pharmacogenomics of GPCR Drug Targets. *Cell*, 172(1), 41-54.e19. <https://doi.org/10.1016/j.cell.2017.11.033>
- Hein, P., Frank, M., Hoffmann, C., Lohse, M. J., & Bünemann, M. (2005). Dynamics of receptor/G protein coupling in living cells. *The EMBO Journal*, 24(23), 4106–4114. <https://doi.org/10.1038/sj.emboj.7600870>
- Hermans, E., Geurts, M., & Maloteaux, J.-M. (1997). Agonist and antagonist modulation of [35S]-GTP $\gamma$ S binding in transfected CHO cells expressing the neurotensin receptor. *British Journal of Pharmacology*, 121(8), 1817–1823. <https://doi.org/10.1038/sj.bjp.0701334>
- Heydenreich, F. M., Plouffe, B., Rizk, A., Milić, D., Zhou, J., Breton, B., Le Gouill, C., Inoue, A., Bouvier, M., & Veprintsev, D. B. (2021). Vasopressin V2 is a promiscuous G protein-coupled receptor that is biased by its peptide ligands. *BioRxiv*, 2021.01.28.427950. <https://doi.org/10.1101/2021.01.28.427950>
- Higashijima, T., Ferguson, K. M., Sternweis, P. C., Smigel, M. D., & Gilman, A. G. (1987). Effects of Mg<sup>2+</sup> and the beta gamma-subunit complex on the interactions of guanine nucleotides with G proteins. *Journal of Biological Chemistry*, 262(2), 762–766. [https://doi.org/10.1016/S0021-9258\(19\)75851-7](https://doi.org/10.1016/S0021-9258(19)75851-7)
- Huang, W., Masureel, M., Qu, Q., Janetzko, J., Inoue, A., Kato, H. E., Robertson, M. J., Nguyen, K. C., Glenn, J. S., Skiniotis, G., & Kobilka, B. K. (2020). Structure of the neurotensin receptor 1 in complex with  $\beta$ -arrestin 1. *Nature*, 579(7798), 303–308. <https://doi.org/10.1038/s41586-020-1953-1>
- Inagaki, S., Ghirlando, R., White, J. F., Gvozdenovic-Jeremic, J., Northup, J. K., & Grisshammer, R. (2012). Modulation of the Interaction between Neurotensin Receptor NTS1 and Gq Protein by Lipid. *Journal of Molecular Biology*, 417(1), 95–111. <https://doi.org/10.1016/j.jmb.2012.01.023>
- Inoue, A., Raimondi, F., Kadji, F. M. N., Singh, G., Kishi, T., Uwamizu, A., Ono, Y., Shinjo, Y., Ishida, S., Arang, N., Kawakami, K., Gutkind, J. S., Aoki, J., & Russell, R. B. (2019). Illuminating G-Protein-Coupling Selectivity of GPCRs. *Cell*, 177(7), 1933-1947.e25. <https://doi.org/10.1016/j.cell.2019.04.044>
- James, A., & Williams, J. (2020). Basic Opioid Pharmacology—An Update. *British Journal of Pain*, 14(2), 115–121. <https://doi.org/10.1177/2049463720911986>
- Jones, J. C., Jones, A. M., Temple, B. R. S., & Dohlman, H. G. (2012). Differences in intradomain and interdomain motion confer distinct activation properties to structurally similar G $\alpha$  proteins. *Proceedings of the National Academy of Sciences*, 109(19), 7275. <https://doi.org/10.1073/pnas.1202943109>

- Kallunki, T., Barisic, M., Jäättelä, M., & Liu, B. (2019). How to Choose the Right Inducible Gene Expression System for Mammalian Studies? *Cells*, 8(8).
- <https://doi.org/10.3390/cells8080796>
- Kato, H. E., Zhang, Y., Hu, H., Suomivuori, C.-M., Kadji, F. M. N., Aoki, J., Krishna Kumar, K., Fonseca, R., Hilger, D., Huang, W., Latorraca, N. R., Inoue, A., Dror, R. O., Kobilka, B. K., & Skiniotis, G. (2019). Conformational transitions of a neurotensin receptor 1–Gi1 complex. *Nature*, 572(7767), 80–85. <https://doi.org/10.1038/s41586-019-1337-6>
- Kenakin, T. (2003). Ligand-selective receptor conformations revisited: The promise and the problem. *Trends in Pharmacological Sciences*, 24(7), 346–354.
- [https://doi.org/10.1016/S0165-6147\(03\)00167-6](https://doi.org/10.1016/S0165-6147(03)00167-6)
- Kenakin, T., Watson, C., Muniz-Medina, V., Christopoulos, A., & Novick, S. (2012). A Simple Method for Quantifying Functional Selectivity and Agonist Bias. *ACS Chemical Neuroscience*, 3(3), 193–203. <https://doi.org/10.1021/cn200111m>
- Khan, S. M., Sleno, R., Gora, S., Zylbergold, P., Laverdure, J.-P., Labbé, J.-C., Miller, G. J., & Hébert, T. E. (2013). The Expanding Roles of G $\beta\gamma$  Subunits in G Protein–Coupled Receptor Signaling and Drug Action. *Pharmacological Reviews*, 65(2), 545–577.
- <https://doi.org/10.1124/pr.111.005603>
- Kitabgi, P. (2006). Differential processing of pro-neurotensin/neuromedin N and relationship to pro-hormone convertases. *Neurotensin: Roles and Mechanisms*, 27(10), 2508–2514.
- <https://doi.org/10.1016/j.peptides.2006.03.038>
- Kleczkowska, P., & Lipkowski, A. W. (2013). Neurotensin and neurotensin receptors: Characteristic, structure–activity relationship and pain modulation—A review. *Pharmacology of Pain*, 716(1), 54–60. <https://doi.org/10.1016/j.ejphar.2013.03.004>
- Klein Herenbrink, C., Sykes, D. A., Donthamsetti, P., Canals, M., Coudrat, T., Shonberg, J., Scammells, P. J., Capuano, B., Sexton, P. M., Charlton, S. J., Javitch, J. A., Christopoulos, A., & Lane, J. R. (2016). The role of kinetic context in apparent biased agonism at GPCRs. *Nature Communications*, 7(1), 10842. <https://doi.org/10.1038/ncomms10842>
- Kobilka, B. K., & Deupi, X. (2007). Conformational complexity of G-protein-coupled receptors. *Trends in Pharmacological Sciences*, 28(8), 397–406.
- <https://doi.org/10.1016/j.tips.2007.06.003>
- Koehl, A., Hu, H., Maeda, S., Zhang, Y., Qu, Q., Paggi, J. M., Latorraca, N. R., Hilger, D., Dawson, R., Matile, H., Schertler, G. F. X., Granier, S., Weis, W. I., Dror, R. O., Manglik, A., Skiniotis, G., & Kobilka, B. K. (2018). Structure of the  $\mu$ -opioid receptor–Gi protein complex. *Nature*, 558(7711), 547–552. <https://doi.org/10.1038/s41586-018-0219-7>

- Kostenis, E., Degtyarev, M. Y., Conklin, B. R., & Wess, J. (1997). The N-terminal Extension of Gαq Is Critical for Constraining the Selectivity of Receptor Coupling \*. *Journal of Biological Chemistry*, 272(31), 19107–19110. <https://doi.org/10.1074/jbc.272.31.19107>
- Locht, C., Coutte, L., & Mielcarek, N. (2011). The ins and outs of pertussis toxin. *The FEBS Journal*, 278(23), 4668–4682. <https://doi.org/10.1111/j.1742-4658.2011.08237.x>
- Mafi Amirhossein, Kim Soo-Kyung, & Goddard William A. (2022). The mechanism for ligand activation of the GPCR–G protein complex. *Proceedings of the National Academy of Sciences*, 119(18), e2110085119. <https://doi.org/10.1073/pnas.2110085119>
- Matthees, E. S. F., Haider, R. S., Hoffmann, C., & Drube, J. (2021). Differential Regulation of GPCRs—Are GRK Expression Levels the Key? *Frontiers in Cell and Developmental Biology*, 9. <https://doi.org/10.3389/fcell.2021.687489>
- Mazella, J., Zsürger, N., Navarro, V., Chabry, J., Kaghad, M., Caput, D., Ferrara, P., Vita, N., Gully, D., Maffrand, J.-P., & Vincent, J.-P. (1998). The 100-kDa Neurotensin Receptor Is gp95/Sortilin, A Non-G-Protein-coupled Receptor\*. *Journal of Biological Chemistry*, 273(41), 26273–26276. <https://doi.org/10.1074/jbc.273.41.26273>
- Milligan, G. (2003). Principles: Extending the utility of [35S]GTPγS binding assays. *Trends in Pharmacological Sciences*, 24(2), 87–90. [https://doi.org/10.1016/S0165-6147\(02\)00027-5](https://doi.org/10.1016/S0165-6147(02)00027-5)
- Mondal, S., Hsiao, K., & Goueli, S. A. (2015). A Homogenous Bioluminescent System for Measuring GTPase, GTPase Activating Protein, and Guanine Nucleotide Exchange Factor Activities. *ASSAY and Drug Development Technologies*, 13(8), 444–455. <https://doi.org/10.1089/adt.2015.643>
- Nehmé, R., Carpenter, B., Singhal, A., Strege, A., Edwards, P. C., White, C. F., Du, H., Grisshammer, R., & Tate, C. G. (2017). Mini-G proteins: Novel tools for studying GPCRs in their active conformation. *PLOS ONE*, 12(4), e0175642. <https://doi.org/10.1371/journal.pone.0175642>
- Neves, S. R., Ram, P. T., & Iyengar, R. (2002). G Protein Pathways. *Science*, 296(5573), 1636. <https://doi.org/10.1126/science.1071550>
- Nishimura, A., Okamoto, M., Sugawara, Y., Mizuno, N., Yamauchi, J., & Itoh, H. (2006). Ric-8A potentiates Gq-mediated signal transduction by acting downstream of G protein-coupled receptor in intact cells. *Genes to Cells*, 11(5), 487–498. <https://doi.org/10.1111/j.1365-2443.2006.00959.x>
- Nobles Muriel, Benians Amy, & Tinker Andrew. (2005). Heterotrimeric G proteins precouple with G protein-coupled receptors in living cells. *Proceedings of the National Academy of Sciences*, 102(51), 18706–18711. <https://doi.org/10.1073/pnas.0504778102>

- Okashah, N., Wan, Q., Ghosh, S., Sandhu, M., Inoue, A., Vaidehi, N., & Lambert, N. A. (2019). Variable G protein determinants of GPCR coupling selectivity. *Proceedings of the National Academy of Sciences*, 116(24), 12054. <https://doi.org/10.1073/pnas.1905993116>
- Oldham, W. M., & Hamm, H. E. (2008). Heterotrimeric G protein activation by G-protein-coupled receptors. *Nature Reviews Molecular Cell Biology*, 9(1), 60–71. <https://doi.org/10.1038/nrm2299>
- Olsen, R. H. J., DiBerto, J. F., English, J. G., Glaudin, A. M., Krumm, B. E., Slocum, S. T., Che, T., Gavin, A. C., McCory, J. D., Roth, B. L., & Strachan, R. T. (2020). TRUPATH, an open-source biosensor platform for interrogating the GPCR transducerome. *Nature Chemical Biology*, 16(8), 841–849. <https://doi.org/10.1038/s41589-020-0535-8>
- Onaran, H. O., Ambrosio, C., Uğur, Ö., Madaras Koncz, E., Grò, M. C., Vezzi, V., Rajagopal, S., & Costa, T. (2017). Systematic errors in detecting biased agonism: Analysis of current methods and development of a new model-free approach. *Scientific Reports*, 7(1), 44247. <https://doi.org/10.1038/srep44247>
- Onfroy, L., Galandrin, S., Pontier, S. M., Seguelas, M.-H., N'Guyen, D., Sénard, J.-M., & Galés, C. (2017). G protein stoichiometry dictates biased agonism through distinct receptor-G protein partitioning. *Scientific Reports*, 7(1), 7885. <https://doi.org/10.1038/s41598-017-07392-5>
- Piliponsky, A. M., Chen, C.-C., Nishimura, T., Metz, M., Rios, E. J., Dobner, P. R., Wada, E., Wada, K., Zacharias, S., Mohanasundaram, U. M., Faix, J. D., Abrink, M., Pejler, G., Pearl, R. G., Tsai, M., & Galli, S. J. (2008). Neuropeptid Y increases mortality and mast cells reduce neuropeptid Y levels in a mouse model of sepsis. *Nature Medicine*, 14(4), 392–398. <https://doi.org/10.1038/nm1738>
- Qin, K., Sethi, P. R., & Lambert, N. A. (2008). Abundance and stability of complexes containing inactive G protein-coupled receptors and G proteins. *The FASEB Journal*, 22(8), 2920–2927. <https://doi.org/10.1096/fj.08-105775>
- Rasmussen, S. G. F., DeVree, B. T., Zou, Y., Kruse, A. C., Chung, K. Y., Kobilka, T. S., Thian, F. S., Chae, P. S., Pardon, E., Calinski, D., Mathiesen, J. M., Shah, S. T. A., Lyons, J. A., Caffrey, M., Gellman, S. H., Steyaert, J., Skiniotis, G., Weis, W. I., Sunahara, R. K., & Kobilka, B. K. (2011). Crystal structure of the β2 adrenergic receptor–Gs protein complex. *Nature*, 477(7366), 549–555. <https://doi.org/10.1038/nature10361>
- Rominger, D. H., Cowan, C. L., Gowen-MacDonald, W., & Violin, J. D. (2014). Biased ligands: Pathway validation for novel GPCR therapeutics. *Respiratory • Musculoskeletal*, 16, 108–115. <https://doi.org/10.1016/j.coph.2014.04.002>

- Schihada, H., Shekhani, R., & Schulte, G. (2021). Quantitative assessment of constitutive G protein-coupled receptor activity with BRET-based G protein biosensors. *Science Signaling*, 14(699), eabf1653. <https://doi.org/10.1126/scisignal.abf1653>
- Seeman, P., Chau-Wong, M., Tedesco, J., & Wong, K. (1975). Brain Receptors for Antipsychotic Drugs and Dopamine: Direct Binding Assays. *Proceedings of the National Academy of Sciences of the United States of America*, 72(11), 4376–4380. JSTOR.
- Seven, A. B., Hilger, D., Papasergi-Scott, M. M., Zhang, L., Qu, Q., Kobilka, B. K., Tall, G. G., & Skiniotis, G. (2020). Structures of Gα Proteins in Complex with Their Chaperone Reveal Quality Control Mechanisms. *Cell Reports*, 30(11), 3699-3709.e6. <https://doi.org/10.1016/j.celrep.2020.02.086>
- Skrzydelski, D., Lhiaubet, A.-M., Lebeau, A., Forgez, P., Yamada, M., Hermans, E., Rostene, W., & Pelaprat, D. (2003). Differential Involvement of Intracellular Domains of the Rat NTS1 Neurotensin Receptor in Coupling to G Proteins: A Molecular Basis for Agonist-Directed Trafficking of Receptor Stimulus. *Molecular Pharmacology*, 64(2), 421. <https://doi.org/10.1124/mol.64.2.421>
- Strange, P. G. (2010). Use of the GTPγS ([35S]GTPγS and Eu-GTPγS) binding assay for analysis of ligand potency and efficacy at G protein-coupled receptors. *British Journal of Pharmacology*, 161(6), 1238–1249. <https://doi.org/10.1111/j.1476-5381.2010.00963.x>
- Strohman, M. J., Maeda, S., Hilger, D., Masureel, M., Du, Y., & Kobilka, B. K. (2019). Local membrane charge regulates β2 adrenergic receptor coupling to Gi3. *Nature Communications*, 10(1), 2234. <https://doi.org/10.1038/s41467-019-10108-0>
- Stryer, L. (1978). Fluorescence Energy Transfer as a Spectroscopic Ruler. *Annual Review of Biochemistry*, 47(1), 819–846. <https://doi.org/10.1146/annurev.bi.47.070178.004131>
- Syrovatkina, V., Alegre, K. O., Dey, R., & Huang, X.-Y. (2016). Regulation, Signaling, and Physiological Functions of G-Proteins. *Molecular Basis of Signal Transduction*, 428(19), 3850–3868. <https://doi.org/10.1016/j.jmb.2016.08.002>
- Szekeres, P. G., & Traynor, J. R. (1997). Delta opioid modulation of the binding of guanosine-5'-O-(3-[35S]thio)triphosphate to NG108-15 cell membranes: Characterization of agonist and inverse agonist effects. *The Journal of Pharmacology and Experimental Therapeutics*, 283(3), 1276–1284.
- Tabarean, I. V. (2020). Neurotensin induces hypothermia by activating both neuronal neurotensin receptor 1 and astrocytic neurotensin receptor 2 in the median preoptic nucleus. *Neuropharmacology*, 171, 108069. <https://doi.org/10.1016/j.neuropharm.2020.108069>

- Takahashi, K., Ehata, S., Miyauchi, K., Morishita, Y., Miyazawa, K., & Miyazono, K. (2021). Neurotensin receptor 1 signaling promotes pancreatic cancer progression. *Molecular Oncology*, 15(1), 151–166. <https://doi.org/10.1002/1878-0261.12815>
- Tanaka, K., Masu, M., & Nakanishi, S. (1990). Structure and functional expression of the cloned rat neurotensin receptor. *Neuron*, 4(6), 847–854. [https://doi.org/10.1016/0896-6273\(90\)90137-5](https://doi.org/10.1016/0896-6273(90)90137-5)
- Tyler-McMahon, B. M., Boules, M., & Richelson, E. (2000). Neurotensin: Peptide for the next millennium. *20th Anniversary Celebratory Special Issue*, 93(1), 125–136. [https://doi.org/10.1016/S0167-0115\(00\)00183-X](https://doi.org/10.1016/S0167-0115(00)00183-X)
- Uhl, G. R., & Snyder, S. H. (1976). Regional and subcellular distributions of brain neurotensin. *Life Sciences*, 19(12), 1827–1832. [https://doi.org/10.1016/0024-3205\(76\)90114-4](https://doi.org/10.1016/0024-3205(76)90114-4)
- Vögler, O., Casas, J., Capó, D., Nagy, T., Borchert, G., Martorell, G., & Escribá, P. V. (2004). The G $\beta\gamma$  Dimer Drives the Interaction of Heterotrimeric Gi Proteins with Nonlamellar Membrane Structures \*. *Journal of Biological Chemistry*, 279(35), 36540–36545. <https://doi.org/10.1074/jbc.M402061200>
- Wacker, D., Stevens, R. C., & Roth, B. L. (2017). How Ligands Illuminate GPCR Molecular Pharmacology. *Cell*, 170(3), 414–427. <https://doi.org/10.1016/j.cell.2017.07.009>
- Wang, J.-G., Li, N.-N., Li, H.-N., Cui, L., & Wang, P. (2011). Pancreatic cancer bears overexpression of neurotensin and neurotensin receptor subtype-1 and SR 48692 counteracts neurotensin induced cell proliferation in human pancreatic ductal carcinoma cell line PANC-1. *Neuropeptides*, 45(2), 151–156. <https://doi.org/10.1016/j.npep.2011.01.002>
- Wu, zherui, Martinez-Fong, D., Trédaniel, J., & Forgez, P. (2013). Neurotensin and its high affinity receptor 1 as a potential pharmacological target in cancer therapy. *Frontiers in Endocrinology*, 3. <https://doi.org/10.3389/fendo.2012.00184>
- Xu, Y., Piston, D. W., & Johnson, C. H. (1999). A bioluminescence resonance energy transfer (BRET) system: Application to interacting circadian clock proteins. *Proceedings of the National Academy of Sciences*, 96(1), 151. <https://doi.org/10.1073/pnas.96.1.151>
- Yajima, I., Kumashita, M. Y., Naito, Y., Yoshikawa, T., Takahashi, H., Funasaka, Y., Suzuki, T., & Kato, M. (2012). Reduced GNG2 expression levels in mouse malignant melanomas and human melanoma cell lines. *American Journal of Cancer Research*, 2(3), 322–329. PubMed.
- Yamada, M., Yamada, M., Watson, M. A., & Richelson, E. (1993). Neurotensin stimulates cyclic AMP formation in CHO-rNTR-10 cells expressing the cloned rat neurotensin receptor. *European Journal of Pharmacology: Molecular Pharmacology*, 244(1), 99–101. [https://doi.org/10.1016/0922-4106\(93\)90064-G](https://doi.org/10.1016/0922-4106(93)90064-G)

- Yin, J., Chen, K.-Y. M., Clark, M. J., Hijazi, M., Kumari, P., Bai, X., Sunahara, R. K., Barth, P., & Rosenbaum, D. M. (2020). Structure of a D2 dopamine receptor–G-protein complex in a lipid membrane. *Nature*, 584(7819), 125–129. <https://doi.org/10.1038/s41586-020-2379-5>
- Zhou, Y., Meng, J., Xu, C., & Liu, J. (2021). Multiple GPCR Functional Assays Based on Resonance Energy Transfer Sensors. *Frontiers in Cell and Developmental Biology*, 9, 779. <https://doi.org/10.3389/fcell.2021.611443>
- Zou, R., Wang, X., Li, S., Chan, H. C. S., Vogel, H., & Yuan, S. (2022). The role of metal ions in G protein-coupled receptor signalling and drug discovery. *WIREs Computational Molecular Science*, 12(2), e1565. <https://doi.org/10.1002/wcms.1565>

## Appendix

### Appendix Tables

**Appendix Table I. Affinity chromatography resins and elution peptides, antibodies, assay kits, ligands, and reagents used during the project.**

Reagent	Source	Identifier
<b>Affinity Chromatography Resins and Elution Peptides</b>		
ALFA Elution Peptide	NanoTag Biotechnologies	N1520
ALFA Selector Peptide Elutable (4% cross-linked agarose)	NanoTag Biotechnologies	N1510-L
Talon® Metal Affinity Resin	Takara Bio	635504
<b>Antibodies</b>		
Anti-Gβ Monoclonal Antibody (H-1) Alex Fluor® 680	Santa Cruz Biotechnology	sc-166123 AF680
Anti-NanoLuc® Monoclonal Antibody	Promega	N7000
FluoTag®-X2 anti-ALFA Alexa Fluor® 647	NanoTag Biotechnologies	N1502
IRDye® 800CW Goat anti-Mouse IgG (H+L) Secondary Antibody	Li-Cor	926-32210
<b>Assay Kits</b>		
GTPase-Glo™ Assay	Promega	V7681
Nano-Glo® Luciferase Assay System	Promega	N1120
Pierce™ BCA Protein Assay Kit	Thermo Fisher Scientific	23225
<b>Ligands</b>		
NT1-13	Kazem Asadollahi (Bio21 Institute)	N/A (Endogenous Production)
NT8-13	GL Biochem (Shanghai, China)	N/A (Synthetic Peptide)
<b>General Reagents and Enzymes</b>		
3-((3-cholamidopropyl) dimethylammonio)-1-propanesulfonate (CHAPS)	Anatrace	C316
Benzonase	Merck Millipore	70746
Bovine Serum Albumin (BSA)	Sigma-Aldrich	A7906
Bromophenol Blue	Cytiva	17-1329-01
Cholesteryl Hemisuccinate Tris Salt (CHS)	Anatrace	CH210
cOmplete™ EDTA-free Protease Inhibitor Cocktail	Roche®, Sigma-Aldrich	5056489001
Dulbecco's Modified Eagle Medium (DMEM)	Gibco™, Thermo Fisher Scientific	10313021
Dulbecco's Phosphate Buffered Saline (DPBS)	Gibco™, Thermo Fisher Scientific	14190136
Ethylenediaminetetraacetic Acid (EDTA) Disodium salt Dihydrate	ChemSupply Australia	EA023
Foetal Bovine Serum (FBS)	Bovogen Biologicals	SFBS-F
FreeStyle™ 293 Expression Medium	Gibco™, Thermo Fisher Scientific	12338018

Glycine	ChemSupply Australia	GA007
Guanosine 5'-diphosphate (GDP) sodium salt	Sigma-Aldrich	G7127
Guanosine 5'-triphosphate (GTP) sodium salt hydrate	Sigma-Aldrich	G8877
HEPES (1 M Solution)	Gibco™, Thermo Fisher Scientific	15630080
HEPES (Powder)	Sigma-Aldrich	H3375
Imidazole	Sigma-Aldrich	792527
Isopropyl $\beta$ -D-1-thiogalactopyranoside (IPTG)	GoldBio	I2481C100
Lauryl Maltose Neopentyl Glycol (LMNG)	Anatrace	NG310
L-Glutamine	Gibco™, Thermo Fisher Scientific	25030081
Lipofectamine 2000	Invitrogen, Thermo Fisher Scientific	11668019
Magnesium chloride hexahydrate	Supelco®, Sigma-Aldrich	105833
Methanol	Supeco®, Sigma-Aldrich	1.06035
n-dodecyl- $\beta$ -d-malatoside (DDM)	Anatrace	D310
Opti-MEM	Gibco™, Thermo Fisher Scientific	31985070
Palmitoyloleoyl phosphatidylcholine (POPC)	Avanti Polar Lipids	850457C
Palmitoyloleoyl phosphatidylglycerol (POPG)	Avanti Polar Lipids	840457C
Penicillin/streptomycin	Gibco™, Thermo Fisher Scientific	15140122
Phenol Red-Free DMEM (PRF-DMEM)	Gibco™, Thermo Fisher Scientific	31053028
Phenylmethylsulfonyl fluoride (PMSF)	GoldBio	P-470-25
Sodium chloride	ChemSupply Australia	SA046
Sodium cholate hydrate	Sigma-Aldrich	C1254
Sodium Dodecyl Sulphate (SDS)	Sigma-Aldrich	L3771
Trizma® base	Sigma-Aldrich	T1503
TWEEN® 20	Sigma-Aldrich	P1379
$\beta$ -mercaptoethanol	Sigma-Aldrich	805740

**Appendix Table II. Plasmids Used during the project and corresponding descriptors.**

Plasmids	Descriptor
pCSC 6xHis Venus <sub>(1-155)</sub> G $\gamma_2$ P2A Venus <sub>(155-239)</sub> G $\beta_1$ IRES G $\alpha_{i3}$ nLuc	G $\alpha_{i3}$ -based BRET sensor used throughout the project, containing a 6xHis-tag for purification
pCSC 6xHis Venus <sub>(1-155)</sub> G $\gamma_2$ P2A Venus <sub>(155-239)</sub> G $\beta_1$ IRES G $\alpha_q$ nLuc	G $\alpha_q$ -based BRET sensor used throughout the project, containing a 6xHis-tag for purification
pMDL Packaging Plasmid	3 <sup>rd</sup> generation lentiviral vector; Contains HIV-1 gag/pol genes for generation of structural proteins and reverse transcriptase
pRSV-Rev Packaging Plasmid	3 <sup>rd</sup> generation lentiviral vector; Encodes Rev to allow for RNA export from the nucleus
pCMV-VSV-G Envelope Plasmid	3 <sup>rd</sup> generation lentiviral vector; Generates the vesicular stomatitis virus G protein envelope glycoproteins
pcDNA3.1/Zeo(+)	Mammalian empty control construct
pcDNA3.1/Zeo(+) Rat NTSR1 WT	Mammalian construct containing wild-type rat NTSR1 utilised for live cell-based BRET assays
pCSC enNTSR1 (M208) Strep. IRES mCherry	Mammalian construct containing enNTSR1 utilised for live cell-based BRET assays
pcDNA3.1/Zeo(+) enNTSR1 WT Nanoluciferase	Mammalian construct containing enNTSR1 with an intracellular nanoluciferase fusion attachment for $\beta$ -arrestin-based BRET assays
pcDNA3.1/Zeo(+) Rat NTSR1 WT Nanoluciferase	Mammalian construct containing rat NTSR1 with an intracellular nanoluciferase fusion attachment for $\beta$ -arrestin-based BRET assays
pcDNA3.1/Zeo(+) $\beta$ -arrestin Venus	Mammalian construct containing $\beta$ -arrestin with a Venus protein attachment for $\beta$ -arrestin-based BRET assays
pCSC SP-PW Kozac HA ALFA 3C Rat NTSR1 WT His IRES mCherry	Mammalian construct containing the HA ALFA tagged wild-type rat NTSR1 for expression and purification
pDS170 10xHis MBP 3C enNTSR1 (M208) 3C muGFP 10xHis	Bacterial construct used to express and purify enNTSR1, containing an N- and C-terminal 10xHis-tag, maltose-binding protein (MBP) fusion, followed by a 3C protease cleavage site, enNTSR1, another 3C protease cleavage site, and muGFP

**Appendix Table III. DNA sequences of BRET sensor G protein subunits indicating nanoluciferase, Venus, and 6xHis-tag insertion sites.**

pCSC 6xHis Venus <sub>(1-155)</sub> G $\gamma$ <sub>2</sub> P2A Venus <sub>(155-239)</sub> G $\beta$ <sub>1</sub> IRES G $\alpha$ <sub>i3</sub> nLuc	
Nanoluciferase-G $\alpha$ <sub>i3</sub>	ATGGGCTGCACGTTGAGCGCCGAAGACAAGGCAGTCAGTGGAGCG AAGCAAGATGATCGACCGCAACTTACGGGAGGACGGGGAAAAAG CGGCCAAAGAACGAAAGCTGCTGCTACTCGGTGCTGGAGAACATCTG GTAAAAGCACCATTGTGAAACACAGATGAAAATCATTGAGGAT GGCTATTGAGGATGAATGTAACAAATATAAAGTAGTTGCTAC AGCAATACTATACAGTCATCATGCAATCATAAGAGCCATGGGA CGGCTATCAGGAGGTGGCGGATCCGTCTCACACTCGAAGATTTC GTTGGGACTGGCGACAGACAGCCGGTACAACCTGGACCAAGT CCTGAACAGGGAGGTGTCCAGTTGTTGAGAACATCTGGGGT GTCCGTAACTCCGATCCAAGGATTGTCCTGAGCGGTGAAAATGG GCTGAAGATCGACATCCATGTCATCATCCGTATGAAGGTCTGAG CGGCGACCAAATGGGCCAGATCGAAAAAAATTAAAGGTGGTGT ACCTGTGGATGATCATCACTTAAGGTGATCCTGCACTATGGCA CACTGGTAATCGACGGGTTACGCCAACATGATCGACTATTCG GACGGCGTATGAAGGCATGCCGTGTTGACGGCAAAAAGATC ACTGTAACAGGGACCCCTGTGGAACGGCAACAAAATTATCGACGA GCGCCTGATCAACCCCGACGGCTCCCTGCTGTTCCGAGTAACCAT CAACGGAGTGACCGGCTGGCGCTGTGCGAACGCATTCTGGCGTC TGGCGGTGGAGGATCCAAGATTGACTTTGGGAAGCTGCCAGGG CAGATGATGCCCGCAATTATTGTTAGCTGGCAGTGCTGAAG AAGGAGTCATGACTCCAGAACTAGCAGGAGTGATTAAACGGTTA TGGCGAGATGGTGGGGTACAAGCTGCTCAGCAGATCCAGGGA ATATCAGCTCAATGATTCTGCTCATATTATCTAAATGATCTGGAT AGAATATCCCAGTCTAACTACATTCCAACACTCAGCAAGATGTTCTT CGGACGAGAGTGAAGACCACAGGCATTGTAGAAACACATTCAC CTTCAAAGACCTATACTCAAGATGTTGATGTAGGTGGCAAAG ATCAGAACGAAAAAAAGTGGATTCACTGTTGAGGGAGTGACAG CAATTATCTCTGTGTCGCCCTCAGTGTAGGAAACACATTCAC TGAGGACGAGGAGATGAACCGAATGCATGAAAGCATGAAACTGT TTGACAGCATTGTAATAACAAATGGTTACAGAAACTTCAATCA TTCTCTCCTAACAGAAAGACCTTTGAGGAAAAAAATAAAGA GGAGTCCGTTAACTATCTGTTATCCAGAAATACACAGGTTCCAATA CATATGAAGAGGCAGCTGCCTATATTCAATGCCAGTTGAAGATC TGAACAGAACGAAAAGATACCAAGGAGATCTAACTCACTCACCT GTGCCACAGACACGAAGAATGTGCAGTTGTTGATGCTGTTA CAGATGTCATCATTAAAAACAACCTAAAGGAATGTGGACTTTAT
Venus <sub>(155-239)</sub> -G $\beta$ <sub>1</sub>	GACAAGCAGAACGGCATCAAGGCCAACTTCAAGATCCGCCA CAACATCGAGGACGGCGCGTGCAGCTGCCGACCACTACCAGC AGAACACCCCCATCGCGACGGCCCCGTGCTGCCGACAACC ACTACCTGAGCTACCAGTCAAACGTGAGCAAAGACCCAAAG AAGCGCGATCACATGGCCTGCTGGAGTCTGACAGCGGCCGGG ATCACTCTCGGCATGGACGAGCTGTACAAGGGCGGATCTGGGGA GGCAGTGAGCTGACCAAGTACGGCAGGAGGCCAGCAACTTAA GAACCAAGATTGAGACGCCAGGAAAGCATGTGCAGATGCAACTC TCTCTCAGATCACAAACACATCGACCCAGTGGGAAGAACATCAA ATGCGCACGAGGAGGACACTGCAGGGGGCACCTGGCCAAGATTAA GCCATGCACTGGGGCACAGACTCCAGGCTCTCGTCAGTGCCTC GCAGGATGGTAAACTTATCATCTGGACAGCTACACCACCAAACAA

	GGTCCACGCCATCCCTCGCGCTCCTGGGTATGACCTGTGCA TATGCCCTCTGGAACTATGTGGCCTGCAGTGGCCTGGATAAC ATTGCTCCATTACAATCTGAAAACTCGTGAGGGAACGTGCGC GTGAGTCGTGAGCTGGCAGGACACACAGGTTACCTGCTGCTGC CGATTCCCTGGATGACAATCAGATCGTACCCAGCTCTGGAGACACC ACGTGTGCCCTGTGGACATCGAGACCGGCCAGCAGACGACCAC GTTTACCGGACACACTGGAGATGTCATGAGCCTTCTTGCTCCT GACACCAGACTGTCGTCTGGTGTGATGCTCAGCCAAA CTCTGGGATGTGCGAGAAGGCATGTGCCGGCAGACCTCACTGGC CACGAGTCTGACATCAATGCCATTGCTTCTCAAATGGCAAT GCATTGCCACTGGCTCAGACGCCACCTGCAGGCTGTTGAC CTTCGTGCTGACCAGGAGCTCATGACTTACTCCCAGACAAACATC ATCTGCGGGATCACCTCTGTCTCCTCTCAAAGAGCAGGGCGCCTC CTCCTGCTGGTACGACACTCAACTGCAACGTCTGGATGCA CTCAAAGCCGACCGGGCAGGTGTCTGGCTGGCATGACAACCAC GTCAGCTGCCTGGCGTGACTGACGATGGCATGGCTGTGGCGACA GGGTCTGGATAGCTCCTCAAGATTGGAAC
6xHis-Venus <sub>(1-155)</sub> -G $\gamma_2$	ATG <b>CATCACCACCATCACGGAGTAGCGGTTCA</b> GTGAGCAAG <b>GGCGAGGAGCTGTTCACCGGGGTGGTACCCATCCTGGTCAGCTG</b> GACGGCGACGTAAACGCCACAAGTCAGCGTGTCCGGCGAGGG CGAGGGCGATGCCACCTACGGCAAGCTGACCTGAAGCTGATCTG CACCAACGGCAAGCTGCCGTGCCCTGGCCACCCCTCGTGACCAC CCTGGGCTACGCCCTGCAGTGCCTGCCGCTACCCGACCACAT GAAGCAGCACGACTTCTCAAGTCCGCATGCCGAAGGCTACGT CCAGGAGCGCACCATCTTCAAGGACGACGGCAACTACAAGA CCCGCGCCGAGGTGAAGTTCGAGGGCGACACCCCTGGTAACCGC ATCGAGCTGAAGGGCATCGACTCAAGGAGGACGGCAACATCCT GGGGCACAAGCTGGAGTACAACACTACAACAGCCACAACGTCTATA TCACCGCCGGCGGATCTGGTGGAGGCATGGCCAGCAACAACACC GCCAGCATAGCACAAGCCAGGAAGCTGGTAGAGCAGCTTAAGAT GGAAGCCAATATCGACAGGATAAAGGTGTCAAAGGCAGCTGCAG ATTGATGGCCTACTGTGAAGCACATGCCAAGGAAGACCCCCCTCC TGACCCCTGTTCCGGCTCAGAAAACCGTTAGGGAGAAGAAGT TTTCTGTGCCATCCTT
<b>pCSC 6xHis Venus<sub>(1-155)</sub> G<math>\gamma_2</math> P2A Venus<sub>(155-239)</sub> G<math>\beta_1</math> IRES G<math>\alpha_q</math> nLuc</b>	
Nanoluciferase-G $\alpha_q$	ATGACTCTGGAGTCCATCATGGCGTGCCTGAGCGAGGAGGCC AAGGAAGCCCGCGGATCAACGACGAGATCGAGCGGCAGCTCCG CAGGGACAAGCGGGACGCCGCCGGAGCTCAAGCTGCTGCTGC TCGGGACAGGAGAGAGTGGCAAGAGTACGTTATCAAGCAGATG AGAATCATCCATGGGTCAAGGATACTCTGATGAAGATAAAAGGGG CTTCACCAAGCTGGTGTATCAGAACATCTCACGGCCATGCAGGC CATGATCAGAGCCATGGACACACTCAAGATCCCATAAGTATGA GCACAATAAGGCTCATGCACAATTAGTCGAGAAGTTGATGTGGA GAAGGTGTCTGCTTTGAG <b>TCA</b> GGAGGTGGCGAT <b>T</b> GTCTTCACA <b>CTCGAAGATTCTGTTGGGACTGGCAGACAGACAGCCGGCTACAAC</b> <b>CTGGACCAAGTCCTGAACAGGGAGGTGTCCAGTTGTTCA</b> G AATCTGGGTGTCCGTAACTCCGATCCAAAGGATTGCTCTGAGC GGTAAAATGGGCTGAAGATCGACATCCATGTCATCATCCGTAT GAAGGTCTGAGCGGCACCAATGGCCAGATCGAAAAAAATT TAAGGTGGTGTACCCGTGGATGATCATCACTTAAGGTGATCCT GCACTATGGCACACTGTAATCGACGGGTTACGCCAAACATGAT CGACTATTCTGGACGCCGTATGAAGGCATGCCGTGTCGACGG

	<b>CAAAAAGATCACTGTAACAGGGACCCTGTGGAACGGCAACAAAAA TTATCGACGAGCGCCTGATCAACCCCCGACGGCTCCCTGCTGTTCC GAGTAACCATCAACGGAGTGACCGGCTGGCGGCTGTGCGAACGC ATTCTGGCGTCTGGCGTGGAGGATCTAATCCATATGTAGATGCA ATAAAGAGTTATGGAATGATCCTGGAATCCAGGAATGCTATGAT AGACGACGAGAAATATCAATTATCTGACTCTACCAAATACTATCTT AATGACTTGGACCGCGTAGCTGACCTGCCTACCTGCCTACGCAA CAAGATGTGCTTAGAGTCAGAGAGAAGAAAATGGATACACTGCTTGAA TACCCCTTGACTTACAAAGTGTCACTTCAGAATGGTCGATGTAG GGGGCCAAGGTCAGAGAGAAGAAAATGGATACACTGCTTGAA AATGTCACCTCTATCATGTTCTAGTAGCGCTTAGTGAATATGATC AAGTTCTCGTGGAGTCAGACAATGAGAACCGAATGGAGGAAAGC AAGGCTCTCTTAGAACAAATTATCACATACCCCTGGTTCCAGAAC TCCTCGGTTATTCTGTTCTAAACAAGAAAGATCTCTAGAGGAG AAAATCATGTATTCCCCTAGTCGACTACTTCCCAGAACATGAT GGACCCCAGAGAGATGCCAGGCAGCCCCGAGAACATTCTGAA GATGTTCGTGGACCTGAACCCAGACAGTGAACAAATTATCTACTC CCACTTCACGTGCGCCACAGACACCGAGAACATCCGCTTGCTT TGCTGCCGTCAAGGACACCATCCCTCAGTTGAACCTGAAGGAGTA CAATCTGGTC</b>
<b>Venus<sub>(155-239)</sub>-G<math>\beta_1</math></b>	Identical to G $\alpha_{i3}$ sequence
<b>6xHis-Venus<sub>(1-155)</sub>-G<math>\gamma_2</math></b>	Identical to G $\alpha_{i3}$ sequence

**Appendix Table IV. Amino acid sequences of BRET sensor G protein subunits indicating nanoluciferase, Venus, and 6xHis-tag insertion sites.**

pCSC 6xHis Venus <sub>(1-155)</sub> G $\gamma_2$ P2A Venus <sub>(155-239)</sub> G $\beta_1$ IRES G $\alpha_{i3}$ nLuc	
Nanoluciferase-G $\alpha_{i3}$	MGCTLSAEDKAAVERSkmIDRNLREdgeKAKEVKKLLLGAGESG KSTIVKQMKIIHEDGYSEDECKQYKVVVSNTIQSIIAIIRAMGRLSG GGGSVFTLEDFVGDRQTAGYNLDQVLEQGGVSSLFQNLGVSVTP IQRIVLsgENGLKIDiHViIPyEGLSGDQMgQIEKIFKVVPVDDHHF KVlHYgtLVIdGVTPNMIDYFGRPyEGIAVFdgkkitVTgtLwNG NKiiderlinPDGSllFrVtINGVtgwrlcerilASGGGGSKIDFGEA ARADDARQLFVLAGSAEEGVMTPELAGVIKRLWRDGGVQACFSRS REYQLNDSASYLNLDLDRISQSNYIPTQQDVLRTRVKTTGIVEFHFT FKDLYFKMFDVGGQRSERKKWIHCFCGVTAIIFCVAlSDYDLVLAE DEEMNRMHESMKLFDSICNNKWFTEtsiILFLNKDLFEEKIKRSPL TICYPEYTGSNTYEEAAAyIQCQFEDLNRRKDTKEIYTHFTCATDTK NVQFVFDATDVIIKNNLKECGLY
Venus <sub>(155-239)</sub> -G $\beta_1$	DKQKNGIKANFKIRHNIEDGGVQLADHYQQNTPIGDGPVLLPDNH YLSYQSKLSKDPNEKRDHMVLLFVTAAGITLGMDELYKGSSGGG SELDQLRQEAEQLKNQIRDARKACADATLSQITNNIDPVGRIQMRT RRTLRGHLAKIYAMHWGTDsRLLVSASQDGKLIWDSYTTNKVHA IPLRSSWVMTCAyAPSGNYVACGGLDNICSiYNLKREGNVRVsRE LAGHTGYLSCCRFLDDNQIVTSSGDTTCALWDIETGQQTTFTGHT GDVMSLsLAPDTRLFVSGACDASAKLWDVREGMCRQTFTGhesDI NAICFFPNGNATGSSDATCRLFDLRADQELMTYSHDNIICGITSV SFSKSGRLLLAGYDDFNcNVWDALKADRAGVLAGHDNRVsCLGV TDDGMAVATGSWDSFLKIWN
6xHis-Venus <sub>(1-155)</sub> -G $\gamma_2$	MHHHHHHGSSGSVSKGEELFTGVVPILVELGDVNghKfsvsGEG EGDATYgkltLkIcttgkLPVPWptLvtLgyglqcfarypdHM KQHdffksampegyvQERTIFFKDDGNYKTRAEVKFEGDTLVNRIE LKGIDFKEDGNILGHKLEYNynshnvYitAGGSGGGMASNNTASIA QARKLVEQLKMEANIDRIKVSKAAADLMAYCEAHAKEDPLTPVP ASENPfrekkFFcaIL
pCSC 6xHis Venus <sub>(1-155)</sub> G $\gamma_2$ P2A Venus <sub>(155-239)</sub> G $\beta_1$ IRES G $\alpha_q$ nLuc	
Nanoluciferase-G $\alpha_q$	MTLESIMACCLSEEAKEARRINDEIERQLRRDKRDARRELKLLLGT GESGKSTFIKQMRIIHGSGYSDEDKRGFTKLVYQNIftAMQAMIRA MDTLKIPYKYEHNKAHAQLVREVDVEKVSafeSGGGSVFTLEDF VGDWRQTAGYNLDQVLEQGGVSSLFQNLGVSVTPiQRIvLsENG LKIDiHViIPyEGLSGDQMgQIEKIFKVVPVDDHHFkVlHYgtLV DGVTpNMIDYFGRPyEGIAVFdgkkitVTgtLwNGNKiiderlinPD GSllFrVtINGVtgwrlcerilASGGGGSNPYVDAIKSLWNDPGIQ EcYDRRREYQLSDSTKYYLNLDRVADPAYLPTQDVLRVrVPTT GIIEPFDLQSvIFRMVDVGGQRserrkwiHCFENVTSIMFLVALSE YDQVLVESDNENRMEEsKALFRtiITYPWFQNSsVILFLNKKDLLEE KIMyShLVDYFPEYDGPQRDAQAAREFILKMFDLNPDSdkIiYsh FTCATDTENIRFVFAAVKDTILQLNLKEYNLV
Venus <sub>(155-239)</sub> -G $\beta_1$	Identical to G $\alpha_{i3}$ sequence
6xHis-Venus <sub>(1-155)</sub> -G $\gamma_2$	Identical to G $\alpha_{i3}$ sequence

**Appendix Table V. Antibodies, respective targets, and usage conditions during immunoblots.**

<b>Antibody</b>	<b>Target</b>	<b>Dilution</b>	<b>Incubation Time</b>	<b>Incubation Temperature</b>
Anti-NanoLuc® Monoclonal Antibody	Nanoluciferase (attached to the G $\alpha_{i3}$ subunit)	1:1000	Overnight (~18 Hours)	4°C
IRDye® 800CW Goat anti-Mouse IgG (H+L) Secondary Antibody	Anti-NanoLuc® Monoclonal Antibody	1:1000	1 Hour	Room Temperature (22-25°C)
Anti-G $\beta$ Monoclonal Antibody (H-1) Alex Fluor® 680	G $\beta$ 1-4 G protein subunit	1:100	1 Hour	Room Temperature (22-25°C)
FluoTag®-X2 anti-ALFA Alexa Fluor® 647	15-amino acid ALFA-tag (SRLEEELRRRLTE)	1:500	1 Hour	Room Temperature (22-25°C)

## Appendix Methods

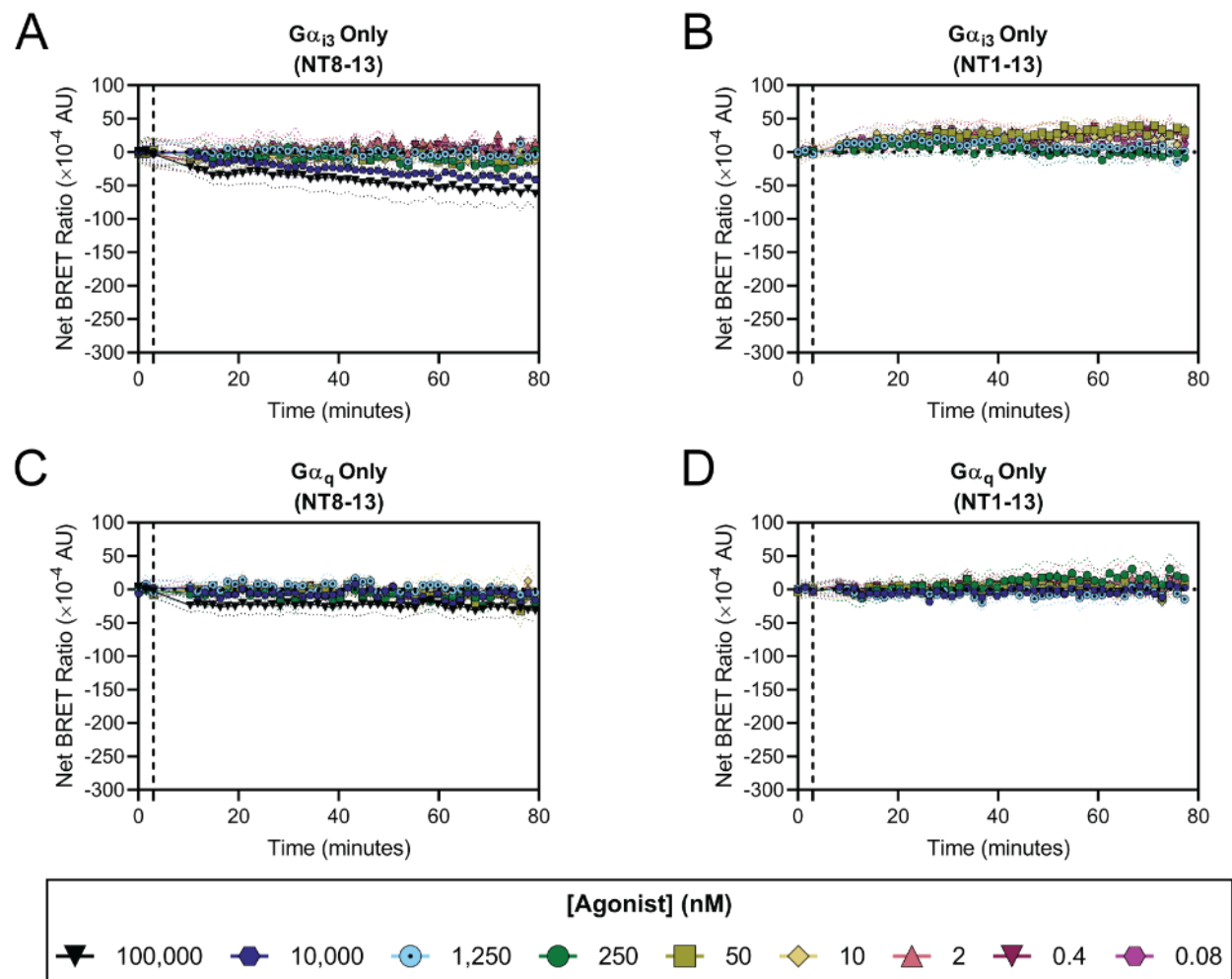
### Saturation Binding Assays

HEK293-F Human NTSR1 WT IRES mCherry stables and HEK293-F cells were plated and transfected as previously described (refer to Live Cell BRET Assays protocol). In the latter case, HEK293-F cells were transfected with either 750 ng of pCSC enNTSR1 (M208) Strep. IRES mCherry or pcDNA3.1/Zeo(+). Cells were harvested from plates and resuspended in 1 mL FSM. 50  $\mu$ L of cells were aliquoted into the wells of a clear, 96-well V-bottom microplates (Corning). 60  $\mu$ L of fluorescein-labelled NT8-13 (FAM NT8-13) at 2X the final concentration (or FSM vehicle) was then added to every well. Half the plate was also treated with 10  $\mu$ L 100  $\mu$ M NT8-13 (10  $\mu$ M NT8-13) to assess competitive binding (the other half was treated with an equivalent volume of FSM). The plate was incubated for 1 hour at room temperature with gentle shaking to allow for agonist binding. Cells were pelleted in the plate, media aspirated, and resuspended 150  $\mu$ L of fresh FSM. Cells in each well of the plate were then read for FAM (excitation at 493 nm and emission at 517 nm) using a CytoFLEX Flow Cytometer (Beckman Coulter).

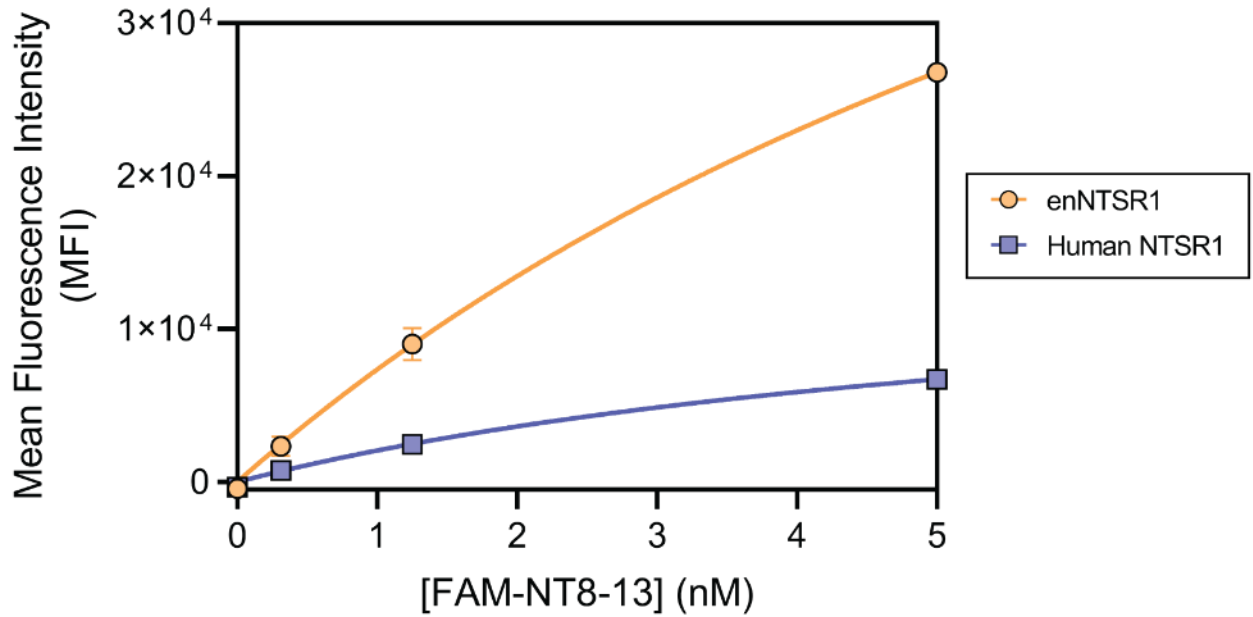
### enNTSR1-G $\alpha$ <sub>i3</sub> Coupling GTP Turnover Assay

Lipid micelles, containing POPC and POPG lipids (Avanti Polar Lipids), were produced and solubilized in chloroform by mixing LMNG, CHS, and lipids in a 5:1:1 molar ratio, respectively. Chloroform was evaporated overnight, and films resuspended in reaction buffer (20 mM HEPES (pH 7.5), 100 mM NaCl). To incorporate lipids into purified enNTSR1, enNTSR1 (2  $\mu$ M) was incubated with a 20-fold dilution of micelles or LMNG (0.02% final) at room temperature for 30 minutes in reaction buffer. enNTSR1 was allowed to couple with G $\alpha$ <sub>i3</sub> heterotrimers (final enNTSR1 concentration of 1  $\mu$ M) by sequentially adding 10 mM MgCl<sub>2</sub>, 1191 ng purified G $\alpha$ <sub>i3</sub> BRET biosensor, 10  $\mu$ M agonist (or equivalent volume of vehicle reaction buffer) and incubating at room temperature for 2.5 hours. GTP hydrolysis was assessed using the GTPase-Glo assay as previously described, with the modifications being to assay in reaction buffer and a reduction in GTP turnover reaction time from 60 minutes to 30 minutes.

## Appendix Figures

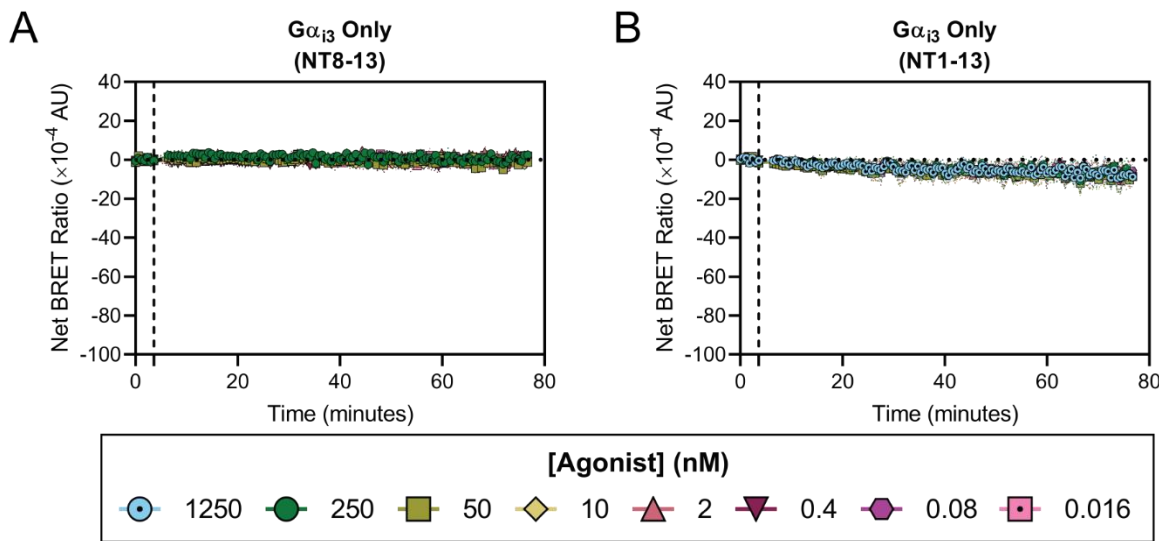


**Appendix Figure A1. HEK293-F cells depict minimal-to-no non-specific activation of G $\alpha_{i3}$  and G $\alpha_q$  BRET biosensors in the presence of saturating NT8-13 and NT1-13.** Change in BRET ratio over time in parental HEK293-F cells for the activation of (A) G $\alpha_{i3}$  in the presence of NT8-13, (B) G $\alpha_{i3}$  in the presence of NT1-13, (C) G $\alpha_q$  in the presence of NT8-13, and (D) G $\alpha_q$  in the presence of NT1-13. The data were baseline corrected against the average of three luminescent signal reads (90 second between each; 3 minutes total) prior to the addition of agonist (vertical black dotted lines). All values are expressed as mean  $\pm$  SEM for three independent experiments conducted in duplicate where duplicates were averaged before calculating SEM.

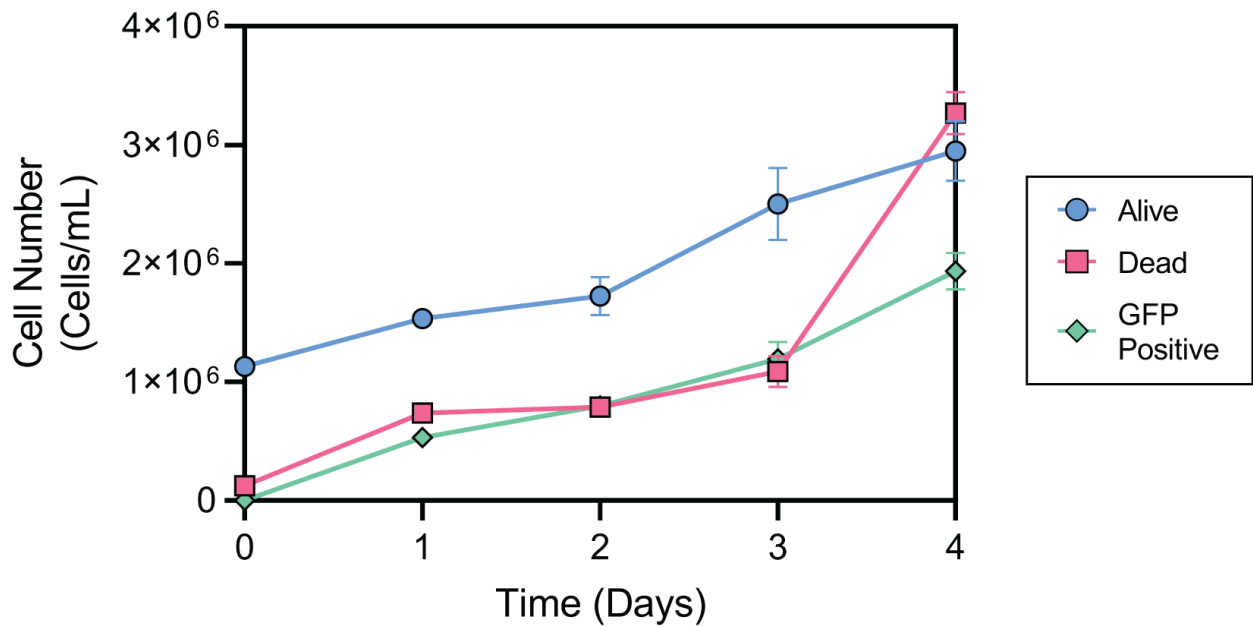


**Appendix Figure A2. Saturation binding of enNTSR1 and human NTSR1 utilising fluorescein amidite-labelled NT8-13 highlights enNTSR1 is expressed to a higher degree.** Values are expressed as mean  $\pm$  SEM and are representative of three independent experiments conducted in triplicate. Points fit to a nonlinear regression using a “One-site – Specific binding” model.

---

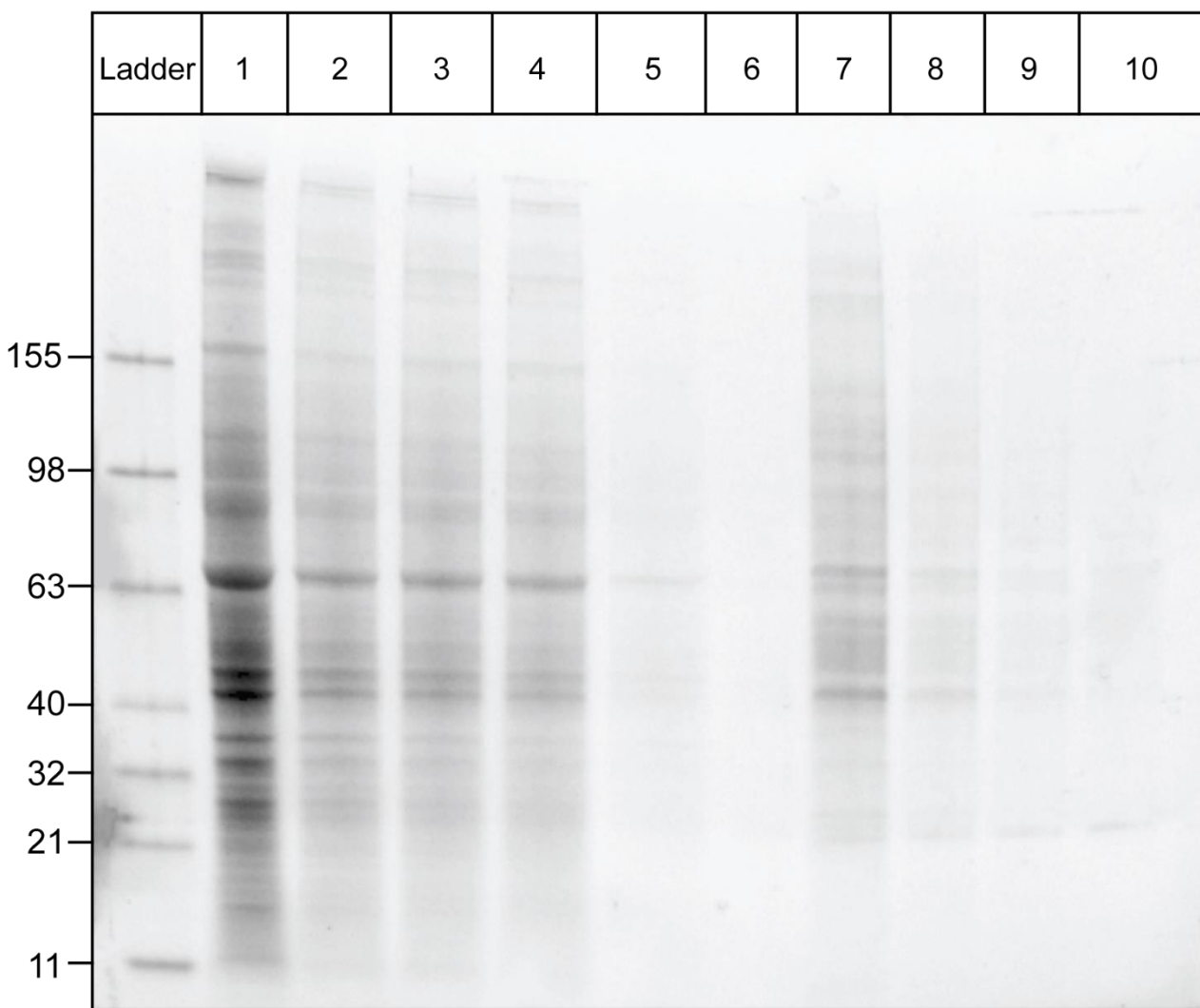


**Appendix Figure A3. Membrane preparations show no non-specific activation of the G $\alpha_{i3}$  signalling pathway due to background binding of NT8-13 or NT1-13 to endogenous human NTSR2.** Change in BRET ratio over time in parental HEK293-F cells for the activation of (A) G $\alpha_{i3}$  in the presence of NT8-13, and (B) G $\alpha_{i3}$  in the presence of NT1-13. The data were baseline corrected against the average of seven luminescent signal reads (36 second between each; 3 minutes 36 seconds total) prior to the addition of agonist (vertical black dotted lines). All values are expressed as mean  $\pm$  SEM for three independent experiments conducted in triplicate where triplicates were averaged before calculating SEM.



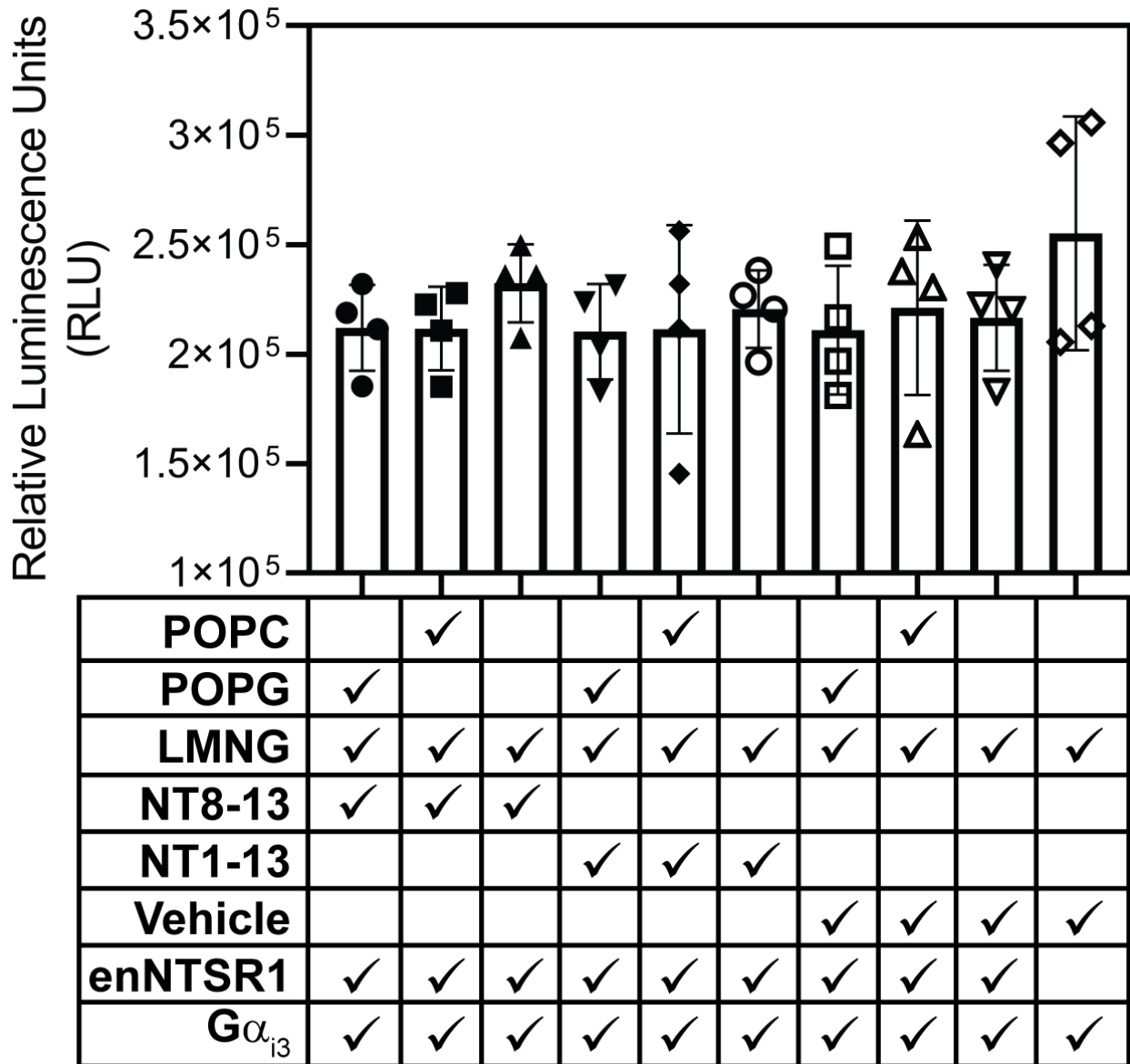
**Appendix Figure A4. Live, dead, and GFP positive cell counts during the time course optimisation and production of the  $\text{G}\alpha_{i3}$  BRET sensor.** Values are expressed as mean  $\pm$  SEM for four independent experiments conducted in quadruplicate where quadruplicates were averaged before calculating SEM.

---



**Appendix Figure A5. Associated stain-free gel image during purification of the 6X-Histidine tagged G $\alpha_{i3}$  BRET sensor from an 80 mL starter culture.** Lanes correspond to (total volumes samples were taken from in brackets): 0, SDS-PAGE ladder lane; 1, Cell lysate (25 mL); 2, Post-solubilisation (50 mL); 3, Post-centrifugation solubilisation supernatant (50 mL); 4, Unbound protein flow through (50 mL); 5, Wash 1 (15 mL); 6, Wash 2 (15 mL); 7, Elution 1 (2 mL); 8, Elution 2 (2 mL); 9, Elution 3 (2 mL); 10, Elution 4 (2 mL). Ladder markers are in kDa.

---



**Appendix Figure A6. Purified enNTSR1 was unable to be reconstituted into a stable complex with purified  $G\alpha_{i3}$  BRET sensor.** Two-way ANOVA indicated mean luminescence for all enNTSR1 containing samples (Columns 1-9) were not significantly different to the mean luminescence of the  $G\alpha_{i3}$ -only control (Column 10) at a significance level of  $p = 0.05$ .